RESEARCH PAPER P-284

ACOUSTIC REVERBERATION AT THE SEA SURFACE: SURFACE AND SUBLAYER SPECTRA VIS-Á-VIS SCATTERING AND REFLECTION

John J. Martin

December 1966

IDA
INSTITUTE FOR DEFENSE ANALYSES
RESEARCH AND ENGINEERING SUPPORT DIVISION

Log No. IDA/HQ 66-5291
Copy 95 of 150

RESEARCH PAPER P-284

ACOUSTIC REVERBERATION AT THE SEA SURFACE: SURFACE AND SUBLAYER SPECTRA VIS-Á-VIS SCATTERING AND REFLECTION

John J. Martin

December 1966

IDA

INSTITUTE FOR DEFENSE ANALYSES
RESEARCH AND ENGINEERING SUPPORT DIVISION

Contract DAHC15-67-C-0011
Task T-37

ACKNOWLEDGMENT

In the course of developing this research paper, I had assistance from numerous individuals. I acknowledge with gratitude their assistance.

At the outset, Dr. R. P. Chapman of the Canadian Naval Research Establishment, Dr. G. R. Garrison of the Applied Physics Laboratory of the University of Washington, and Dr. M. Schulkin made available to me much of the data which they had used in the preparation of their referenced papers. In this relation, Messrs. R. J. Urick of the U. S. Naval Ordnance Laboratory, White Oak, Maryland, and R. M. Richter of the U. S. Naval Weapons Services Office, Philadelphia, saved my needlessly pursuing data of theirs that were no longer available.

During the course of the work reported here, Dr. R. D. Turner of IDA aided me in a critical matter relating to spectra. In addition to this, Miss Joan Begelman showed inexhaustible patience in graph-reading most of the data appearing in Appendix B, Mrs. Marion L. Fickett prepared the many graphs of Appendix B and made the overall calculation of rms errors, and Mrs. Marguerite Bradley Stavriotis patiently typed numerous iterations of the paper.

When the paper was substantially completed, Prof. Walter H. Munk of the Institute of Geophysics of the University of California, and Dr. J. Menkes of IDA reviewed my efforts and their comments were useful in arranging and clarifying some of the matters I had treated.

CONTENTS

I. INTRODUCTION

The reverberation of sound from an ensonified area at the surface of the ocean is a process in which diffuse scattering from the sea surface and a subsurface volume (sublayer) as well as specular reflection from the surface take part; this has been recognized for some time.[1*] The reverberation of acoustic energy from the surface and its sublayer is, patently, associated with the "texture" of the sea surface and turbulent fluctuations below the surface. This paper separates the total reverberation strength of ocean surface into scattering and reflection contributions and analyzes scattering into that due to the rough sea surface itself, and that due to a turbulent sublayer. There are two bases for this analysis: (1) acoustic reverberation data over a range of frequencies, grazing angles, and sea-surface wind speeds, and (2) optical laboratory and sea measurement of air-driven water-surface slope and slope spectral densities, modified to interpret acoustic scattering data and describe acoustic reflection data.

This paper begins by presenting from the literature the theoretical bases used, as they relate to mathematical, statistical, and physical aspects of the analysis. Next, the paper continues by presenting in tabular or graphical form the acoustic and optical experimental data immediately pertinent to the analysis given here.

The analysis which then follows, proceeds by using the previously developed relationship between acoustic scattering strength and acoustic frequency, grazing angle, and sea-surface elevation power spectral density (psd) to compare elevation psd derived from

*References and footnotes are numbered at the end of the main paper.

acoustic and optical data. Scattering from a stochastic surface is described by decomposing the surface to sinusoids of varying amplitude and then computing the scattering strength due to resonant interactions of radiant field and Fourier components of the surface. The comparison of elevation psd from these two sources shows sufficient agreement in character and magnitude to develop confidence, with some qualification, in psd's developed from acoustic reverberation data. In the process of analyzing acoustically-based elevation psd, three sea-surface wind speed regimes are found.

Next, given acoustically based elevation spectra of the sea surface as a function of wind speed, the paper continues by using the general dependence of turbulent volume scattering upon accustic frequency, grazing angle, and turbulent volume psd--based on small enough grazing angles--to separate volume and surface scattering and to determine a turbulent volume spectral density. This scattering, due to index of refraction fluctuations in a turbulent volume, is analyzed in a manner related to the resonant interaction described above for rough surfaces. From this it is possible to estimate sea-surface sublayer scattering. Presently there is no basis for choosing the physical field whose fluctuations cause scattering.

Finally, starting with optically based slope psd, both sea-surface elevation and curvature-related psd's may be calculated. From these, the reflection strength of facets of the sea surface may be found as a function of sea-surface wind speed, incidence angle, and frequency, using previously developed relationships.

In summary, this paper makes use of acoustic and optical experimental data to derive appropriate wind-driven sea-surface statistics, from which scattering strength of the sea surface and its sublayer, and reflection strength of the surface are determined as a function of grazing or incidence angle, acoustic frequency, and sea-surface wind speed. The paper relies upon many of the ideas presented in a related paper previously published.[2]

II. THEORETICAL BASIS

As it is true that surface and volume scattering and surface reflection of acoustic energy from the surface and near surface of the sea are dependent upon the statistics of the irregularities of the scattering and reflecting spaces as well as upon the frequency and incidence angle of that energy, this section will present theoretical relationships for surface scattering strength (N_s) and surface reflection strength (N_R) of the sea, and for the volume scattering strength of the sea-surface sublayer (N_v) in terms of acoustic frequency (f_r) or acoustic wave number ($k_r = 2\pi f_r/c$), grazing angle (φ), and some appropriate function of surface elevation power spectral density (psd $\equiv$ E, with suitable subscripts). Since E is a function of air or wind speed v, it is through psd's that total reverberation strength (N_T) depends upon wind speed. Thus, with N in decibels (for definition, cf. Appendix B)

$$10^{N_T/10} = 10^{N_s/10} + 10^{N_v/10} + 10^{N_R/10} . \qquad (1)$$

A. SPECTRA[3]

The relationships among one- and two-dimensional (1-D and 2-D) spectra, together with related statistics and functions, are summarized here. Scattering due to elevation irregularities of the sea surface is considered next, then scattering strength due to the subsurface volume, followed by a discussion of reflection strength of, presumably, suitably disposed sea-surface "facets" at near normal incidence of the acoustic energy to the surface. When dealing with spectra of the sea surface at large wave numbers, it is necessary for lack of better information at the present time to assume both

isotropic and homogeneous conditions. That this is untrue is known and, in fact, is almost self-evident to any sea-watcher; on the other hand, it is likely that at the scale of horizontal distances of interest in acoustic scattering the elevation of roughness does not vary greatly from upwind-downwind direction to crosswind direction. In any case, the sea surface is treated here as if isotropic and homogeneous, and some justification will be given.

Probably the root mean square (rms) elevation (σ_z) of the sea surface is the physical quantity about which one has the best intuitive feeling, and it is therefore a likely starting point. Thus, along a given line on a rough surface, the variance (σ_z^2) of the elevation along that line is just the integral of the power spectral density of elevation $[E_z(k_s,v)]_1$,

$$\sigma_z^2 = \int_{-\infty}^{\infty} [E_z(k_s,v)]_1 \, dk_s \quad . \tag{2}$$

In this functional dependence of E, the subscript z indicates that elevation z is the quantity whose density is being expressed, k_s is a spatial wave number (as opposed to acoustic wave number k_r), v is the characteristic speed of the air or wind over the water surface, and the subscript 1 means that the spectrum is for the 1-D case, i.e., along a line. The spatial wave number $k_s = 2\pi/\lambda_s$ is a convenient independent variable for describing the Fourier components of a stochastic process. The radiation wave number $k_r = 2\pi/\lambda_r$ is a similarly convenient variable for describing the radiant energy oscillations on the same scale. If elevation irregularities of the surface in question are isotropic and homogeneous, then the elevation psd is identical along all lines.

Frequently, roughness characteristics of a line or surface are expressed by recourse to a correlation function $B_z(x,y)$ where x, y, and z are mutually orthogonal axes. For an isotropic, homogeneous surface, the correlation function is not a function of direction and

can be expressed in terms of a single variable as $B_z(r)$. Now fundamentally it is true that

$$B_z(r,v) = \langle z(p,v) \cdot z(p+r,v) \rangle \quad , \tag{3}$$

where p is a point on the surface, and r is distance from that point, and $\langle \; \rangle$ indicate averaging over all points on the surface. The correlation function is expressible not only as an average over the surface of the product of elevations at a given distance r, but also as a transformation of the elevation psd. Thus,

$$B_z(r,v) = \int_{-\infty}^{\infty} \exp(ik_s r)[E_z(k_s,v)]_1 \; dk_s \quad . \tag{4}$$

The correlation function $B_z(r,v)$ allows the definition of the correlation length $r_z(v)$ of the surface as

$$B_z(r_z,v)/B_z(0,v) = e^{-1} \quad . \tag{5}$$

Depending upon the distribution of elevation variance in wave number space or, on the other hand, the form or shape of the related correlation function, it happens that

$$r_z(v) = O(\sigma_z/\sigma_{z'}) \tag{6}$$

as, for example, one may demonstrate for exponential or Gaussian $B_z(r,v)$.

Though it is true that the correlation function for an isotropic surface is the same whether the averaging is done over the whole surface or only along some given line on that surface (Appendix A), it is not true that the 1-D elevation psd is the same as the 2-D psd; in fact, 1-D and 2-D spectra are incommensurate as they have different units. In Appendix A, the relationship between $[E_z(k_s,v)]_1$ and $[E_z(k_s,v)]_2$ is given; the result is that[4] (Appendix A)

$$[E_z(k_s,v)]_{2i} = \sqrt{2/\pi} \int_{k_s}^{\infty} \frac{[E_z'(k_s',v)]_1}{(k_s'^2-k_s^2)^{3/2}}\, dk_s' \quad , \tag{7}$$

where the prime on E_z indicates differentiation with respect to k_s'. The subscript i is appended to the psd of the left side of Eq. 7 to emphasize that for this relation to be valid, the surface must be isotropic; subsequently the i is not used as isotropicity is assumed. Relative to elevation variance, the significance of Eq. 7 is that[5]

$$\sigma_z^2 = \int_{-\infty}^{\infty} 2\pi k_s [E_z(k_s,v)]_2\, dk_s \quad . \tag{8}$$

Finally, the relationship between elevation irregularities and surface slope irregularities and elevation second derivative irregularities needs to be considered. If, as before, $[E_z(k_s)]_1$ is the 1-D psd of elevation irregularities at wave number k_s then the 1-D psd of slope irregularities of a water surface is

$$[E_{z'}(k_s)]_1 = k_s^2 [E_z(k_s,v)]_1 \quad . \tag{9}$$

By analogy with the foregoing, the rms slope in a given direction is

$$\sigma_{z'}^2 = \int_{-\infty}^{\infty} k_s^2 [E_z(k_s)]_1\, dk_s \quad . \tag{10}$$

Generally the 1-D psd of irregularities of the n^{th} derivative of z is given by

$$[E_{z(n)}(k_s,v)]_1 = k_s^{2n} [E_z(k_s,v)]_1 \quad . \tag{11}$$

Thus, the variance of the second derivative of surface elevation along a line is

$$\sigma_{z''}^2 = \int_{-\infty}^{\infty} k_s^4 [E_z(k_s,v)]_1\, dk_s \quad . \tag{12}$$

As a practical matter, for arbitrarily chosen $E_z(k_s, v)$, $\sigma^2_{z(s)}$ need not remain bounded.

B. SURFACE SCATTERING

Analysis of wave scattering at an isotropically irregular surface yields the theoretical relationship for backscattering strength with grazing angle φ not too near $\pi/2$ as[6]

$$10^{N_s/10} = 4|R|^2 k_r^4 \sin^4\varphi [E_z(2k_r \cos\varphi]_2 \quad , \tag{13}$$

where R is a reflection coefficient given by

$$R = \frac{\hat{\rho} - \dfrac{\hat{c}}{\sin\varphi}\left(1 - \dfrac{\cos^2\varphi}{\hat{c}^2}\right)^{\frac{1}{2}}}{\hat{\rho} + \dfrac{\hat{c}}{\sin\varphi}\left(1 - \dfrac{\cos^2\varphi}{\hat{c}^2}\right)} + \frac{2\hat{\rho}(\hat{\rho}-1)\cot^2\varphi}{\left[\hat{\rho} + \dfrac{\hat{c}}{\sin\varphi}\left(1 - \dfrac{\cos^2\varphi}{\hat{c}^2}\right)^{\frac{1}{2}}\right]^2} \ . \tag{14}$$

In Eq. 13, N_s is surface backscattering strength of the scatterer in decibels; $[E_z(k_s)]_2$ is the power spectrum of an isotropically rough surface; k_r is acoustic radiation wave number; φ is the grazing angle; i.e., the angle measured from the surface to the incident ray; $\hat{\rho}$ is the ratio (in the present case) of air density to water density; and $\hat{c}$ is the ratio of speed of sound in water to speed of sound in air. With the values of $\hat{\rho}(\cong 1/800)$ and $\hat{c}(\cong 5)$ of interest here, one can show $R \cong -1$ so that backscattering strength N_s for the sea surface becomes

$$10^{N_s/10} = 4k_r^4 \sin^4\varphi [E_z(2k_r \cos\varphi), v_{sea}]_2 \quad , \tag{15}$$

where v_{sea} is the sea-surface wind speed. Since sea-surface wind speed is a characteristic number, v_{sea} must be measured outside the appreciable effect of any boundary layers. Inasmuch as $k_r = 2\pi f_r/c$, where f_r is acoustic frequency and c is the speed of sound in water, then the foregoing equation shows surface reverberation strength to

be a function only of acoustic frequency, grazing angle, and sea-surface wind speed for an isotropic surface. For an anisotropic surface, there may be an additional dependence upon azimuth. At grazing angles near zero, shadowing of the surface by nearby crests may cause Eq. 15 to overestimate scattering.[7]

C. VOLUME (SUBLAYER) SCATTERING

Analysis of scattering from an isotropically turbulent volume of fluid shows that, in a generalized theoretical form, backscattering volume reverberation strength varies as[8] (Appendix B)

$$10^{N_v/10} = \left\{ 2\pi k_r^4 \sum_{i=1}^{n} (V_i/x_i^2)[E_{x_i}(2k_r)]_3 \right\} / r_{ref}^2 \quad , \tag{16}$$

where N_v is a turbulent volume backscattering strength, at a reference distance r_{ref} from the scattering volume, V_i is the scattering volume of the X_i turbulent field, and x_i is a characteristic value for the field and possibly a function of k_r, $[E_{x_i}(k_s)]_3$ is the power spectrum of the X_i field in an isotropically irregular volume.[9] In the sea sublayer, X_i may be from among temperature and salinity fluctuation, bubbles and possibly others. As a working assumption, at this point, it will be assumed that fluctuations of a single field are the dominant scattering means, i.e., if more than one field is significant that index of refraction fluctuations are congruent among these. Thus, the relationship for backscattering from turbulent fluctuations for the sea sublayer becomes

$$10^{N_v/10} = 2\pi k_r^4 V[E_x(2k_r, v_{...})]_3 / x^2 r_{ref}^2 \quad . \tag{17}$$

There remains the scattering volume, V, to be considered. Since sea-surface reverberation strengths are reduced on a sea-surface reference area ($A_{ref} = r_{ref}^2$) basis, the effective scattering volume per unit of surface area in Eq. 17 is

$$V = r_{ref}^2 z_0(k_r) \sin\varphi \quad , \tag{18}$$

because the density of radiation in the scattering volume V varies as sin φ, and because the volume of a cylinder or pyramidal frustrum depends only on its height for fixed base area. In this, $z_0(k_r)$ is the effective depth to which scattering of acoustic energy of wave number k_r takes place.

It is likely that fluctuations in the sublayer are not isotropic or homogeneous[10] and this contradicts a fundamental assumption of Eq. 16. Besides this, reflection and refraction at small grazing angles may cause anomalous effects. In practical cases, these effects may be ameliorated in part because at large wave numbers there is a tendency to isotropy as, certainly, there is no preferred direction for the ultimate dissipation due to eddies.

Thus, subsurface volume scattering strength N_v may be written

$$10^{N_v/10} = 2\pi z_0(k_r)k_r^4 \sin\varphi[E_x(2k_r,\ v_{...})]_s/x^2 \quad . \qquad (19)$$

One interesting aspect of this relation is the implication that sublayer reverberation strength varies as the sine of grazing angle φ, and there is some indication in the experimental data of Appendix B to confirm this.

D. SURFACE REFLECTIONS

A recently published paper[2] developed a relationship for reverberation strength due to surface reflections from an isotropically rough surface as

$$10^{N_R/10} = \frac{(A_R)_{eff}}{\pi^3}\left(\frac{\sigma_{z''}}{\sigma_{z'}}\right)^2 \exp\left[-\frac{1}{2}\left(\frac{\cot\varphi}{\sigma_{z'}}\right)^2\right] \quad , \qquad (20)$$

where N_R is reverberation strength due to surface reflections from suitably disposed facets, $\sigma_{z'}^2$, and $\sigma_{z''}^2$ are the variances of the first and second derivatives of surface elevation, and $(A_R)_{eff}$ is the effective reflecting area of each facet. Formally $(A_R)_{eff}$ has limiting values as follows: $(A_R)_{eff}$ = constant for $\sigma_{z''}/\sigma_{z'''} \gg c/f_r = \lambda_r$,

and $(A_R)_{eff} = \pi(\sigma_{z''}/\sigma_{z'''})^2$ for $(\sigma_{z''}/\sigma_{z'''})$ about the order of λ_r or less. As stated previously, depending upon $E_z(k)$, $\sigma_{z''}/\sigma_{z'''}$ may be approximately equal to correlation length $r_{z''}$ for surface second derivative. Thus Eq. 20 takes two forms:

$$10^{N_R/10} = \text{constant}\left\{\frac{1}{\pi^2}\left(\frac{\sigma_{z''}}{\sigma_{z'}}\right)^2 \exp\left[-\frac{1}{2}\left(\frac{\cot\varphi}{\sigma_{z'}}\right)^2\right]\right\}, \quad \sigma_{z''}/\sigma_{z'''} >> \lambda_r , \tag{21a}$$

and

$$10^{N_R/10} = \frac{1}{\pi}\left(\frac{\sigma_{z''}^2}{\sigma_{z'}\,\sigma_{z'''}}\right)^2 \exp\left[-\frac{1}{2}\left(\frac{\cot\varphi}{\sigma_{z'}}\right)^2\right], \quad \sigma_{z''}/\sigma_{z'''} \leq O(\lambda_r) . \tag{21b}$$

The ratios of variances in these equations are, of course, wind-speed dependent as indicated by Eqs. 8 and 11, but it would be laborious to indicate this.

III. DATA BASIS

As stated, the experimental basis of this paper consists of both acoustic[1,11-18] and optical[7,19] data. Through recourse to the literature[1,11-16] and through private[17,18] correspondence, 2459 data relating reverberation strength to acoustic frequency, grazing angle, and wind speed were obtained (Appendix B). These data which are not, of course, uniformly dense in the frequency-grazing angle-wind speed "space" were sampled for the scattering analysis at grazing angles of φ = 10, 30, and 50 deg. For the reflection analysis, the data are segregated in a group with 70 deg $\leq \varphi \leq$ 90 deg for acoustic frequency f_r = 60 kcps. It was deemed necessary to sample the scattering data so that a relatively broad, prolifically reported experiment would not outweigh a perhaps equally competent, less elaborate one. Because of the relative paucity of data for sea-surface wind speeds less than five knots and greater than 15 knots and, separately, for grazing angles near 90 deg, these vicinities were treated as possible within the data available. From Appendix B, Table 1 in this section gives the sampled values of acoustic reverberation data for sea-surface wind speeds (v_{sea}) less than five knots; Table 2 for wind speeds of v_{sea} = 5, 10, and 15 knots; and Table 3 for sea-surface wind speeds greater than 15 knots. Table 4 gives reverberation data from Appendix B for 70 deg $\leq \varphi \leq$ 90 deg, where it is deemed[2] that reflection effects dominate.

In addition to acoustic data which, as will be seen, may be used to imply a sea-surface 2-D isotropic roughness elevation psd, optical data are available in the literature which relate to air-driven water surface 1-D slope psd as a function of air speed (v_{lab}) over the water surface; the air speeds appropriate to these data are $v_{lab} \simeq$

Table 1 -- SAMPLED ACOUSTIC REVERBERATION STRENGTH (db)
EXPERIMENTAL DATA FOR SEA-SURFACE WIND SPEED ≤ 5 KNOTS

Grazing Angle, deg	Wind Speed, knots	Acoustic Frequency, kcps	Reverberation Strength
30	2.0	60.0	-40
	2.5	1.2	-46
	2.5	2.4	-49
	2.5	4.8	-42
	2.5	9.6	-53
	.5	60.0	-42
	2.5	60.0	-37
	3.5	60.0	-37
	4.5	60.0	-34
50	2.0	60.0	-38
	2.5	1.2	-34
	2.5	2.4	-38
	2.5	4.8	-31
	2.5	60.0	-28
	3.5	60.0	-37
	4.0	60.0	-39
	4.5	60.0	-32

NOTE: At all frequencies, except 60 kcps, the frequency given is the center of an octave-wide bandpass.

Table 2 -- SAMPLED ACOUSTIC REVERBERATION STRENGTH (db)
EXPERIMENTAL DATA FOR SEA-SURFACE WIND
SPEED = 5, 10, and 15 KNOTS

Grazing Angle, deg	Wind Speed, knots	Acoustic Frequency, kcps	Reverberation Strength
10	5	.6	-66
		1.2	-60
		2.4	-65
		4.8	-58
		9.6	-53
		60.0	-48
	10	.6	-64
		1.2	-52
		2.4	-45
		4.8	-34
		9.6	-45
	15	60.0	-28
30	5	.6	-45
		1.2	-48
		2.4	-52
		4.8	-50
		9.6	-47
		60.0	-36
	10	.6	-44
		1.2	-41
		2.4	-40
		4.8	-30
		9.6	-38
		60.0	-36
	15	.6	-42
		1.2	-38
		2.4	-39
		4.8	-29
		9.6	-34
		60.0	-22
50	5	.6	-32
		1.2	-45
		2.4	-41
		4.8	-43
		9.6	-40
		60.0	-33
	10	.6	-32
		1.2	-38
		2.4	-39
		4.8	-28
		9.6	-32
		60.0	-30
	15	.6	-30
		1.2	-33
		2.4	-30
		4.8	-23
		9.6	-28
		60.0	-21

NOTE: At all frequencies, except 60 kcps, the frequency given is the center of an octave-wide bandpass.

Table 3 -- SAMPLED ACOUSTIC REVERBERATION STRENGTH (db) EXPERIMENTAL DATA FOR SEA-SURFACE WIND SPEED > 15 KNOTS

Grazing Angle, deg	Wind Speed, knots	Acoustic Frequency, kcps	Reverberation Strength
10	17	60.0	-27
	17.5	1.2	-51
		2.4	-52
		4.8	-45
		9.6	-43
	19.5	60.0	-31
	20.0	60.0	-28
	21.0	60.0	-32
	22.0	60.0	-30
	25.0	4.8	-34
	30.0	.6	-40
		1.2	-35
30	17.0	60.0	-25
	17.5	1.2	-42
		2.4	-45
		4.8	-40
		9.6	-32
	19.5	60.0	-22
	20.0	1.2	-32
		2.4	-31
		60.0	-23
	21.0	60.0	-22
	33.0	60.0	-26
50	17.5	2.4	-28
	19.5	60.0	-19
	20.0	1.2	-28
		2.4	-39
		60.0	-22
	21.0	60.0	-20
	22.0	60.0	-24

NOTE: At all frequencies, except 60 kcps, the frequency given is the center of an octave-wide bandpass.

Table 4 -- NEAR-NORMAL REVERBERATION STRENGTH (db)
$70 \leq \varphi \leq 90$ deg
f_r = 60 kcps

Speed, v, knots	Grazing Angle, φ, deg	Reflection Strength, N_t
2	71	-36
	74	-32
		-33
	75	-35
	78	-19
3	70	-21
		-31
	73	-33
		-43
	79	-14
		-26
	80	-36
	81	-31
3.5	70	-25
	76	-15
	90	- 2
		-11
4	70	-30
		-31
	80	-23
		-25
4.5	71	-27
	73	-21
	74	-19
	79	- 9
		-13
5	70	-27
	74	-24
	78	-14
5.5	70	-27
	74	-21
	78	- 8
6.5	75	-18
	82	- 7
		- 8
	90	- 1
		- 2
		- 3
		- 4
		- 6
		- 8
8.5	74	-24
	75	-12
		-16
		-22
	84	-11
		-13
	90	- 7
		- 8
11.5	69	-20
	74	-14
		-17
		-20
12	70	-24
	72	-20
	75	-21
	80	-10
	90	-11
		-11
		-15
16	75	-26
	80	-22
21	70	-17
	72	-15
	75	-10
	79	- 5

3, 6, 9, and 12 m/sec.[20] As the relationships between 1-D elevation psd and 1-D slope psd, and between 1-D and 2-D psd's for isotropic surfaces are known, the optical data may be used to estimate acoustic reverberation strength and to interpret the elevation psd derived from acoustic reverberation data. Figure 1 shows the fundamental optical data[19] used in this paper and, as stated, it is possible to transform these frequency-biased 1-D slope spectra of $fS(f) \equiv f[E_{\zeta'}(f)]_1$ into the 1-D elevation spectra $[E_\zeta(k_s)]_1$. It is suggested by the author of the optical data that the spectral peak near a frequency of 1.7 cps is related to system noise due primarily to electrical supply 60-cps "pick-up," and that the rise at the highest frequencies is probably not real. As a consequence, these questionable data are smoothed or ignored in the analysis.

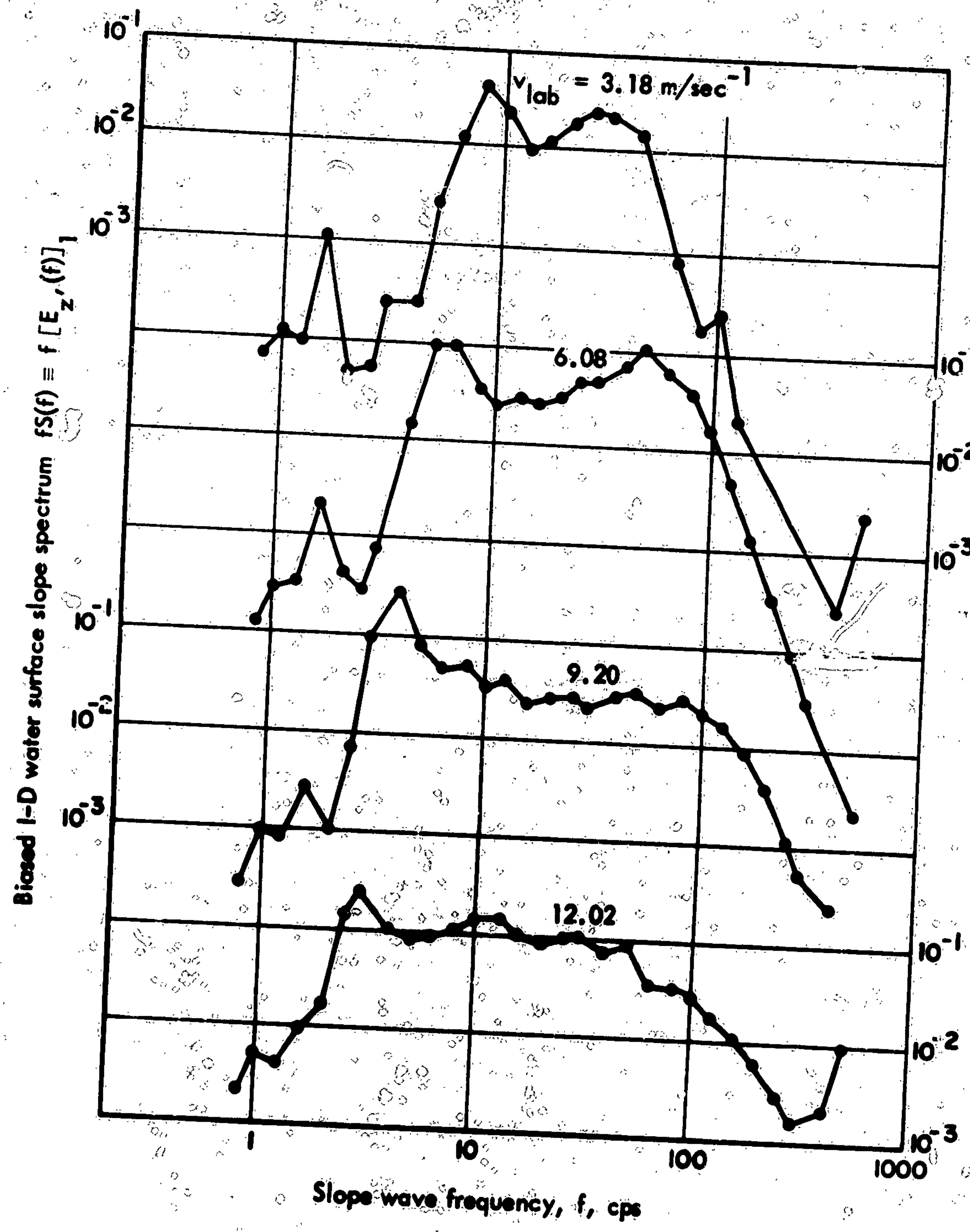

FIGURE 1 Slope Spectrum Times Frequency, fS(f), of Up- and Down-Wind Slopes as a Function of Frequency, f, for Four Wind Speeds v_{lab}, as Shown

IV. ANALYSIS

Traditionally, it has been popular to describe acoustic reverberation of the sea surface as some logarithmic and perhaps trigonometric function of acoustic frequency, grazing angle, and sea-surface rms height or wind speed.[2,13,21,22] It will be informative in contradistinction, therefore, to develop from Fig. 1 and Eqs. 7 and 9 an isotropic elevation psd from which, with Eq. 15, some idea may be obtained of the possible trends and magnitudes of backscattering strength N_s with variations of acoustic frequency and wind speed. The point of departure from optical data rather than acoustic data bears explaining. Because of the scale of sea-going acoustic experiments, an averaging over reasonably large and, perhaps, inhomogeneously and anistropically rough surfaces is inherent and this introduces an undesirable smoothing effect; it is not uncommon to obtain acoustic data from explosive shots averaged over an octave of acoustic frequency which introduces further smoothing; inconstancy of sea-surface wind speeds (gustiness) and difficulties in wind speed measurement introduce additional smoothing; averaging over variations of near surface temperatures tends to smooth over grazing angles due to refraction; lastly, unclean (slick) surfaces may inhibit the formation of sea-surface roughness and scattering strengths may be irregular and low. Thus, a "controlled" experiment at sea may be a formidable accomplishment. On the other hand, optical experiments in a laboratory may be reasonably well controlled, need not suffer from any unknown refraction and may average over areas of less than 1 mm^2 (smaller than the inside of the letter "o"). Furthermore, water surfaces in the laboratory may be kept especially clean allowing full roughness to develop.

Before discussing the optically based elevation spectra, it appears that some comment about laboratory air speeds and sea-surface wind speeds is warranted. Reference 19 suggests that the relationship between laboratory air speed v_{lab} over water surface and sea-surface wind speed v_{sea} is as[23]

$$v_{sea} \ln (h/\sigma_z)_{sea} = v_{lab} \ln (h/\sigma_z)_{lab} \quad , \tag{22}$$

where h is the distance above the water mean surface level at which wind speed measurements are made and σ_z is the rms elevation of the water surface. Equation 22 essentially assumes a logarithmic boundary layer profile of air speed above the sea. Thus, given appropriate values of h/σ_z as in Appendix C, a numerical solution transforms v_{lab} to v_{sea} as in Table 5.

Table 5 -- RELATION BETWEEN OPTICAL LABORATORY AIR SPEEDS AND EQUIVALENT SEA-SURFACE WIND SPEEDS

Air Speed Over Water Surface, v_{lab}	Sea-Surface Wind Speed, v_{sea}	
	(m/sec)	(knots)
3.18	2.2	4.3
6.08	4.2	8.1
9.20	7.0	13.5
12.02	9.7	19.0

The results of Table 5 which show $v_{sea} < v_{lab}$ are at odds with Ref. 19 which estimates $v_{sea} \approx 2.2 v_{lab}$; the discrepancy arises from the assumptions on σ_z which here are functionally dependent on v_{lab}, and in Ref. 19 are assumed to be 0.1 cm for both laboratory measurements and open sea measurements.

A. SEA-SURFACE SCATTERING STRENGTH

Now, the 1-D slope psd of Fig. 1 may be modified to 2-D isotropic surface elevation psd according to Eqs. 7 and 9 (see also

Appendices A and C). This transformation is shown graphically in Fig. 2. These optically based data of Fig. 2 have been pieced together without adjustment with comparable data taken mechanically[24] as in Fig. 3. The reasonably good agreement of the two diversely obtained data sets in the vicinity of $k_s = 0.05\ cm^{-1}$ as well as the agreement in trends (Appendix C, Fig. C-4), is taken as giving added credence to the transformations which have been accomplished for the optical data in going from $[fE_z,(f)]_1$ to $[E_z(k_s)]_2$.

An inspection of Fig. 2 yields some interesting points. Grossly, one notes that $[E_z(k_s, v_{lab})]_2$ varies about as k_s^{-4} to k_s^{-3}, which with Eq. 15 suggests that on the average reverberation due to surface diffuse scattering will slightly increase with frequency; a theoretical guideline with slope -11/3 is drawn for later reference to acoustically based surface and sublayer spectra. However, the curves of Fig. 2 do show some systematic variation which suggests that at a given wind speed, scaling laws will depend importantly on the frequencies and frequency bandwidths for which data are taken. The most obvious systematic variation of the psd curves of Fig. 2 is the "hump" between about 1 to 10 cm^{-1} at $v_{lab} \cong 3$ m/sec which broadens as air speed is increased. It is interesting, and probably significant, that at low air speed this hump is centered at about 4 cm^{-1} (Table C-3). The relationship for surface wave phase velocity[25] c_{ph} is

$$c_{ph}^2 = g/k_s + \gamma k_s/\rho_w \quad , \tag{23}$$

where g is acceleration due to gravity and γ and ρ_w are, respectively, the air interface surface tension and density of water. From this, it develops that $(c_{ph})_{min}$ occurs at $k_s \cong 3.7\ cm^{-1}$. One may suppose that for $v < (c_{ph})_{min}$ wind energy may not couple to the water surface because the wind speed is less than the minimum phase velocity of waves, and that as free-stream wind speed increases, so does the speed of air at the air-sea interface, there being an eventual and increasing effect as wind speeds increase. This interpretation is strengthened by experimental data[26] on the turbulence spectra of wind

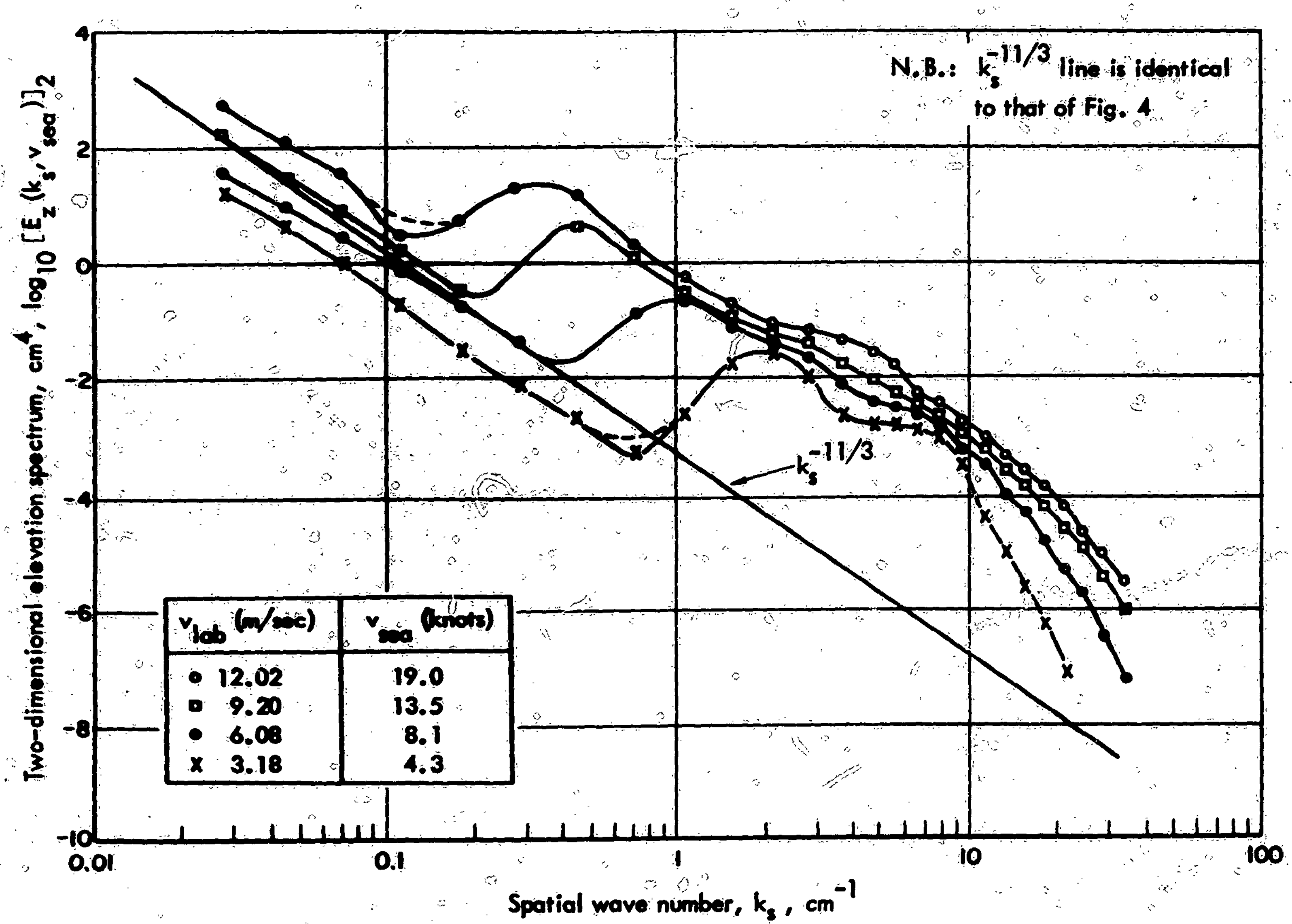

FIGURE 2 Two Dimensional Water Surface Elevation Spectrum, Optically Based vs. Wave Number and Air Speed

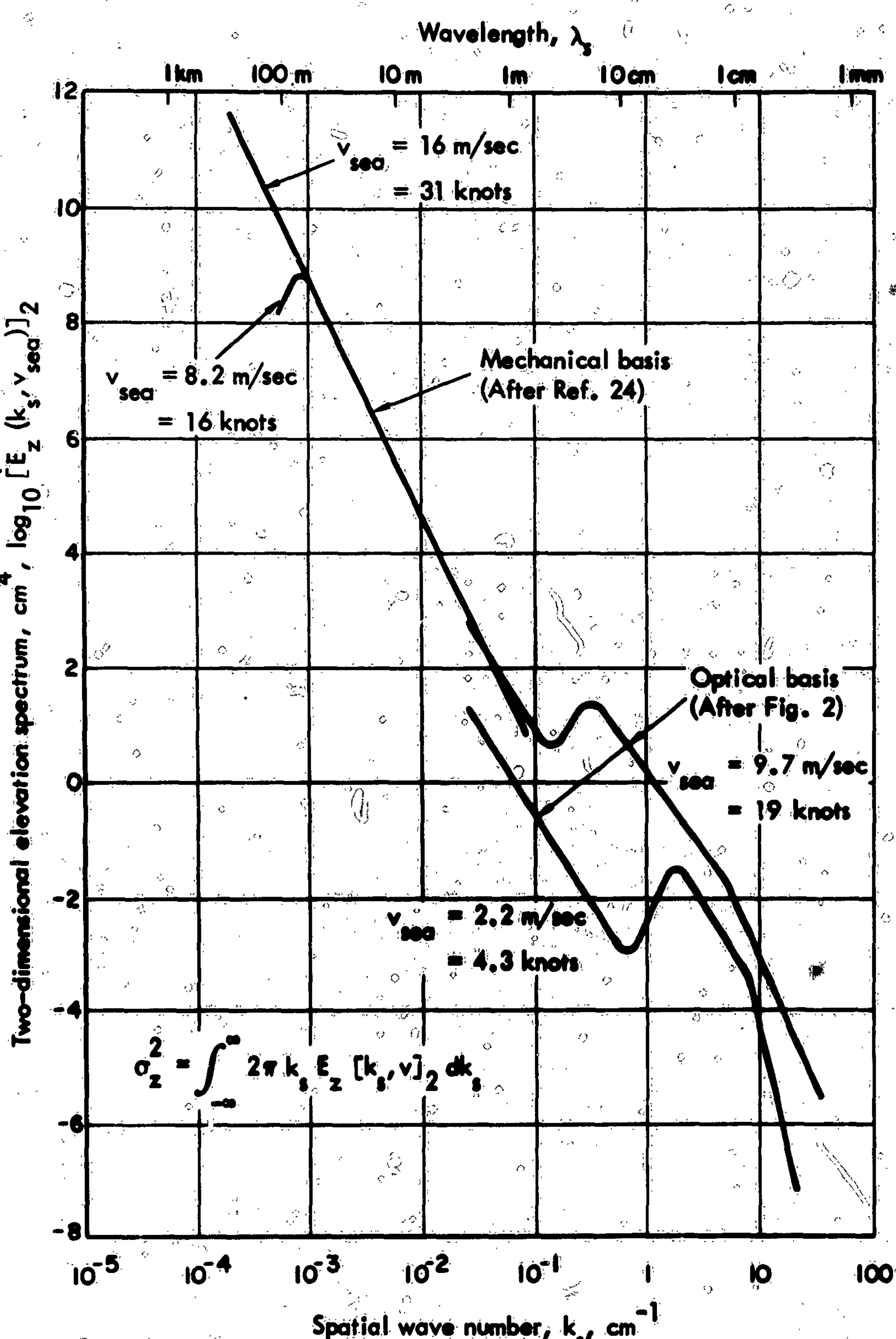

FIGURE 3 Two-Dimensional Sea-Surface Elevation Spectrum vs. Wave Number and Air Speed

over waves which show dissipation of wind energy at a maximum at $k_s \cong 2\ cm^{-1}$ suggesting that the sea is extracting energy from the atmosphere in the wave number vicinity of the hump of Fig. 2.

To continue, Fig. 2 shows that with increasing wind speed the isotropic surface elevation psd fills out to both smaller and larger wave numbers, maintaining more or less the same variation with k_s, both before the sudden increase in the 0.2 to 2 cm^{-1} region of k_s, and after. Thus, it appears that at a given wind speed, scattering strength for a clean water surface may increase relatively gently up to a critical frequency at which, with increasing frequency, scattering strength undergoes a sudden increase and then increases gently again to very high frequencies (of the order of $f_r = c/\lambda_r = k_r c/2\pi = k_s c/2\pi \cong 0.25$ Mcps). From the point of view of psd variation with air speed, Figs. 2 and 3 have interesting implications: With increasing wind speed the surface of wind-driven water becomes more "ordered" both at small and large wave numbers, i.e., at wavelengths characterized by dekameters, or greater, and by centimeters. Further, the local minima of $[E_I(k_s, v_{1.s})]_s$ in the range $0.1 < k_s < 1\ cm^{-1}$ suggests that at a given air speed, large wavelengths and small wavelengths are energetically isolated[27] and that wind and sea are in equilibrium at very small wave numbers, $k_s < 0.1$ to $1.0\ cm^{-1}$; at large wave numbers ($k_s > 0.1$ to $1.0\ cm^{-1}$), it appears that energy input to the surface flows to large wave numbers and is there dissipated. It is possible that pressure forces dominate at small wave numbers, and viscous forces at large wave numbers.

The reasonable agreement of optically and mechanically based data for $[E_I(k_s, v_{s.s})]_s$ as shown in Fig. 3 gives some credence to the foregoing interpretations, as does the allusion to atmospheric turbulence dissipation. In addition, one may use acoustic data with Eq. 15 to derive $[E_I(k_s, v_{s.s})]_s$ under the assumption that the sea surface is isotropically rough, at least at large wave numbers, and that if φ is near its midrange, reverberation is due to surface scattering to the exclusion of volume or reflection effects. Under

such an assumption, the data of Table 2 have been converted to isotropic surface elevation psd and these are shown in Fig. 4 for v_{sea} = 5, 10, and 15 knots and φ = 50 deg; it is deemed φ = 50 deg in both large enough grazing angle that subsurface effects are negligible and small enough that reflection effects are not important either. For 5 knots $\leq v_{sea} \leq$ 15 knots, $[E_Z(k_s, v_{sea})]_2$ based on the data of Table 2 has a least square fit (lsf) given by

$$[E_Z(k_s, v_{sea})]_2 = 8.36(10)^{-6} v_{sea}^{2.359} k_s^{-3.672} \quad (\mathrm{cm}^4) \qquad (24)$$

with v_{sea} in knots, and k_s in cm^{-1}. The rms error introduced into N_s by using Eq. 24 is less than 4 db.

In Fig. 4, wind speeds of v_{sea} = 5, 10, and 15 knots are used and, for these, $[E_Z(k_s, v_{sea})]_2$ is plotted as a function of wave number k_s. As a guide and reference, a line of slope $k_s^{-11/3}$ is drawn as in Fig. 2. In the acoustic reverberation measurements, there is a suggestion of the "hump" of Fig. 2 for $0.1 < k_s < 1.0$ cm^{-1}. There is indication also of increasing spectral densities for $v_{sea} \geq$ 5 knots but for $v_{sea} <$ 5 knots, spectral densities (not shown) are only marginally less as will become apparent in Fig. 6. The suggestion in Fig. 6--as would appear of course from the reverberation data directly--is that for $v_{sea} <$ 5 knots elevation psd is substantially constant and, perhaps, roughness is convected into the measurement area from contiguous disturbed areas; above 5 knots the coupling between wind and sea becomes important and spectral densities increase. As $(c_{ph})_{min} \cong 0.5$ knots, the difference between 5 knots and $(c_{ph})_{min}$ gives a measure of sea-surface shear required to generate appreciable local roughness.

That extraneous, perhaps subsurface, effects are in fact appreciable at sufficiently small grazing angles is demonstrated by Fig. 5, where elevation psd is shown at, for example, a sea-surface wind speed, v_{sea} = 15 knots and φ = 10, 30, 50 deg. One sees that as the grazing angle $\varphi \to 0$, the apparent elevation psd (hence, reverberation strength) increases markedly, and that the major portion of this

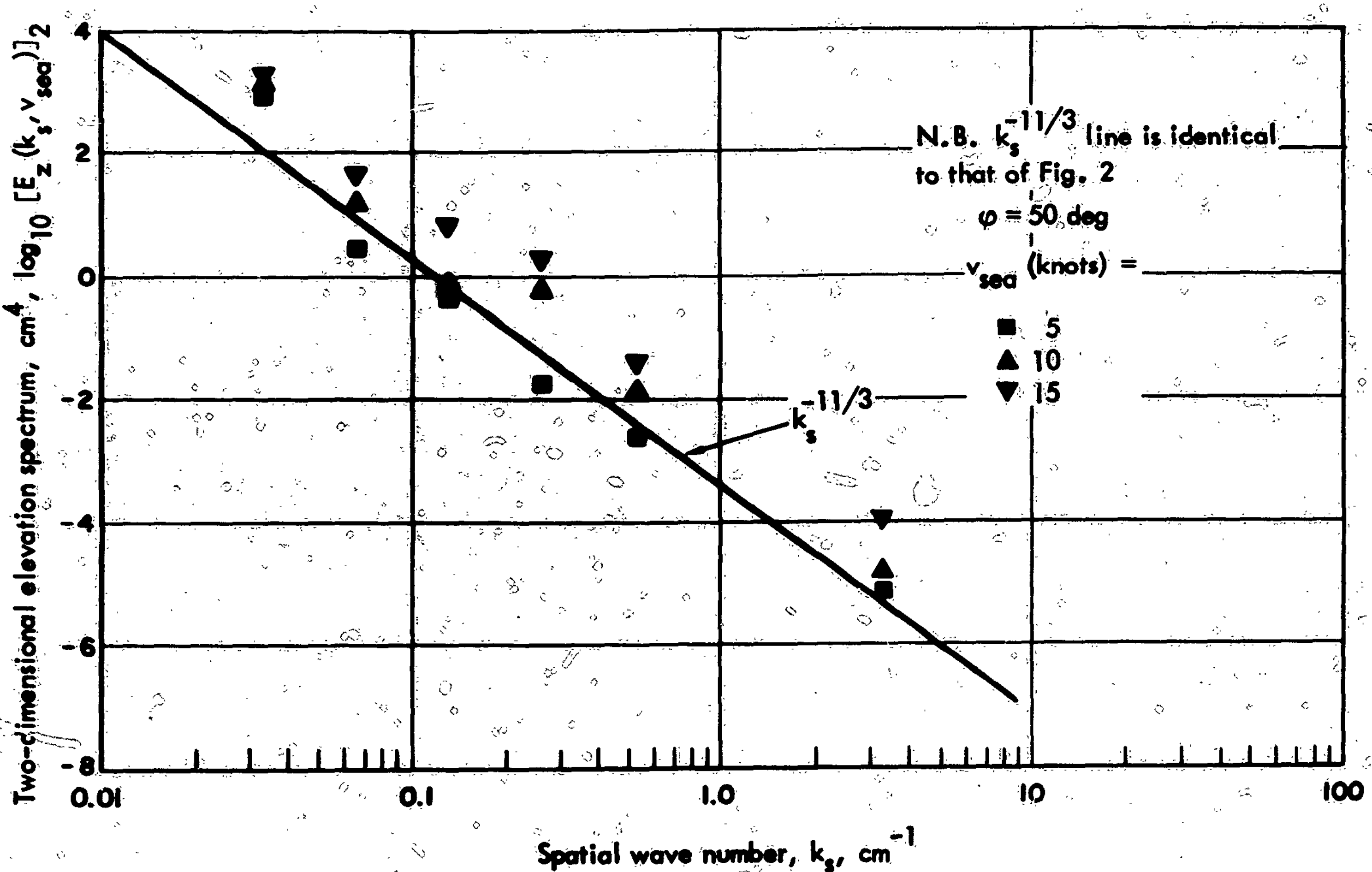

FIGURE 4 Two-Dimensional Sea-Surface Elevation Spectrum, Acoustically Based vs. Wave Number and Wind Speed

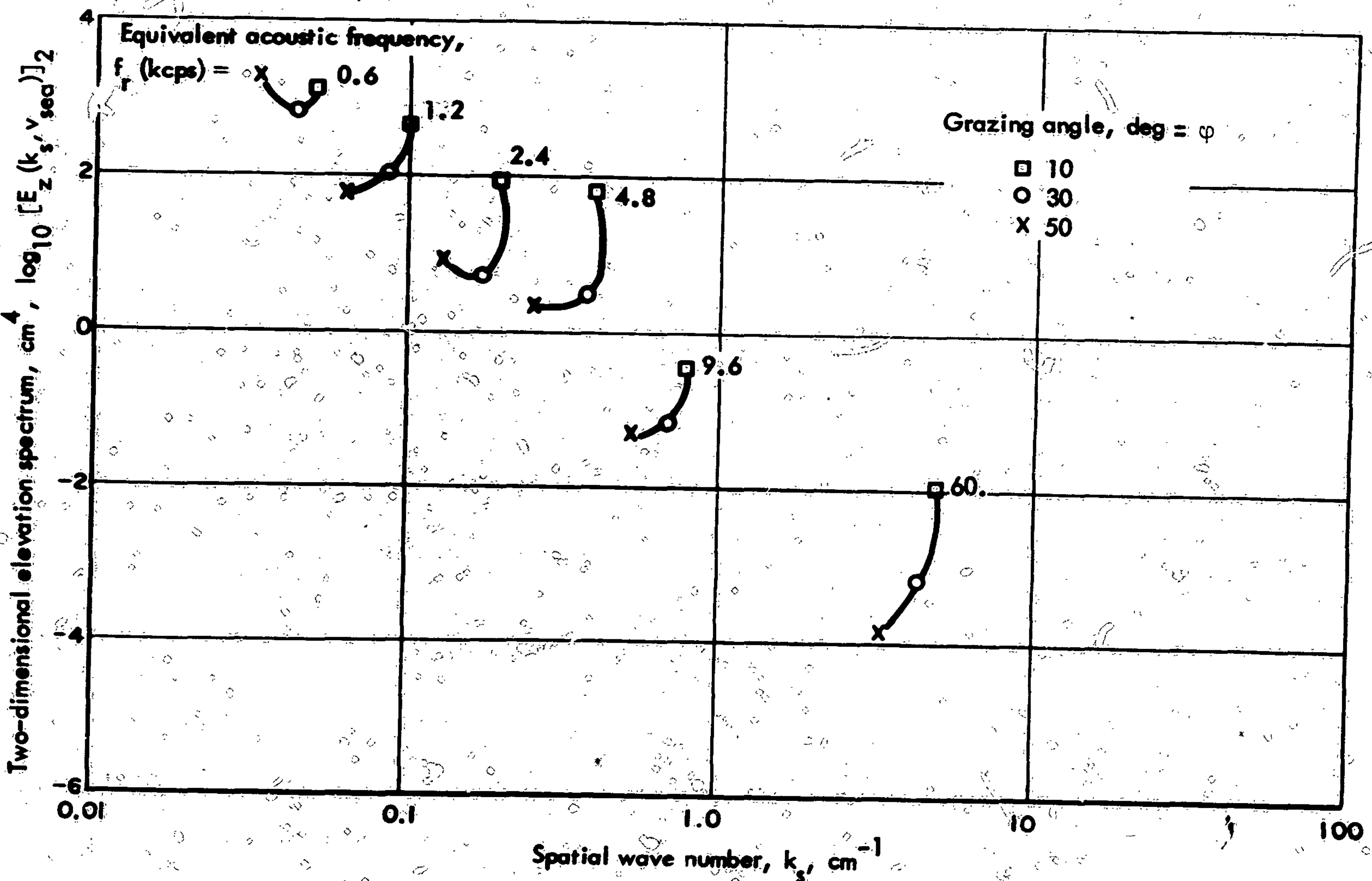

FIGURE 5 Two-Dimensional Sea-Surface Elevation Spectrum, Acoustically Based vs. ing Angle

R10-7-66-R

change occurs between 30 and 10 deg and remains reasonably constant between 50 and 30 deg. The magnitude of increases of elevation psd with grazing angle bears some probing. At small wave numbers corresponding to low acoustic frequencies (Fig. 5), subsurface effects are characterized by a change of a few tenths in the logarithm of $[E_z(k_s, v_{s.a})]_a$, i.e., surface and sublayer effects are nearly comparable. Furthermore, it appears also that at small wave numbers, the effect of the grazing angle is felt only as $\varphi \rightarrow 10$ deg and smaller. However, at large wave number (acoustic high frequency) sublayer effects are characterized by changes in the logarithm of $[E_z(k_s)]_a$ of unity or more, i.e., sublayer scattering is an order of magnitude or more larger than surface scattering.

As a pecularity of the amount of data available at acoustic frequency f_r = 60 kcps, it is possible to augment Figs. 4 and 5 by elevation psd calculations at 10 and 50 deg as a function of several wind speeds. This is shown in Fig. 6, in which the apparent $[E_z(k_s, v)]_a$ is plotted. Figure 6 shows that elevation psd may tend to be substantially constant at sea for sea-surface wind speeds less than about 5 knots ($\approx$ 2.5 m/sec), and that apparent elevation psd increases with wind speed from about 5 knots (2.5 m/sec) to about 15 knots (7.7 m/sec), above which it remains substantially constant as if an exponential integral fit were appropriate. If, in fact, at grazing angle φ = 10 deg, the elevation psd is only apparent, being really a subsurface effect, then the nearly congruent behavior of the φ = 10 deg and φ = 50 deg curves of Fig. 6 suggests that the subsurface effect is closely tied to surface effect, or that the sublayer contributes appreciably even at the 50-deg grazing angle. This latter possibility is considered subsequently. One such connection is, of course, surface elevation and subsurface turbulent motions which may affect the sea-surface elevation and concurrently cause convection, for example, of temperature or density fluctuations below the surface. The implications of Fig. 6 in terms of scattering strength of the sea surface are immediately apparent from Eq. 15; thus at 60 kcps surface

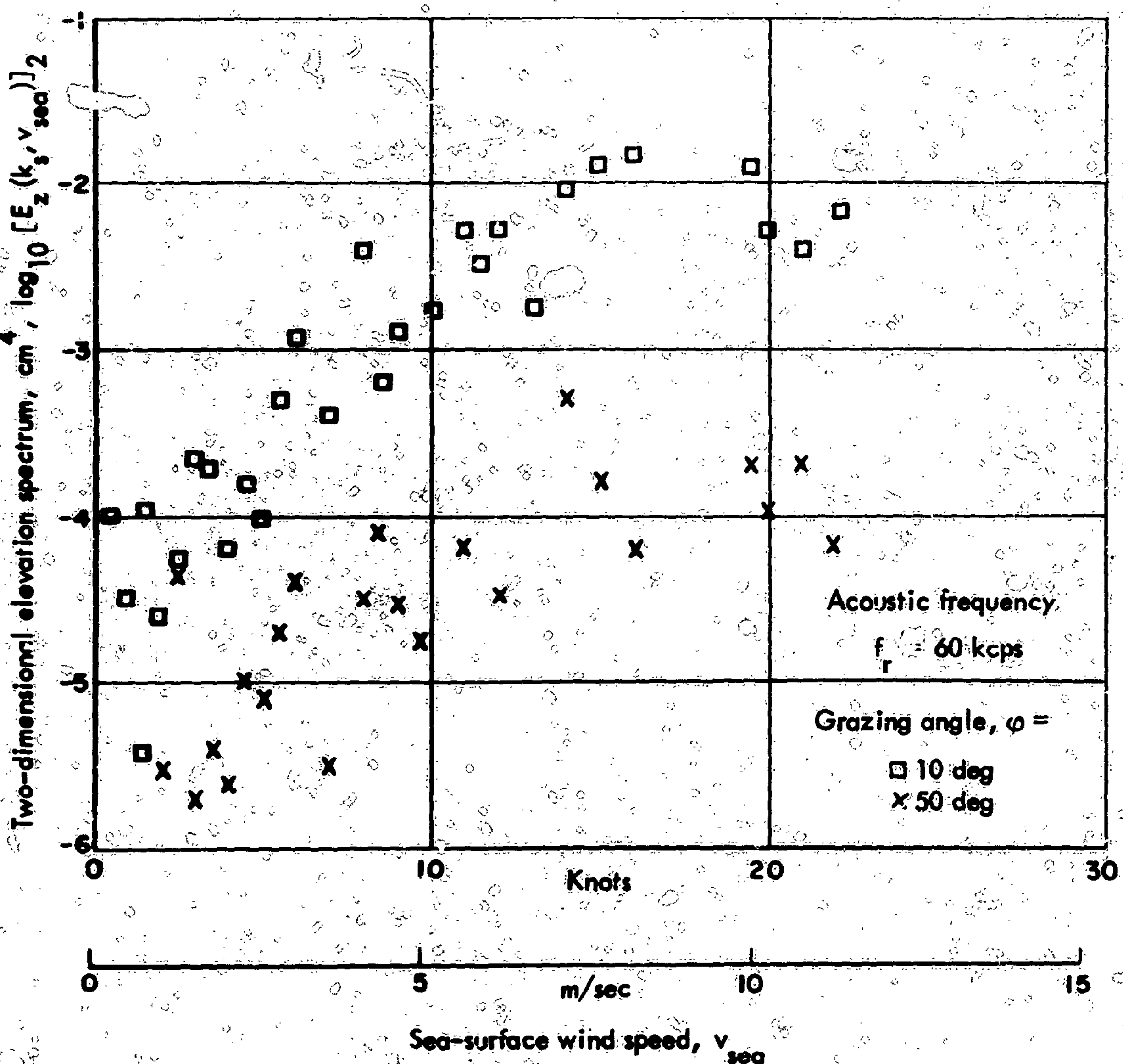

FIGURE 6 Two-Dimensional Sea-Surface Elevation Spectrum at 60 kcps Acoustic Frequency vs. Wave Number and Grazing Angle (typical)

R10-7-68-6

scattering strength is substantially constant for $v_{sea} < 5$ knots and $v_{sea} > 15$ knots and increases about as $v_{sea}^{2.4}$ between these wind speed extremes. Judging from Figs. 2 and 4, it appears unlikely that these wind speed limits and scaling law can describe the situation at low frequencies, though some related behavior may be anticipated.

Having connected optical laboratory air speeds to wind speeds over the sea as in Table 5 and having transformed 1-D slope psd to 2-D isotropic elevation psd and, finally, having available the relationship between surface scattering strength and elevation psd, one may calculate surface acoustic scattering strengths from optical slope data and compare these with directly measured acoustic data; this, of course, is just an inverse exercise to what has gone before. In Fig. 7, acoustic data have been calculated at grazing angle φ = 50 deg and are attributed to the sea-surface wind speeds of Table 5, i.e., v_{sea} = 4.3, 8.1, 13.5, and 19 knots. It is suggested that not all of the irregularities in the optically based curves of Fig. 7 are real, but they are maintained to indicate that spectra are one possible source of uncertainty in scattering strengths. If the laboratory air speeds (transformed to v_{sea}) are taken to be nominally 5, 10, 15, and 20 knots, then the optically based acoustic scattering strengths, relative to the acoustic measurements have an rms difference of 8 db. This implies that, with suitable care, acoustical reverberation data for various sea-surface wind speeds may be deduced from experimental measurements by optical means of water surface slopes.

As much of the 8-db rms error between the acoustic and optical data of Fig. 7 is contributed at f_r = 60 kcps, some consideration of this is warranted. One may argue that the acoustic data taken at sea are lower than they might be under some other water surface circumstances. The argument goes as follows: The relationship between elevation and slope spectra which is given by Eq. 9 shows that the behavior of the elevation psd at large wave numbers has an important influence upon the slope variance through the k_3^2 dependence of the slope

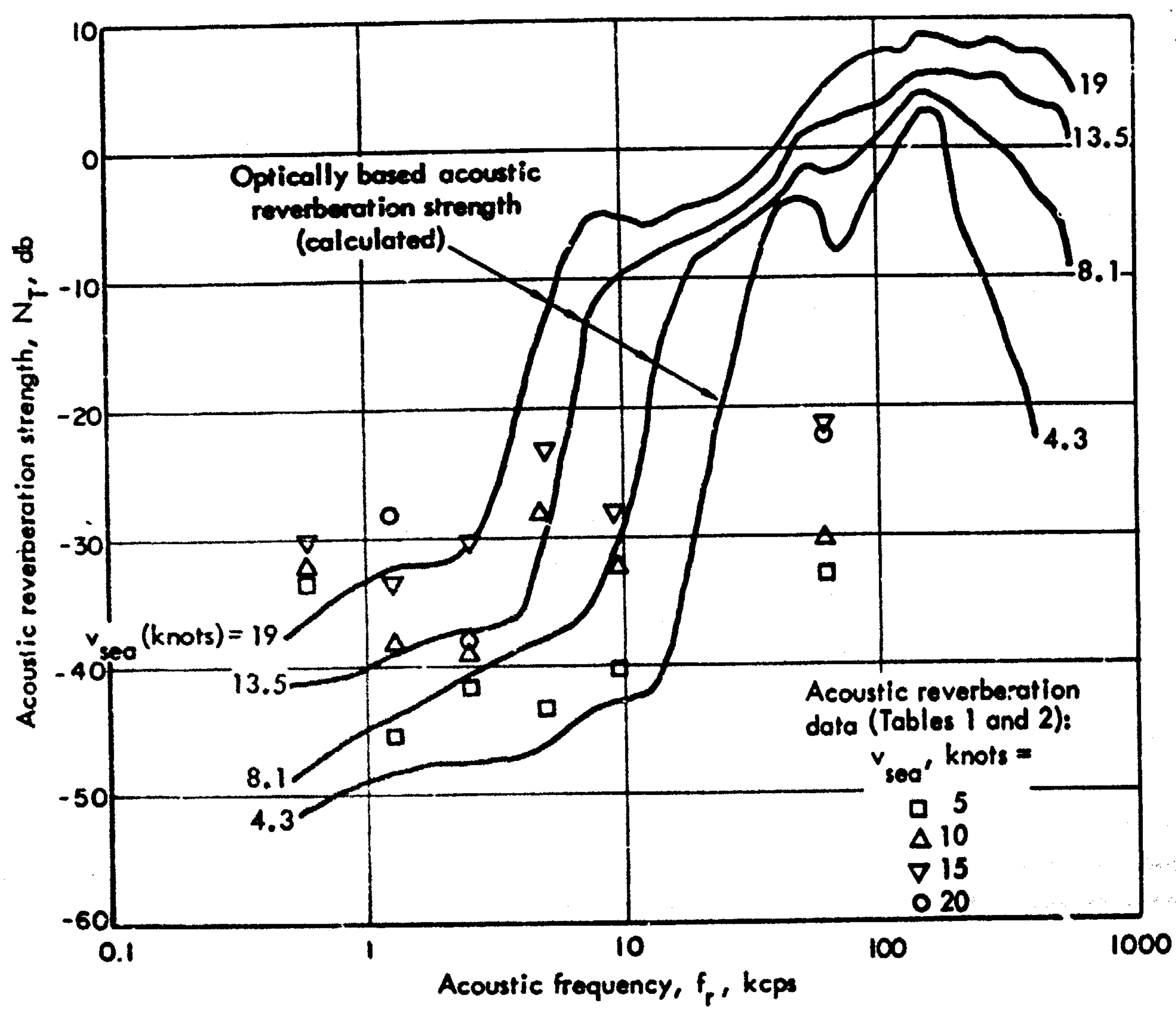

FIGURE 7 Acoustic Reverberation Strength, Optical and Acoustic Basis vs. Acoustic Frequency and Wind Speed

psd. Thus, if the elevation spectrum is deficient at large wave numbers, then slope variance may be disproportionally affected. Measurements at sea have shown that slope variance is markedly decreased when slicks appear on the sea surface,[7] i.e., the slick tends to inhibit the formation of short (capillary) wavelengths corresponding to large wave numbers. With regard to the optically based curves of Fig. 7, special effort was made to remove any fouling matter on the water surface on a continuous basis and, therefore, one may reason that the laboratory water surface was "clean." On the other hand, the acoustic measurements at f_r = 60 kcps were made in Dabob Bay of Puget Sound and near Key West, Florida. Both of these, either directly or by diffusion or convection, may have been affected by the oily jetsam of maritime traffic to a degree which is not attained at great distances from traffic lanes. Apparently, the inhibiting effect of slick--if it be this--is not operable at low frequencies (in the vicinity of 1 kcps), and it is difficult to estimate from the acoustic data where in frequency space the slick becomes important. This is so because, in the vicinity of 10 kcps, the rise of scattering strength with sea-surface wind speed may be so precipitous that a small error in wind speed can cause apparent discrepancies comparable to the slick effect.

B. SEA SUBLAYER SCATTERING STRENGTH

Notwithstanding the uncertainties of elevation psd, referred to in connection with the discussion above, one is led to the possibility of estimating an elevation psd which is relatively unaffected by volume and reflection effects, e.g., at 50 deg. Then, this elevation psd may be used as a basis for separating, at sufficiently small grazing angles, the contribution to total reverberation strength from both surface scattering and surface sublayer scattering.

Assume that sufficiently far from $\varphi = \pi/2$, where reflection strength N_R is negligible, one may write

$$10^{N_T/10} = 10^{N_S/10} + 10^{N_V/10} . \qquad (25)$$

In this equation N_T is to be considered as acoustic experimental reverberation strength, and N_s is to be determined from Eq. 15, using an isotropic surface elevation psd evaluated, for now, from acoustic experimental data at $\varphi = 50$ deg where, as stated, it is assumed N_v is negligible compared to N_s. Hence, using Eqs. 15, 24, and 25, it appears that a biased approximation to the turbulent spectrum of the scattering field of the sea-surface sublayer is given by

$$\left[\frac{z_0(kr)[E_x(2k_r)]_3}{x^2}\right] = \left(\frac{1}{2\pi k_r^4 \sin\varphi}\left\{10^{N_T(\varphi)/10} - 4k_r^4 \sin^4\varphi[E_7(2k_r\cos\varphi)]_2\right\}\right) \tag{26}$$

for v_{sea} = constant.

Given Eq. 26, the acoustic reverberation data of Table 2, at grazing angles $\varphi = 10$ deg and 30 deg, may be used to estimate the variation of the biased isotropic volume approximation to the spectrum of fluctuations beneath the surface of the sea which cause scattering. The results of such a calculation are shown in Fig. 8. The data points of Fig. 8 were calculated by estimating the term

$$4k_r^4 \sin^4\varphi[E_7(2k_r\cos\varphi)]_2 = 10^{N_s(\varphi)/10} \quad , \tag{27}$$

as follows. The data of Fig. 4 show $[E_7(2k_r\cos\varphi)]_2$ varies grossly as $(2k_r\cos\varphi)^{-4}$; thus

$$\begin{aligned} N_s(\varphi_2) = N_s(\varphi_1) &+ 10\log(\sin\varphi_2/\sin\varphi_1)^4 \\ &+ 10\log(2k_r\cos\varphi_2/2k_r\cos\varphi_1)^{-4} \quad . \end{aligned} \tag{28}$$

Hence, given the scattering strength $N_s(\varphi_1)$ at grazing angle φ_1 the scattering strength $N_s(\varphi_2)$ at φ_2 is given approximately by[28]

$$N_s(\varphi_2) = N_s(\varphi_1) + 40\log(\tan\varphi_2/\tan\varphi_1) \quad . \tag{29}$$

Thus, the data of Fig. 8 were found by adjusting data N_s(50 deg) to N_s(10 deg) and N_s(30 deg) according to this relationship.

Because of the accuracy lost in the subtraction of Eq. 26, probably only the general features of Fig. 8 are pertinent. For each of the three sea-surface wind speeds the same reference line with $k_s^{-11/3}$ variation is shown to facilitate comparison. The exponent -11/3 is chosen from turbulence theory as being pertinent for fully developed turbulence in the "equilibrium range" of wave numbers.[8] Sometimes the fluctuations of an isotropic turbulent volume are described by a $k_s^{-5/3}$ law: if $\sigma^2 = \int \Phi(k_s)\,dk_s = \int 4\pi k_s^2[E(k_s)]\,dk_s$, then, of course, if $E(k_s) \sim k_s^{-11/3}$, then for the equality to exist, $\Phi(k_s) \sim k_s^{-5/3}$. There is apparently a systematic increase in biased psd levels with increasing wind speed and with decreasing wave number. At the smallest wave numbers there is an indication of a leveling off of biased psd levels at about 1 to 10 cm^4, the implication being that the sublayer reverberation is relatively less important at acoustic low frequencies (less than about 1 kcps) than at the higher frequencies. In what follows, it will be convenient to have an lsf to the data of Fig. 8 in terms of wind speed and wave number, and this is

$$\frac{z_0(k_s)[E_x(k_s)]_b}{x^2} = 1.25(10)^{-6}\, v_{sea}^{2.91}\, k_s^{-3.143},\ 0.05 \le k_s \le 5\ cm^{-1} \quad . \tag{30}$$

The approximation of Eq. 30 causes about a 5-db rms error in estimates of N_v; the leveling off of sublayer spectra at small wave numbers may tend to overestimate N_v by much more than this. The $k_s^{-3.143}$ dependence of the sublayer turbulence biased psd tends to confirm the assumption of scattering by a turbulent sublayer when compared with the theoretical $k_s^{-11/3}$ dependence for isotropic, homogeneous turbulence; in fact, the dependence of the biased psd upon k_s for v_{sea} = 10 and 15 knots and for $k_s \ge 0.4\ cm^{-1}$ is as $k_s^{-3.667}$, indicating perhaps that low wind speeds and small wave numbers are not or cannot be fully turbulent in the equilibrium range of wave numbers.

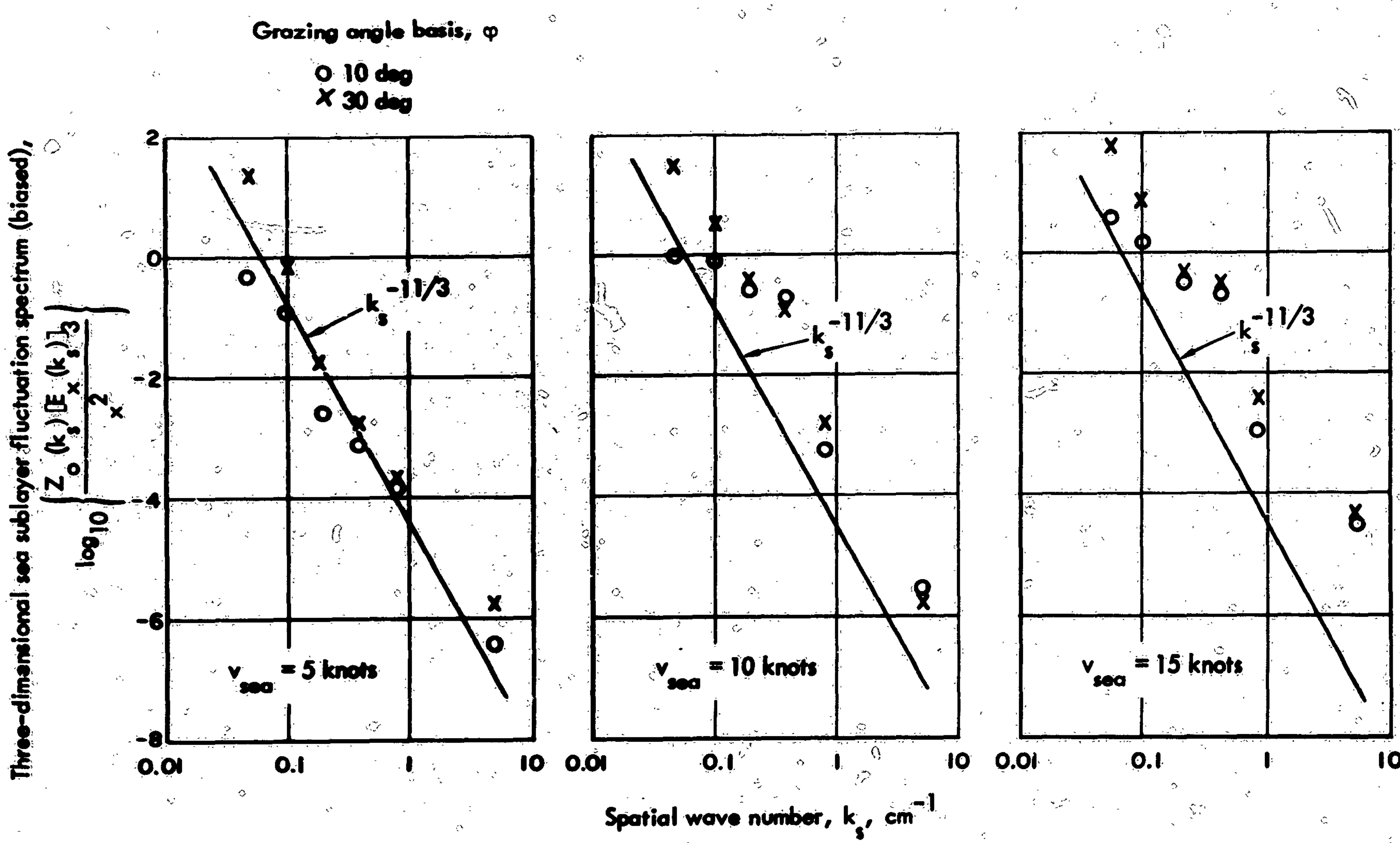

FIGURE 8 Turbulent Sublayer Biased Power Spectral Density vs. Wave Number and Wind Speed

C. SEA-SURFACE REFLECTION STRENGTH

There remains now consideration of reverberation strength estimates for φ near $\pi/2$, i.e., at large grazing angles at which specular reflections from the surface occur in distinction to diffuse scattering at the smaller grazing angles. Now in Eq. 20, which is a model for estimating reflection strength of a rough surface, the term

$$\frac{1}{\pi^2}\left(\frac{\sigma_{z''}}{\sigma_{z'}}\right)^2 \exp\left[-\frac{1}{2}\left(\frac{\cot\varphi}{\sigma_{z'}}\right)\right]^2$$

estimates the number of facets suitably disposed for causing specular reflections and $(A_R)_{eff}$ is the area, averaged over all suitably disposed facets, effective in causing specular reflections. Given the data of Table 4 at f_r = 60 kcps, Eq. 20 may be tested for its propriety by rewriting it as

$$10^{N_R/10} = 10^{N_{R_0}/10} \exp\left[-\frac{1}{2}\left(\frac{\cot\varphi}{\sigma_{z'}}\right)^2\right] , \tag{31}$$

where, of course,

$$N_{R_0} = 10 \log\left[\frac{(A_R)_{eff}}{\pi^2}\left(\frac{\sigma_{z''}}{\sigma_{z'}}\right)^2\right] \tag{32}$$

It is convenient to develop Eq. 31 further to

$$N_R = N_{R_0} + S \cot^2\varphi , \tag{33}$$

in which

$$S = -\frac{5/\ln 10}{\sigma_{z'}^2} . \tag{34}$$

Now the data of Table 4 give N_R as a function of φ and v_{sea}, and it is possible for v_{sea} = constant to make an lsf of N_R as a function of $\cot^2\varphi$ using Eq. 33; this lsf will yield both N_{R_0} and $\sigma_{z'}^2$. The results

of such a calculation are given in Table 6 and shown graphically in Fig. 9. In this figure, the data corresponding to $v_{sea} = 3.5$, 8, 10, and 15 knots are emphasized as those in which one may have greater confidence. This confidence derives from the fact that the data range over much of the range 70 deg $\le \varphi \le$ 90 deg, and further that except for $v_{sea} = 3.5$ knots there are many data points with which to operate.

Included in Fig. 9 are four curves: in the plot of slope variance data the results of optical measurements for clean sea surface[7]

$$
\begin{aligned}
\langle \sigma_{z'}^2 \rangle &= \frac{1}{2}(0.003 + 0.00512\, v_{sea}), \qquad v(\mathrm{m/sec}) \\
&= \frac{1}{2}(0.003 + 0.00264\, v_{sea}), \qquad v(\mathrm{knots})
\end{aligned}
\tag{35}
$$

and for slick sea surface[7]

$$
\begin{aligned}
\langle \sigma_{z'}^2 \rangle &= \frac{1}{2}(0.008 + 0.00156\, v_{sea}), \qquad v(\mathrm{m/sec}) \\
&= \frac{1}{2}(0.008 + 0.00082\, v_{sea}), \qquad v(\mathrm{knots})
\end{aligned}
\tag{36}
$$

In the plot of N_{R_0}, for comparison with Fig. 10, an lsf of N_{R_0} to log v_{sea} for the "confident" data is shown and this relation for 60 kcps acoustic frequency is

$$
N_{R_0} = -0.823 - 10 \log v_{sea}^{0.738} , \tag{37}
$$

i.e., N_{R_0} decreases about as the 3/4 power of sea-surface wind speed. Also shown is the parameter $(\sigma_{z''}^2/\sigma_{z'}\sigma_{z'''})^2/\pi = N_{R_0}$, as in Eq. 21b, to be discussed subsequently.

The suggestion of slope variance data of Fig. 9 is that the water surface for acoustic experiments in Dabob Bay and off Key West was clean in the same sense as was the surface for optical experiments off Monterey, California, although one may still need to distinguish "cleanliness" at sea with that of the laboratory. Further,

Table 6 -- SEA-SURFACE SLOPE VARIANCE AND NORMAL INCIDENCE REVERBERATION STRENGTH FROM ACOUSTIC DATA

Wind Speed, knots	Sea-Surface Slope Variance	Sea-Surface rms Slope	N_{R_0} lsf to Table 4 with Eq. 33	N_{R_0} lsf to Table 4 with Eq. 35
2	1.18 $(10)^{-2}$	0.108	- 16	3
3	67.5	8.21	- 30	- 27
3.5*	1.56	0.125	- 6	- 2
4	3.39	0.184	- 22	- 14
4.5	1.20	0.109	- 4	+ 2
5	1.51	0.123	- 9	- 2
5.5	1.02	0.101	0	0
6.5*	-	-	-	- 2
8*	1.12	0.106	- 4	- 4
8.5*	-	-	-	- 6
10*	1.60	0.127	- 9	- 9
11.5	4.71	0.217	- 13	- 7
12	-	-	-	- 9
15*	2.39	0.155	- 12	- 12
16	2.20	0.149	- 19	- 22
21	1.67	0.129	0	- 7

*Data of greater significance due to range or numerical value of grazing angle.

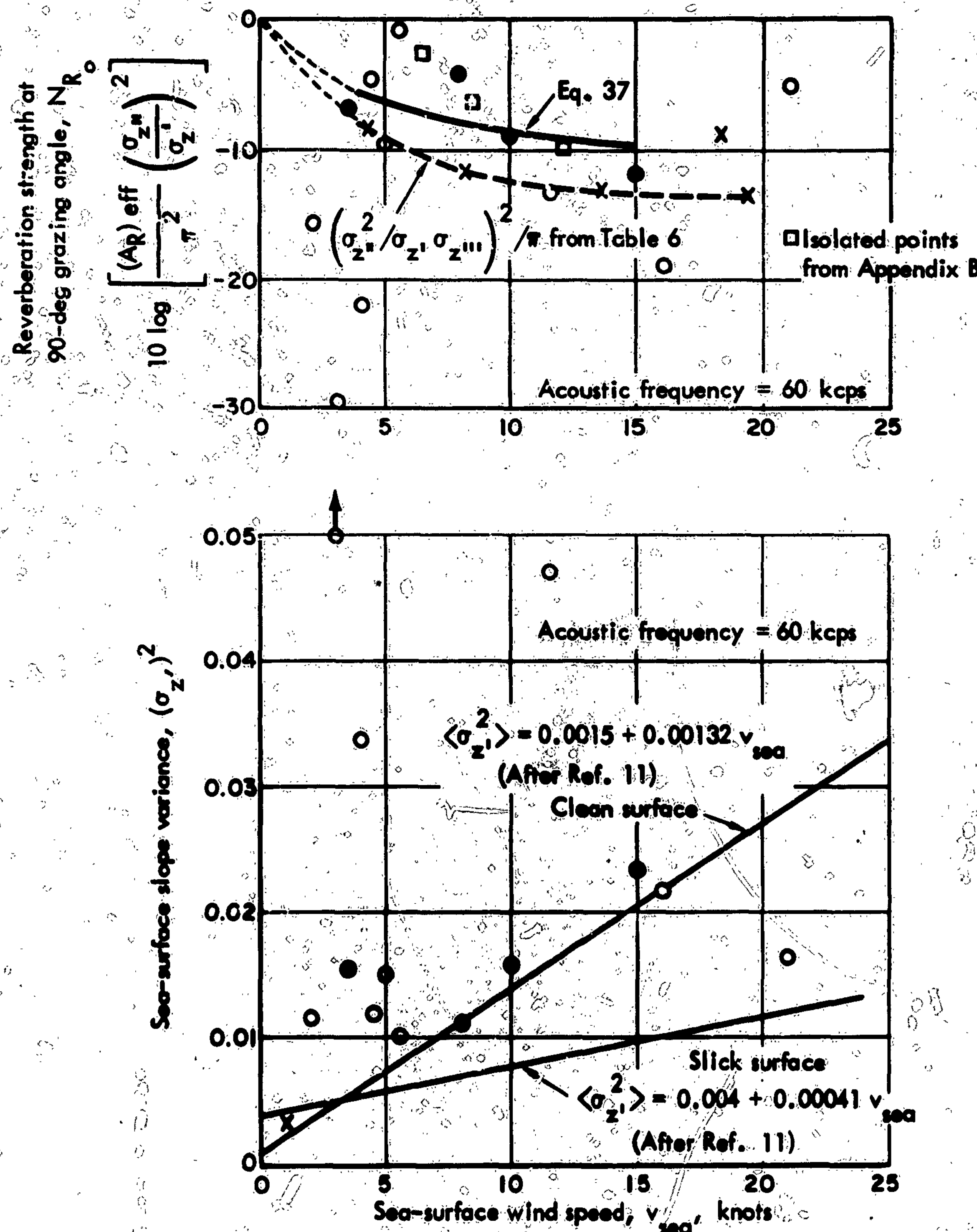

FIGURE 9 Normal Incidence Reverberation Strength and Sea-Surface Slope Variance, Acoustically Based vs. Wind Speed

R10-7-66-9

for those acoustic measurements in which the range 70 deg $\leq \varphi \leq$ 90 deg was sufficiently covered, the agreement between $\langle \sigma_{z'}^2 \rangle_{acoustic}$ and $\langle \sigma_{z'}^2 \rangle_{optical}$ is good enough that some confidence in the model of Eq. 20 is warranted.

Relative to the values of N_{R_0}, the decrease of N_{R_0} with sea-surface wind speed has been suggested previously[2] by analogy with the term $(\sigma_{z''}^2 / \sigma_{z'} \sigma_{z'''})^2$ for the sea surface with the same term for air flow, which later decreases to an apparent limiting value with increasing wind speed. Further, from Fig. 9 apparently

$$\left[\frac{(A_R)_{eff}}{\pi^2} \left(\frac{\sigma_{z''}}{\sigma_{z'}}\right)^2\right] = O\,(0.1) \quad , \tag{38}$$

so that

$$\left[(A_R)_{eff}\right] = O\left[\left(\frac{\sigma_{z'}}{\sigma_{z''}}\right)^2\right] \quad . \tag{39}$$

Depending upon the form of correlation function $B_{z'}(r)$ for surface slope, $(\sigma_{z'} / \sigma_{z''})^2$ is more or less equal to $r_{z'}^2$, the square of correlation length for surface slope. Thus,

$$\left[(A_R)_{eff}\right] = O\left[(r_{z'}^2)\right] \quad , \tag{40}$$

which has some intuitive appeal.

Now, if slope variance for acoustic experiments may be taken as that of Eq. 35 then the variable S of Eq. 34 may be removed as an unknown and N_{R_0} redetermined. This has been done and the results are shown in Fig. 10 and Table 6. The data in this figure for v_{sea} = 3, 4, and 16 knots appear to be spurious; the remaining data show again a decreasing trend with increasing sea-surface wind speed and suggest that for sea-surface wind speed large enough

$$\lim_{v_{sea} \to \infty} N_{R_0} = (N_{R_0})\ \lim \cong -13\ \text{db} \tag{41}$$

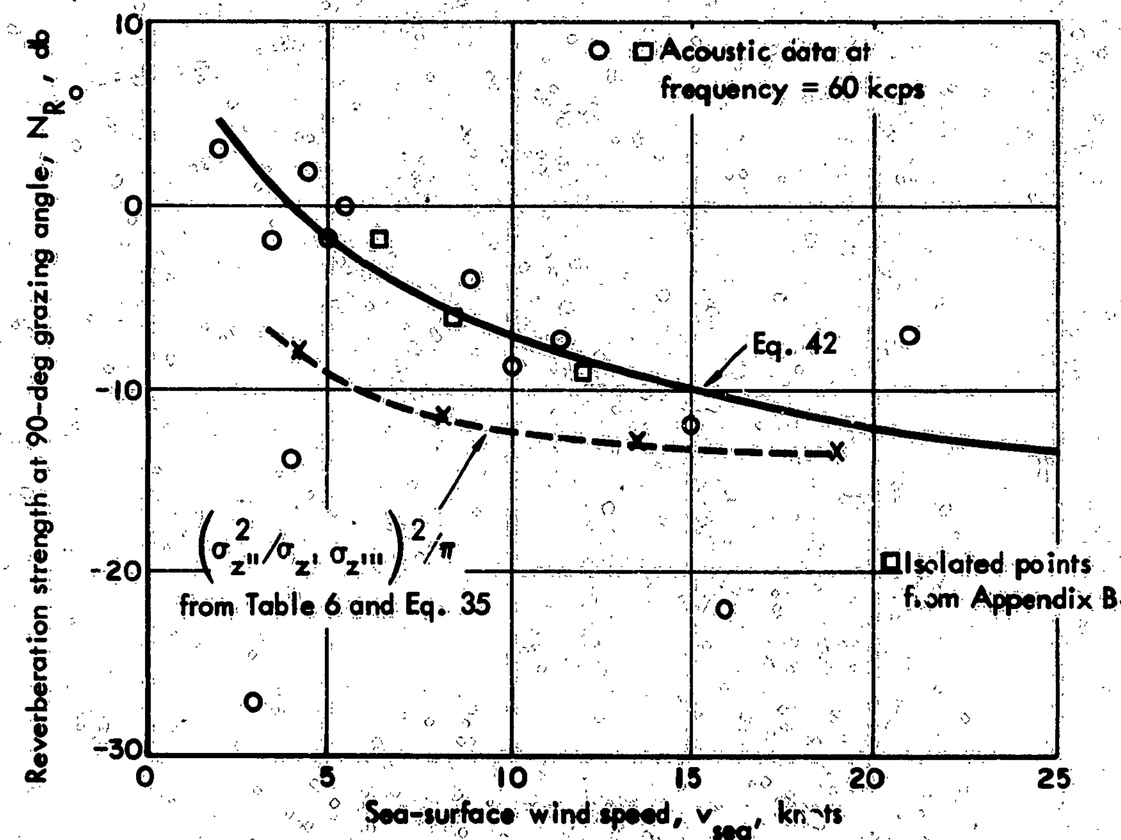

FIGURE 10 Normal Incidence Reverberation Strength, Adjusted

RIO-7-66-10

and that between zero and 4 knots N_{R_0} may be greater than zero-decibels. Finally, it is noted that in Fig. 10 an error in wind-speed estimation of about 1 knot could account for most of the scatter of the "non-spurious" data. An lsf to the data of Fig. 10 is given by

$$N_{R_0} = 10 - 10 \log v_{sea}^{1.68}, \quad 2 \le v_{sea} \le 20 \text{ knots} \quad , \qquad (42)$$

in which N_{R_0} has units of decibels and sea-surface wind speed v_{sea}, knots. The rms error in N_{R_0} associated with Eq. 42 is less than 2 db.

Now that the acoustic data for frequency $f_r = 60$ kcps and φ near $\pi/2$ have been analyzed, it is of interest to determine the variation of K_{s_0} to be expected from direct calculations of $\sigma^2_{z'}$, $\sigma^2_{z''}$, $\sigma^2_{z'''}$ as from the transformation of Fig. 2 with Eqs. 8 to 11. Now

$$\sigma^2_{z'} = \int_0^\infty \left[E_{z'}(k_s)\right]_r \, dk_s \quad , \tag{43}$$

and

$$\sigma^2_{z''} = \int_0^\infty k_s^2 \left[E_{z'}(k_s)\right]_i \, dk_s \quad , \tag{44}$$

and

$$\sigma^2_{z'''} = \int_0^\infty k_s^4 \left[E_{z'}(k_s)\right]_i \, dk_s \quad , \tag{45}$$

and Table 7 give the results of these integrations together with ratios of variances appropriate to Eqs. 21a and 21b. Included in this table are ratios employing σ_z^2 in cm² based on[22]

$$\begin{aligned} \sigma_z^2 &= (0.41\, v_{s.s.}^{5/2})^2 , \quad v_{s.s.}\,(\mathrm{m/sec}) \\ &= 0.0444\, v_{s.s.}^5 , \quad v_{s.s.}\,(\mathrm{knots}) \end{aligned} \tag{46}$$

as appear appropriate from experiment.

In Table 6 the values of $\sigma^2_{z'}$ are about a factor of three larger than that calculated from Eq. 35 and this may be due--as discussed previously--to the difference between the capabilities of clean sea water and laboratory clean water to sustain large elevation spectral density at large wave numbers, i.e., to generate capillary waves. This uncertainty of about three in $\sigma^2_{z'}$ makes the ratio of $\sigma_z/\sigma_{z'} = O(r_z)$ uncertain by a factor of about $\sqrt{3}$. Notwithstanding this, depending upon the distribution of $[E_{z'}(k_s)]_i$, one would expect that ratios of variances would be less affected by this uncertainty and

that the trends indicated are valid. Thus, Table 7 permits the following lsf's of the various parameters with v_{sea} in knots[29]

$$\sigma_{z'} = 0.0062\ v_{sea}^{0.811} \qquad (-) \qquad (47)$$

$$\sigma_{z''} = 0.286\ v_{sea}^{0.956} \qquad (cm^{-1}) \qquad (48)$$

$$\sigma_{z'''} = 1.07\ v_{sea}^{1.522} \qquad (cm^{-2}) \qquad (49)$$

$$\sigma_{z} / \sigma_{z'} = 6.6\ v_{sea}^{1.689} \qquad (cm) \qquad (50)$$

$$\sigma_{z'} / \sigma_{z''} = 0.216\ v_{sea}^{-0.146} \qquad (cm) \qquad (51)$$

$$\sigma_{z''} / \sigma_{z'''} = 0.263\ v_{sea}^{-0.565} \qquad (cm) \qquad (52)$$

where the latter three, Eqs. 50 to 52 are related, respectively, to correlation lengths r_z, $r_{z'}$, and $r_{z''}$. The values of $(\sigma_{z''} / \sigma_{z'} \sigma_{z'''})^2$ of Table 7 are shown in Figs. 9 and 10 in the form

$$10 \log (\sigma_{z''} / \sigma_{z'} \sigma_{z'''})^2 / \pi$$

to correspond to the coefficient of Eq. 21b.

Now for f_r = 60 kcps, $\lambda_r \cong 2.5$ cm and from Table 7 it seems clear that for $v_{sea} \geq 4.3$ knots, $\sigma_{z''} / \sigma_{z'''} \ll \lambda_r$. Thus, Eq. 21b applies to the data of Figs. 9 and 10 and one is led on the basis of $\sigma_{z'}^2$ to the speculation that wind speed measurements for $v_{sea} < 5$ knots for the data of Table 6 may have been subject to some error. The agreement between the lsf to acoustical data of Figs. 9 and 10 and the plot of 10 log $[(\sigma_{z''} / \sigma_{z'} \sigma_{z'''})^2 / \pi]$ to 5 db or better appears to be unexpectedly good, in view of the uncertainty in elevation derivative variances.[30] At acoustic frequencies below 60 kcps, λ_r, of course, becomes larger, so that for 0.6 kcps $\leq f_r \leq$ 60 kcps, $\sigma_{z''} / \sigma_{z'''} \ll \lambda_r$ and only Eq. 21b need be of interest. In fact, it appears that until $f_r \cong 1$ Mcps, Eq. 21b is suitable. Thus, one may approximate N_{R_0} using Eq. 42, and use $N_{R_0} = (N_{R_0})_{lim} = -13$ db for $v_{sea} \gtrsim 20$ knots. The

curves of Figs. 9 and 10 probably may be extrapolated to $N_{R_0} = 0$ db at $v_{sea} = 0$ because the reflection strength of a dead calm sea is at this level.

Table 7 -- VARIANCES AND VARIANCE RATIOS FOR LABORATORY[19] WIND WAVES

Water Surface Air Speed					
v_{lab}	m/sec	3.18	6.08	9.20	12.02
v_{sea}	knots	4.3	8.1	13.5	19.0
σ_z^2*	cm^2	66	1,560	20,200	113,500
$\sigma_{z'}^2$	--	0.044	0.105	0.24	0.51
$\sigma_{z''}^2$	cm^{-2}	1.40	4.20	11.9	23.9
$\sigma_{z'''}^2$	cm^{-4}	97.1	708	3,460	8,150
$\sigma_z / \sigma_{z'}$	cm	39	122	291	474
$\sigma_{z'} / \sigma_{z''}$	cm	0.17	0.16	0.141	0.146
$\sigma_{z''} / \sigma_{z'''}$	cm	0.12	0.077	0.059	0.054
$(\sigma_{z''} / \sigma_{z'} \sigma_{z'''})^2$	--	0.49	0.24	0.173	0.137

*Based on v_{sea}.

V. SUMMARY

One should at this point congregate the relations for surface, sublayer, and reflection strengths, N_s, N_v, and N_R, together with their limitations from the foregoing and then relate these to total reverberation strength. As previously,

$$10^{N_T/10} = 10^{N_s/10} + 10^{N_v/10} + 10^{N_R/10} \quad . \tag{1}$$

The elements of N_T are, first, sea-surface scattering strength N_s,

$$10^{N_s/10} = 4k_r^4 \sin^4 \varphi [E_2(2k_r \cos \varphi,\ v_{sea})]_s \tag{15}$$

in which $[E_2(2k_r \cos \varphi,\ v_{sea})]_s$ may be evaluated from Eq. 24 if not otherwise available. If Eq. 24 is used, then the limitations on k_r, f_r, v_{sea}, and φ are

$$\begin{aligned} &0.05 \le 2k_r \cos \varphi \le 5\ \mathrm{cm}^{-1} \\ &0.6 \le f_r \cos \varphi \le 60\ \mathrm{kcps} \\ &5 \le v_{sea} \le 15\ \mathrm{knots} \\ &(\pi/2 - \varphi)\ \text{"not too small."} \end{aligned} \tag{53}$$

It will develop below that this latter means $N_s = N_s(v_{sea}, k_r, \varphi)$ for $\varphi \le 60$ deg and $N_s(v_{sea}, k_r, \varphi \ge 60\ \mathrm{deg}) = N_s(v_{sea}, k_r, 60\ \mathrm{deg})$. The indication of the experimental data (Fig. 6) is that

$$N_s(v_{sea} \le 5\ \mathrm{knots}, k_r, \varphi) = N_s(5\ \mathrm{knots}, k_r, \varphi) \tag{54}$$

and

$$N_s(v_{sea} \geq 15 \text{ knots}, k_r, \varphi) = N_s(15 \text{ knots}, k_r, \varphi) . \quad (55)$$

The second element of N_T is sea-surface sublayer scattering strength N_v,

$$10^{N_v/10} = 2\pi \sin \varphi k_r^4 \left\{ \frac{z_0(k_r)[E_x(2k_r)]_3}{x^2} \right\} , \quad (19)$$

where the bracketed biased psd may be evaluated from Eq. 30 in the absence of better spectra in which case, the following restrictions apply

$$\begin{aligned} 0.05 &\leq 2k_r \leq 5 \text{ cm}^{-1} \\ 0.6 &\leq f_r \leq 60 \text{ kcps} \\ 5 &\leq v_{sea} \leq 15 \text{ knots} \end{aligned} \quad (56)$$

The indication of the experimental data (Fig. 6) is that

$$N_v(v_{sea} \leq 5 \text{ knots}, k_r, \varphi) = N_v(5 \text{ knots}, k_r, \varphi) \quad (57)$$

$$N_v(v_{sea} \geq 15 \text{ knots}, k_r, \varphi) = N_v(15 \text{ knots}, k_r, \varphi) . \quad (58)$$

Finally, the reflection contribution N_R to N_T is

$$10^{N_R/10} = \frac{1}{\pi} \left(\frac{\sigma_{z''}}{\sigma_{z'} \sigma_{z'''}} \right)^2 \exp \left[-\frac{1}{2} \left(\frac{\cot \varphi}{\sigma_{z'}} \right)^2 \right], \ f_r < 1 \text{ Mcps} , \quad (21b)$$

in which

$$\frac{1}{\pi} \left(\frac{\sigma_{z''}}{\sigma_{z'} \sigma_{z'''}} \right)^2 \equiv 10^{N_{R_0}/10} \quad (59)$$

and, N_{R_0} and $\sigma_{Z'}$ may be evaluated from Eqs. 42 and 35 if not otherwise available.

If Eq. 42 is used, then

$$\left.\begin{aligned} N_{R_0} &= N_{R_0}(v_{sea}), \text{ for} \\ 2 &\le v_{sea} \le 20 \text{ knots} \\ k_r &\gtrsim 50 \text{ cm}^{-1} \\ f_r &\gtrsim 1 \text{ Mcps} \end{aligned}\right\} \qquad (60)$$

and

$$\left.\begin{aligned} N_{R_0} &= \left(N_{R_0}\right)_{lim} \cong -13 \text{ db, for} \\ v_{sea} &\gtrsim 20 \text{ knots} \quad . \end{aligned}\right\} \qquad (61)$$

If Eq. 35 is used then

$$\left.\begin{aligned} \sigma^2_{Z'} &= \sigma^2_{Z'}(v_{sea}), \text{ for} \\ 0 &\le v_{sea} < 27 \text{ knots} \quad . \end{aligned}\right\} \qquad (62)$$

With Eqs. 15, 19, and 21b written with their limitations, it is possible to study the compatibility and acceptability of the relationships, i.e., whether N_V and N_s, and N_s and N_R, as pairs, match suitably, where they "cross-over" one another, and with what confidence they may be used.

First, $N_s \doteq N_V$ when according to Eqs. 15 and 19

$$4k_r^4 \sin^4\varphi[E_Z(2k_r\cos\varphi,\ v_{sea})]_2$$
$$\doteq 2\pi k_r^4 \sin\varphi \left\{\frac{z_0(k_r)[E_X(2k_r,\ v_{sea})]_1}{X^2}\right\} \quad . \qquad (63)$$

A detailed calculation of each side of Eq. 63 shows for $5 \leq v_{sea} \leq 15$ knots and for $0.6 \leq f_r \leq 60$ kcps, that the angle of cross-over of N_s and N_v is approximately $28 \text{ deg} \leq \varphi(N_s = N_v) \leq 50$ deg. Only a small dependence upon sea-surface wind speed is exhibited in this calculation and at 15 knots, $\varphi(N_s = N_v)$ progresses from 30 to 50 deg as f_r progresses from 0.6 to 60 kcps. In view of the approximate $\tan^4\varphi$ scaling of Eq. 29, the gist of this calculation is that at $f_r = 60$ kcps and $v_{sea} = 15$ knots the spectrum of Fig. 4 based on $\varphi = 50$ deg may be a factor of two high, and there is some indication of this. At lesser frequencies the errors involved are, of course, much less. On the other hand, when $\varphi(N_s = N_v) \gtrsim 40$ deg the implication is that turbulent sublayer spectra based on $\varphi = 10$ and 30 deg are credible, as the general similarity between the results for these two grazing angles suggests. Further, in view of the turbulent sublayer scattering ($\sim \sin\varphi$ when referenced to sea-surface unit area) which is an effective bias to surface scattering ($\sim \tan^4\varphi$) for grazing angle less than about 40 deg, one could deduce an empirical Lambert scattering rule ($\sim \sin^2\varphi$) as a description of sea-surface scattering.[2]

Next, there remains a consideration of grazing angle variation of N_s and N_R near $\varphi = \pi/2$, and when and if they merge suitably. The statement "when and if" is made because detailed calculations of $N_s(v_{sea}, k_r, \varphi)$ and $N_R(v_{sea}, \varphi)$ show generally that $N_s(\varphi, v_{sea}) > N_R(\varphi, v_{sea})$. Considering that the elevation psd developed previously from acoustic reverberation data leads to an approximate $\tan^4\varphi$ scaling law for N_s, and that N_R varies near $\varphi = \pi/2$ approximately as

$$1 - \frac{1}{2}\left(\frac{\pi/2 - \varphi}{\sigma_{z'}}\right)^2 ,$$

then as $\varphi \to \pi/2$, $N_s(\varphi) \to \infty$, N_R remains bounded at (N_{R_0}), and it is to be expected that anomalies will occur.

Now, if the necessary elevation psd were available, it is probably true that a numerical calculation of the theory of Eq. 15 could give guidance to matching N_s and N_R, presuming all the assumptions of

that development apply (isotropic, homogeneous surface, normal joint probability distribution for expanding quadruple correlations to double correlation, etc.). In lieu of this, taking guidance from the numerical calculation of Eqs. 15 and 21b, and from the graphed data in Appendix B, it is proposed that N_s be defined as follows: for $\varphi \leq$ 60 deg, $N_s(\varphi)$ is to be given by Eq. 15; and for $\varphi > 60$ deg, $N_s(\varphi) = N_s(60 \text{ deg})$. Hence, $(\pi/2 - \varphi)$ not too small means $\varphi \leq 60$ deg.

When the summary equations are compared with all the data of Appendix B, the resulting rms error over the 2459 data points is less than 6.1 db; if the data for 60 kcps are removed from the data field, the rms error is approximately 6.4 db. Generally the average error for the entire data field is less than 1 db and is 1.6 db when all except 60 kcps data are used. Hence, on the average, the fit of the summary equations is slightly better at high frequencies.

Table 8 -- RMS ERROR BETWEEN SUMMARY EQUATION AND DATA OF TABLES 1, 2, 3, AND 4

Table	Bounds on Data	RMS Error, db
1	$v_{sea} < 5$ knots	4.6
2	5 knots $\leq v_{sea} <$ 15 knots	4.8
3	$v_{sea} >$ 15 knots	5.2
4	70 deg $\leq \varphi \leq$ 90 deg	3.8*

*Values of v_{sea} = 3, 4, and 16 knots omitted.

VI. CONCLUSION

This paper describes reverberation from the sea surface and from an intimately associated sublayer based on theoretical treatments, and the analysis of acoustic and optical data relating to wind-roughened water surfaces in terms of these theoretical treatments. Three mechanisms are elucidated:

(1) diffuse scattering from a turbulent sublayer volume which is relatively important for grazing angles between 0 and 50 deg, and

(2) diffuse scattering from the rough sea surface which is relatively important for grazing angles between 30 and 70 deg, and

(3) specular reflection from the rough sea surface which is relatively important for grazing angles between 70 and 90 deg (normal incidence).

Based on previous theoretical work, sea-surface elevation, slope and curvature-related spectra are deduced from acoustic and optical data under the assumption of sea-surface isotropicity and homogeneity and these are sufficiently in accord, except at large wave numbers, as to make the analytical treatments based on these spectra credible. Discrepancies in elevation spectra at large wave numbers (capillary wavelengths) are discussed in terms of inhibiting slicks on the sea surface, and the relationship this has to diffuse scattering and specular reflections from the sea surface is indicated. It is postulated that sea-surface elevation spectra at small and large wave numbers are energetically isolated; at small wave numbers, sea and atmosphere are in equilibrium due to energy transferred by pressure forces; and, at large wave numbers, energy flows from atmosphere to sea surface, due to viscous forces, from which it is dissipated at still larger wave numbers.

Based on yet other previous theoretical work, biased spectra of the turbulent volume of the sea-surface sublayer are deduced under the assumption of isotropicity and homogeneity of turbulent volume fluctuations. The spectra are biased for, at this point, there is no basis for determining whether temperature, salinity, or some other fluctuations cause index of refraction variations nor for determining, as a function of acoustic frequency, the effective depth to which scattering takes place. Nevertheless, there is sufficient agreement relative to wave number dependence of the biased spectra with isotropic, homogeneous turbulence spectra to justify the assumption of a scattering sublayer. Notwithstanding anistropy, inhomogeneity, reflections, possible refraction, and other effects attending the sublayer, the similarity of the biased spectra with theoretical estimates suggest that the quotient of the effective depth of sublayer scattering and the square of the characteristic value of the turbulent field is substantially a constant for all acoustic frequencies.

Finally, and based also on previous theoretical work, a Gaussian variation of surface facet reflection strength with normal incidence angle is justified. A lower limiting value of reflection strength at normal incidence with increasing wind speed is found acoustically and optically, and this is likened to a similar phenomenon in air turbulence experiments. The relationship between normal incidence acoustic reflection strength and ratios of elevation derivative variances is demonstrated.

The agglomeration of the various theories and data used here results in a sea-surface reverberation strength theory which, when used as a correlation formula, permits determination of values as a function of acoustic frequency (0.6 to 60 kcps), grazing angle (0 to 90 deg) and sea-surface wind speed ($v_{***} > 2$ knots) with an average rms error of 4.6 db. A consideration of published correlations formulas (Appendix B) indicates that, in general, this rms error of about 5 db is as low as current techniques permit and that a systematic consideration of sources of errors is required before it may be reduced.

One inference of this paper is that acoustic reverberation due to surface and sublayer scattering and surface reflections ought to be considered on non-acoustical bases. That is, suitable optical (perhaps laser) and hydrodynamic (perhaps radioactive) techniques may elucidate surface and sublayer spectra and their dependence upon the contaminants (oil, air, etc.) of the water-free surface. Given these fundamental data, a more accurate assessment of the sources of reverberation and their apparent deviation from theoretical estimates would be possible and, at the same time, a substantially better understanding of reverberation would be at hand.

Another implication of the paper is that the sea-surface energy (on an atomic and molecular scale) may be decisive in determining elevation spectral densities of roughness, hence surface scattering and surface reflection of energy. As the sea-surface structure has relevance to electromagnetic as well as acoustic waves, one may expect that our understanding of the scattering and reflection of light and microwaves from the sea would be enhanced as well.

Finally, if as it appears, the sea-surface elevation spectrum is energetically divided by wavelengths of the order of one centimeter, and more or less one dekameter, respectively, and these two regimes are predominantly affected at short wavelengths by viscous forces and at long wavelengths by pressure forces, then this "variables-separable" view of waves may present a more tractable model from which a better understanding of the sea surface may be developed.

VII. REFERENCES

1. R. J. Urick and R. M. Hoover, "Backscattering of Sound from the Sea Surface: Its Measurements, Causes, and Application to the Prediction of Reverberation Levels," J. Acoust. Soc. Am., 28, pp. 1038-1042, 1956.

2. J. J. Martin, "Sea-Surface Roughness and Acoustic Reverberation--An Operational Model," J. Acoust. Soc. Am., 40(3), to be published, September 1966. Also, IDA Research Paper P-217.

3. The matter of spectra and related functions may be pursued in texts on Fourier transforms, time series analysis, turbulence, etc.

4. R. D. Turner, private communication, July 1966.

5. The implication of Eq. 8 is that $[E_t]_s$ has units of $(\text{length})^4$.

6. E. Y. T. Kuo, "Wave Scattering and Transmission at Irregular Surfaces," J. Acoust. Soc. Am., 36(11), November 1964.

7. C. Cox and W. Munk, "Measurement of the Roughness of the Sea Surface from Photographs of the Sun's Glitter," J. Opt. Soc. Am., 44(11), pp. 838-850, November 1954.

8. V. I. Tatarski, Wave Propagation in a Turbulent Medium, New York, Toronto, London, McGraw-Hill Book Company, Inc., pp. 81-90, 1961.

9. $[E_{x_1}]_s$ has units of $x_1(\text{length})^3$.

10. D. H. Shonting, "Preliminary Studies of the Turbulent Characteristics of Ocean Waves," U.S. Naval Underwater Ordnance Station, TM No. 342, July 1965.

11. Principles of Underwater Sound, Natl. Defense Res. Council, Div. 6, Sum. Tech. Rept. Vol. 7, Chapt. 5, pp. 99-109, Washington, D. C., 1946.

12. G. R. Garrison, S. R. Murphy, and D. S. Potter, "Measurements of the Backscattering of Underwater Sound from the Sea Surface," J. Acoust. Soc. Am., 32(1), pp. 104-111, January 1960.

13. R. P. Chapman and J. H. Harris, "Surface Backscattering Strengths Measured with Explosive Sound Sources," J. Acoust. Soc. Am., 34(10), pp. 1592-1597, October 1962.

14. R. M. Richter, "Measurements of Backscattering from the Sea Surface," J. Acoust. Soc. Am., 36(5), pp. 864-869, May 1964.

15. R. P. Chapman and H. D. Scott, "Surface Backscattering Strengths Measured Over an Extended Range of Frequencies and Grazing Angles," J. Acoust. Soc. Am., 36, pp. 1735-1737, 1964.

16. G. B. Hayes, "Environmental Acoustic Measurements at Halifax, Nova Scotia," U.S. Naval Underwater Sound Lab., USL Report 670, 1965.

17. R. P. Chapman, private communication, September 1965.

18. G. R. Garrison, private communication, September 1965.

19. C. S. Cox, "Measurements of Slopes of High-Frequency Wind Waves," J. Marine Res., 16(33), pp. 199-225, 1958.

20. In this paper units appear to be mixed between metric and nautical. There is some consistency however: laboratory measurements are metric and sea-going experiments are nautical. When convenient these are related, but knots multiplied by 0.5149 gives m/sec.

21. H. W. Marsh, "Sea Surface Statistics Deduced from Underwater Sound Measurements," Annals of the New York Academy of Sciences, Vol. 118, Art. 2, pp. 135-146, September 23, 1964.

22. M. Schulkin and R. Shaffer, "Backscattering of Sound from the Sea Surface," J. Acoust. Soc. Am., 35(2), pp. 240-244, February 1963.

23. Relating to this, there are apparently three typographical errors in the first equation of Sec. 4 of Ref. 19.

24. R. W. Burling, "Wind Generation of Waves on Water," Doctoral Dissertation, Imperial College University of London. [Quoted from H. W. Marsh and R. H. Mellen, "Boundary Scattering Effects in Underwater Sound," Radio Science, 1 (New Series) (3), pp. 339-346, March 1966.]

25. C. A. Coulson, Waves, Edinburgh, Oliver and Boyd, pp. 71-75, 1961.

26. S. Pond, R. W. Stewart and R. W. Burling, "Turbulence Spectra of the Wind Over Waves," J. Atmos. Sci., 20, pp. 319-324.

27. G. K. Batchelor, "The Theory of Homogeneous Turbulence," London, Cambridge University Press, pp. 82-88, 1959.

28. Reference 21 proposes a $\tan^4 \varphi$ scaling law for acoustic frequencies low in the present context.

29. Based on v_{sea} of Table 5.

30. The decreasing trend of $(\sigma_{z''}/\sigma_{z'}\sigma_{z'''})^2$ with increasing wind speed is to be expected. Suppose $E_z(k_s)$ is stylized as $E^* k_s^{\alpha}$ between limits $k_0(v_{sea})$ and $k_1(v_{sea})$ and is zero everywhere else. Thus using Eqs. 8-11,

$$(\sigma_{z''}^2/\sigma_{z'}\sigma_{z'''})^2 = \frac{(7-\alpha)(3-\alpha)(k_1^{5-\alpha} - k_0^{5-\alpha})^2}{(5-\alpha)^2(k_1^{3-\alpha} - k_0^{3-\alpha})(k_1^{7-\alpha} - k_0^{7-\alpha})} .$$

Now if $\alpha \simeq 1$, and $k_1 \gg k_0$ then

$$(\sigma_{z''}/\sigma_{z'}\sigma_{z'''})^2 \simeq 3\, k_0/k_1 .$$

From Fig. 3 it appears $k_0(v_{sea}) \to 0$ and $k_1(v_{sea}) \to \infty$, thus $(\sigma_{z''}/\sigma_{z'}\sigma_{z'''})^2 \to 0$ as $v_{sea} \to \infty$.

A1. The brackets $\langle \; \rangle$ denote an ensemble average.

A2. The subscripts "1i" and "2i" will be used only where clarity requires it for distinguishing one- and two-dimensional isotropic surfaces. In what follows $k_s \equiv k$.

A3. Ian N. Sneddon, Fourier Transforms, New York, Toronto, London, McGraw-Hill Book Company, 1951, p. 52, Eqs. (14) and (15), for example.

A4. W. Grobner and N. Hofreiter, Integraltafel, Vol. II, Springer-Verlag, 1958, p. 200, Eq. (2a).

B1. M. Schulkin, private communication, December 1965.

C1. N. Bowditch, American Practical Navigator, U.S. Navy Hydrographic Office, U.S. Government Printing Office, Washington, D. C., 1962, p. 731.

APPENDIX A

RELATIONSHIPS BETWEEN ONE- AND TWO-DIMENSIONAL POWER SPECTRA OF A SURFACE[4]

Let $z(x, y)$ denote the elevation of a statistically isotropic and homogeneous zero-mean random surface. The 2-D autocorrelation or covariance function of z is[A1]

$$B_z(x, y) = [z(x', y')z(x' - x, y' - y)] \quad . \tag{A1}$$

$B_z(x, y)$ is independent of x' and y' because of the homogeneity assumption. (Homogeneity is the spatial equivalent of stationarity for a time-dependent process.)

The isotropy assumption means that $B_z(x, y)$ is invariant under a rotation of the coordinate system, which implies that $B_z(x, y)$ can be written in the form[A1]

$$B_z(x, y) = \Big[B_z(r)\Big]_{2i} \quad , \tag{A2}$$

where

$$r = \sqrt{x^2 + y^2} \quad . \tag{A3}$$

The 1-D autocorrelation function of z can be written

$$B_z(x) = [z(x' - x, y')z(x', y')] \quad . \tag{A4}$$

It follows that

$$\Big[B_z(x)\Big]_1 = \Big[B_z(|x|)\Big]_{2i} \equiv B_z(x) \quad . \tag{A5}$$

Next, the 2-D psd function of z is, by the Wiener-Khinchine theorem, the 2-D Fourier transform of $B_z(x, y)$, i.e.,

$$E_z(k_x, k_y) = (1/2\pi) \int_{-\infty}^{\infty} \int_{-\infty}^{\infty} \exp[i(k_x x + k_y y)]\, B_z(x, y)\, dx\, dy \tag{A6}$$

Transforming to polar coordinates in x and y and invoking Eq. A2 yields

$$E_z(k_x, k_y) = (1/2\pi) \int_0^{\infty} \int_0^{2\pi} \exp[i(k_x r \cos \varphi + k_y r \sin \varphi)][B_z(r)]\, r dr \,, \tag{A7}$$

in which φ is a polar coordinate and is not related to the grazing angle. Now putting

$$k_x = k \cos \theta, \qquad k_y = k \sin \theta \quad .$$

causes Eq. A7 to become

$$E_z(k_x, k_y) = (1/2\pi) \int_0^{\infty} \int_0^{2\pi} \exp[ikr \cos(\varphi - \theta)]\, B_z(r)\, r\, dr\, d\varphi \quad . \tag{A8}$$

Evaluating the integral over φ gives

$$E_z(k_x, k_y) = \int_0^{\infty} J_0(kr)\, B_z(r)\, r dr \quad . \tag{A9}$$

Eq. A9 implies that, under the foregoing assumptions, $E_z(k_x, k_y)$ is a function of

$$k = \sqrt{k_x^2 + k_y^2} \tag{A10}$$

only, i.e.,

$$E_z(k_x, k_y) = \left[E_z(k)\right]_{a1} \tag{A11}$$

Eq. A9 further states that $E_z(k)$ is the Hankel transform of $B_z(r)$:

$$E_z(k) = \int_0^{\infty} J_0(kr)\, B_z(r)\, r dr \quad , \qquad \text{(A12)}$$

which in turn implies that[A3]

$$E_z(r) = \int_{-\infty}^{\infty} J_0(kr)\left[E_z(k)\right]_{21} kdk \quad . \qquad \text{(A13)}$$

Correspondingly, the 1-D psd function is given by

$$\left[E_z(k)\right]_1 = (1/\sqrt{2\pi}) \int_{-\infty}^{\infty} e^{ikx}[B_z(x)]\, dx \quad . \qquad \text{(A14)}$$

It follows from the homogeneity assumption, or from Eq. A5, that $B_z(x)$ is an even function of x, so that Eq. A14 can be rewritten as

$$\left[E_z(k)\right]_1 = \sqrt{2/\pi} \int_0^{\infty} \cos kx[B_z(x)]\, dx \quad . \qquad \text{(A15)}$$

Inverting Eq. A14 and invoking the evenness of $[E_z(k)]_1$ implied by Eq. A15 yields

$$B_z(x) = \sqrt{2/\pi} \int_0^{\infty} \cos kx\left[E_z(k)\right]_1 dk \quad . \qquad \text{(A16)}$$

Next, using Eqs. A5, A12, and A16 affords a representation of $[E_z(k)]_{21}$ in terms of $[E_z(k)]_1$.

$$\left[E_z(k)\right]_{21} = \int_0^{\infty} J_0(kr)\left[\sqrt{2/\pi} \int_0^{\infty} \cos k'r\left[E_z(k')\right]_1 dk'\right] rdr \qquad \text{(A17)}$$

At this point, it would be advantageous to be able to interchange the order of integration in Eq. A17, but the integral over r that is obtained is improper. To circumvent this difficulty, the integral over k′ will first be integrated by parts. Assuming that $[E_z(k')]_1$ vanishes as k′ becomes arbitrarily large, the result is that

$$\left[E_z(k)\right]_{21} = \int_0^\infty J_0(kr)\left[(-1/r)\sqrt{2/\pi}\left[E_z'(k')\right]_1 \sin k'r \, dk'\right] r dr \quad , \qquad (A18)$$

where $[E_z'(k')]_1 = (d/dk')[E_z(k')]_1$. It is now permissible to interchange the order of integration, with the result that

$$\left[E_z(k)\right]_{21} = -\sqrt{2/\pi}\int_0^\infty \left[E_z'(k')\right]_1\left[\int_0^\infty J_0(kr)\sin k'r \, dr\right] dk' \quad . \qquad (A19)$$

The integral over r is a standard form,[A4] so that Eq. A19 becomes

$$\left[E_z(k)\right]_{21} = -\sqrt{2/\pi}\int_k^\infty \left[E_z'(k')\right]_1 (k'^2 - k^2)^{-\frac{1}{2}} \, dk' \quad . \qquad (A20)$$

This expression can be integrated by parts to give $[E_z(k)]_{21}$ in terms of $[E_z(k)]_{11}$; the result is

$$\left[E_z(k)\right]_{21} = \sqrt{2/\pi}\int_0^\infty \left\{\left[E_z(k)\right]_1 - \left[E_z(k')\right]_1\right\}(k'^2 - k^2)^{-3/2} \, k'dk' \qquad (A21)$$

Either Eq. A20 or Eq. A21 is suitable for transforming the 1-D spectra.

APPENDIX B

ACOUSTIC REVERBERATION STRENGTH DEFINITION, DATA, AND CORRELATION FORMULAS

A. DEFINITION

The acoustic reverberation data used in this report are attributed to the sea surface (i.e., considered to be an area phenomenon). Thus, one may approach a definition of reverberation strength operationally. Consider Fig. B-1, where a transducer (transmitter-receiver) ensonifies at grazing angle φ a patch of sea surface with area A and with steradiant intensity $dI_i/d\Omega$. The ensonified surface scatters and reflects, more or less, as appropriate to φ. Some of the energy reverberates ("backscatters") from all points (p_1, p_2, ...) on the surface to the transducer and corresponds there to a reverberated radiant intensity $dI_r/d\Omega$, i.e., energy/unit area at the transducer may be converted through the geometry of the situation to energy/steradian. Now, if transducer depth z_t is sufficiently large and ensonifying beam half-width $\Delta\varphi$ is sufficiently small, then one may assume that reverberated steradiant intensity is proportional to area A. Now $dI_i/d\Omega$ and $dI_r/d\Omega$ are measured at the transducer and $dI_i/d\Omega$ suffers a change due to attenuation and perhaps refraction, as does $dI_r/d\Omega$, in traversing the distance from transducer to surface. The convention then in defining reverberation strength is to correct $dI_i/d\Omega$ and $dI_r/d\Omega$ to a distance of one yard from the scattering surface and to normalize $dI_r/d\Omega$ to a one square yard surface. Thus, reverberation strength N_r is in db given by

$$N_r = 10 \log_{10} \left(\frac{dI_r/d\Omega}{dI_i/d\Omega}\right)_{yd,\ yd^2} , \tag{B1}$$

where the subscript is self-explanatory in view of the foregoing.

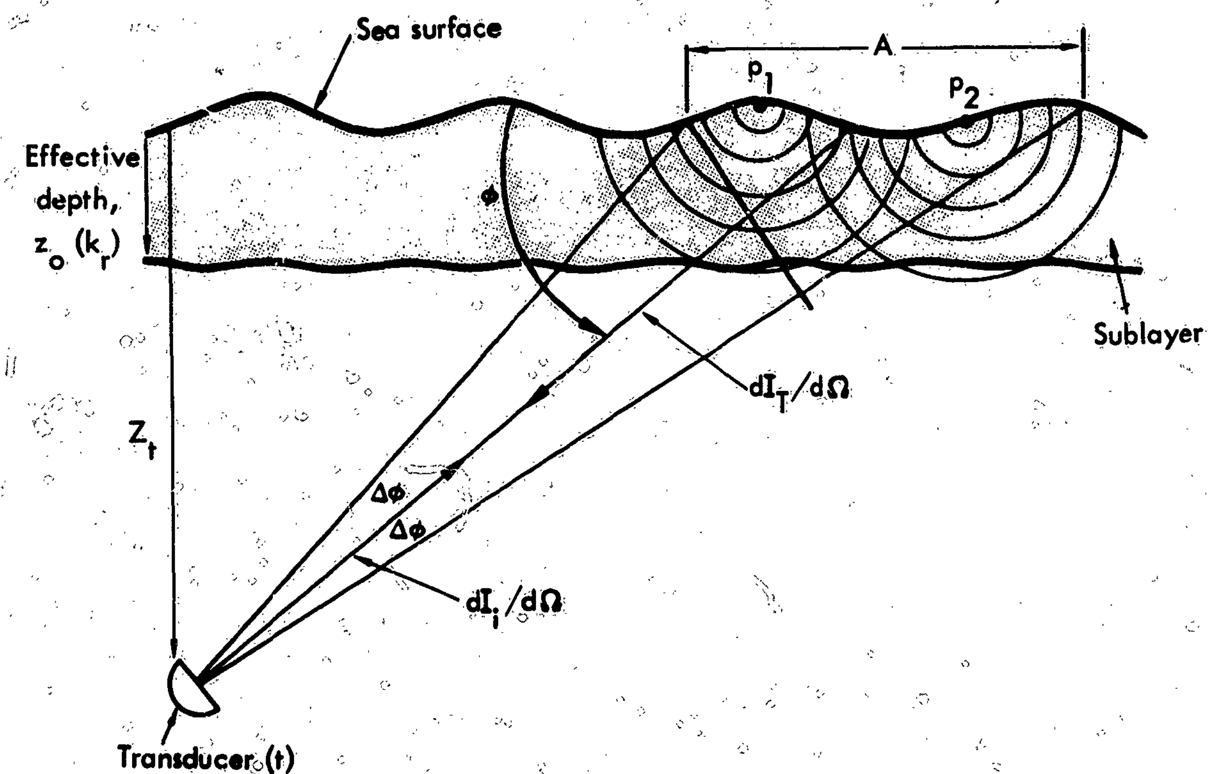

FIGURE B-1 Reverberation Strength Measurement Geometry

R10-7-68-11

Now a reverberation strength for volume may be defined on the same basis as that for area, except that a unit volume rather than a unit area is required. In the present analysis, however, it develops that volume (sublayer) reverberation has been attributed by the various authors to a unit area of the surface. Thus, the reverberation strength of the sublayer referred to the unit surface area appears to vary as sin φ because the volume of reverberation/unit surface area

remains constant with φ, but the energy density in the reverberating volume varies as the projected area A′ of the surface area A (i.e., as sin φ).

B. DATA

The acoustic reverberation data used in this paper have been taken from the literature where necessary and augmented by private correspondence where possible. In either case graphical presentations were converted to tabular data with a given data point described by frequency (or octave mid-point), wind speed, grazing angle, and reverberation strength. These data are presented graphically in Figs. B-2 through B-8 (pp. 69 to 83) and are coded as in Table B-1.

Table B-1 -- CORRESPONDENCE BETWEEN DATA SOURCE OF REVERBERATION DATA GRAPHS

Source	Reference	Symbol
Urick & Hoover	1	⧓
National Defense Research Council	3	✱
Garrison, Murphy, Potter	4, 10	+
Chapman & Harris	5, 9	⧗
Richter	6	▲
Hayes	8	⏻
Marsh	21	

Some of the data in the figures of this Appendix and in the literature were not directly used. Data of Ref. 11 correspond only to a grazing angle of 3 deg, much below the arbitrarily chosen minimum grazing angle for the analysis. Data of Ref. 16 at normal incidence were not used in view of the greater abundance of data at 60 kcps over a wider range of grazing angles near normal incidence. The data of Ref. 21 were not used because wind conditions were not reported specifically but alluded to as being for sea states 0 to 4, i.e., $0 \leq v_{sea} \leq 20$ knots, approximately.

C. CORRELATION FORMULAS

Correlation formulas have been fitted to some of the data of this Appendix; generally they are of logarithmic-trigonometric form and as they appear here, employ units of kilocycles per second, knots, and radians. The first of these, applying to acoustic frequencies between 0.4 and 6.4 kcps, is given by[13]

$$N_T = 3.3 \left[\frac{158}{v_{sea}^{0.58} (1000 f_r)^{0.193}} \right] \log \frac{180\varphi}{30\pi} - 42.4 \log \left[\frac{158}{v_{sea}^{0.58} (1000 f_r)^{0.193}} \right] + 2.6 \quad . \qquad \text{(B2)}$$

The somewhat unusual form of this equation is used in deference to the authors and also to maintain units of knots, kilocycles per second, and radians as is customary. Equation B2 may be approximated and placed in a more usual form by using mean values of v_{sea} = 10 knots and f_r = 1600 cps so as to fix the coefficient of log φ. Then, there results,

$$N_T \cong -56.8 + 33.0 \log \varphi + 24.6 \log v_{sea} + 8.2 \log f_r \quad , \qquad \text{(B3)}$$

for $v_{sea} \cong 10$ knots $f_r \cong 1.6$ kcps.

The next correlation formula[21] to appear is for frequencies $0.268 \leq f_r \leq 1.2$ kcps and sea states 0 to 4. This is given by

$$N_T = -36 + 40 \log \tan \varphi \qquad \text{(B4)}$$

with no wind speed or frequency dependence indicated.

The first correlation formula to appear which analyzed all of the data in the literature[22] was applied to frequencies $0.4 \leq f_r \leq 60$ kcps, all wind speeds, and grazing angles $\varphi \leq 60$ degs (i.e., some of the data of Refs. 1, 11, 12, and 13). The suggested form of this correlation formula is

$$N_T = -71.1 + 9.9 \log \sin \varphi + 24.8 \log v_{sea} + 9.9 \log f_r \quad , \qquad \text{(B5a)}$$

although the least squares fit to the data is given by[B1]

$$N_r = -76.9 + 7.3 \log \sin \varphi + 32.9 \log v_{sea} + 7.3 \log f_r \quad . \tag{B5b}$$

Finally, the predecessor paper[2] of this present one gave as a correlation function (interpreted in the light of sea-surface roughness spectra) the following relation for $24(v_{sea}/10)^6 \leq f_r(\text{kcps}) \leq 24(v_{sea}/0.7)$, and for $0 < \varphi < 60$ deg,

$$N_s = -72.9 + 20 \log \sin \varphi + 40 \log v_{sea} - 5 \log f_r \quad . \tag{B6}$$

The coefficients of Eqs. B3 through B6 are congregated in Table B-2. Inasmuch as grazing angle functional dependence is not consistent throughout these equations, doing this may appear to be anomalous. However, $\varphi \cong \tan \varphi \cong \sin \varphi$ for φ not too large, and in Eq. B3 the coefficient of $\log \varphi$ is a variable at best. Thus, for the sake of concise comparison, Table B-2 appears warranted. Included in Table B-2 is a reference value of N_s at φ = 30 deg, v_{sea} = 10 knots, and f_r = 1.6 kcps.

Table B-2 -- COMPARISON OF CORRELATION FORMULAS FOR SEA-SURFACE REVERBERATION STRENGTH

Source	Constant	$\log f(\varphi)$*	$\log v_{sea}$	$\log f_r$	N_s (30 deg, 10 knots, 1.6 kcps)
Chapman & Harris	-56.8	33.0	24.6	8.2	-39.4
Marsh	-36.0	40.0	0	0	-45.6
Schulkin & Shaffer	a -71.1	9.9	24.8	9.9	-47.3
	b -76.9	7.3	32.9	7.3	
Martin	-72.9	20.0	40.0	-5	-37.9

*Cf. Eqs. B3 through B6.

Finally, it is worth comparing reverberation strengths determined according to the main text of the paper, based on approximations to surface and sublayer spectra with the correlation formulas of Eqs. B3 through B6, over the particular ranges for which these apply. Such a calculation has been made, the results of which are given in Table B-3; in this table both average and rms errors are given so that biases are evident as well.

Table B-3 -- COMPARISON OF CORRELATIONS FORMULAS WITH RESULTS OF PRESENT ANALYSIS*

Source	Average Error, db	RMS Error, db
Chapman & Harris	0	5
Marsh	1	7
Schulkin & Shaffer	a -3 b 0	5 7
Martin	0	7

*Cf. Summary of main text; a positive average error means that results according to the present analysis yield larger, i.e., less negative, results.

The gist of Table B-3 is as follows: The present analysis gives results on the average not much different from previously published correlation formulas. This is not unusual, for the present analysis has used only an augmentation of previously published data and has sought out constituent phenomena for spectral representation based on the augmented data. The rms errors listed in Tables 8 and B-3 suggest that, with present techniques, errors in any experiment as they arise from lack of knowledge of radiated and received power, attenuation, refraction, effective beamwidth, surface and sublayer statistics, wind speed, bandpass filtering, etc., leave a residual uncertainty which in any event may not be reduced below about 5 db. Perhaps, at this point, it is worth investigating the individual variances ($\sigma^2_{V_{sea}}$, $\sigma^2_{f_r}$, σ^2_{φ}, $\sigma^2_{E_z}$, etc.) as they contribute to the total variance ($\sigma^2_{N_T}$), if surface reverberation estimates are to be improved.

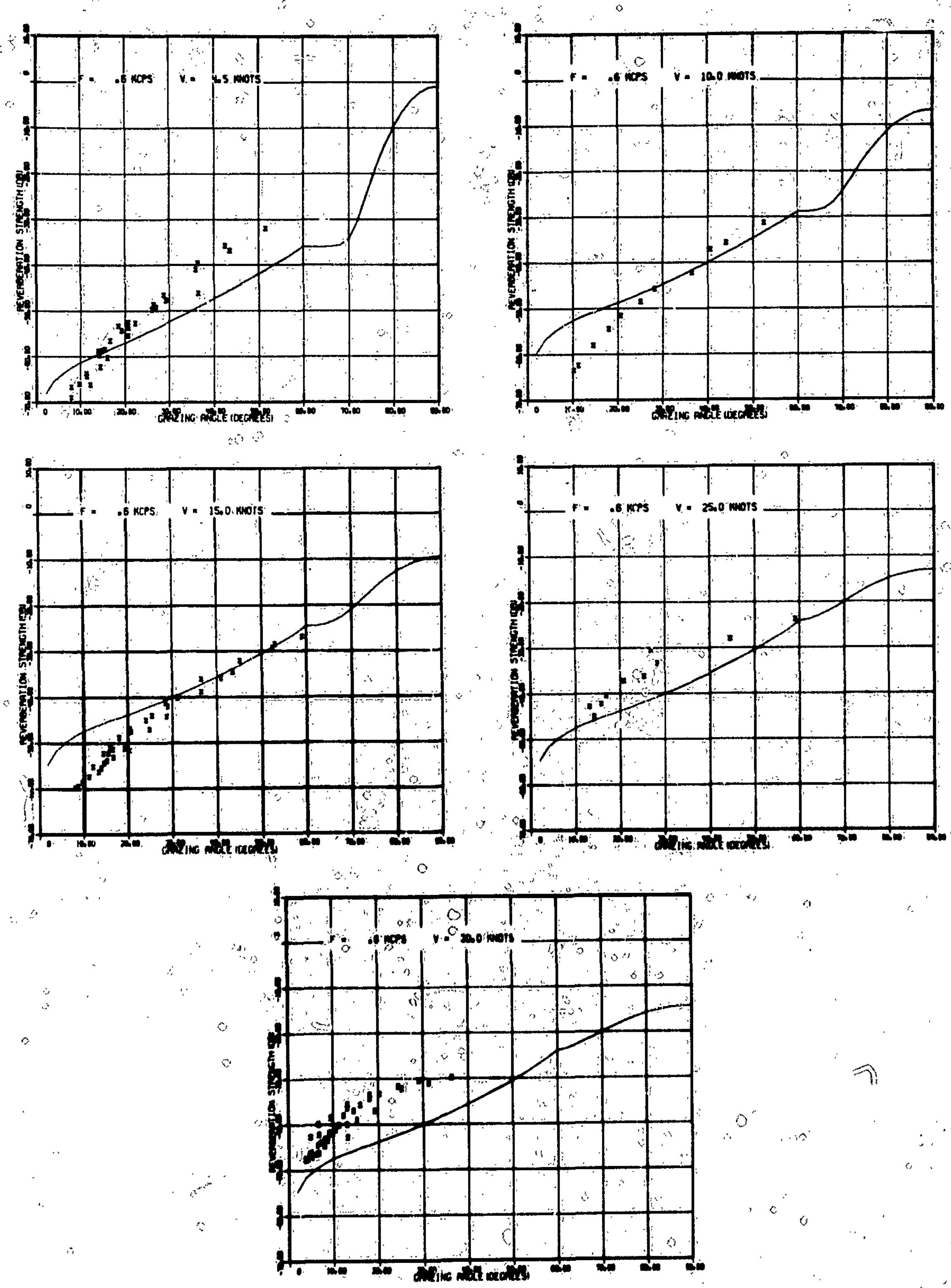

FIGURE B-2 Comparison of Experimental Acoustic Reverberation Data with Present Theory (0.6 kcps)

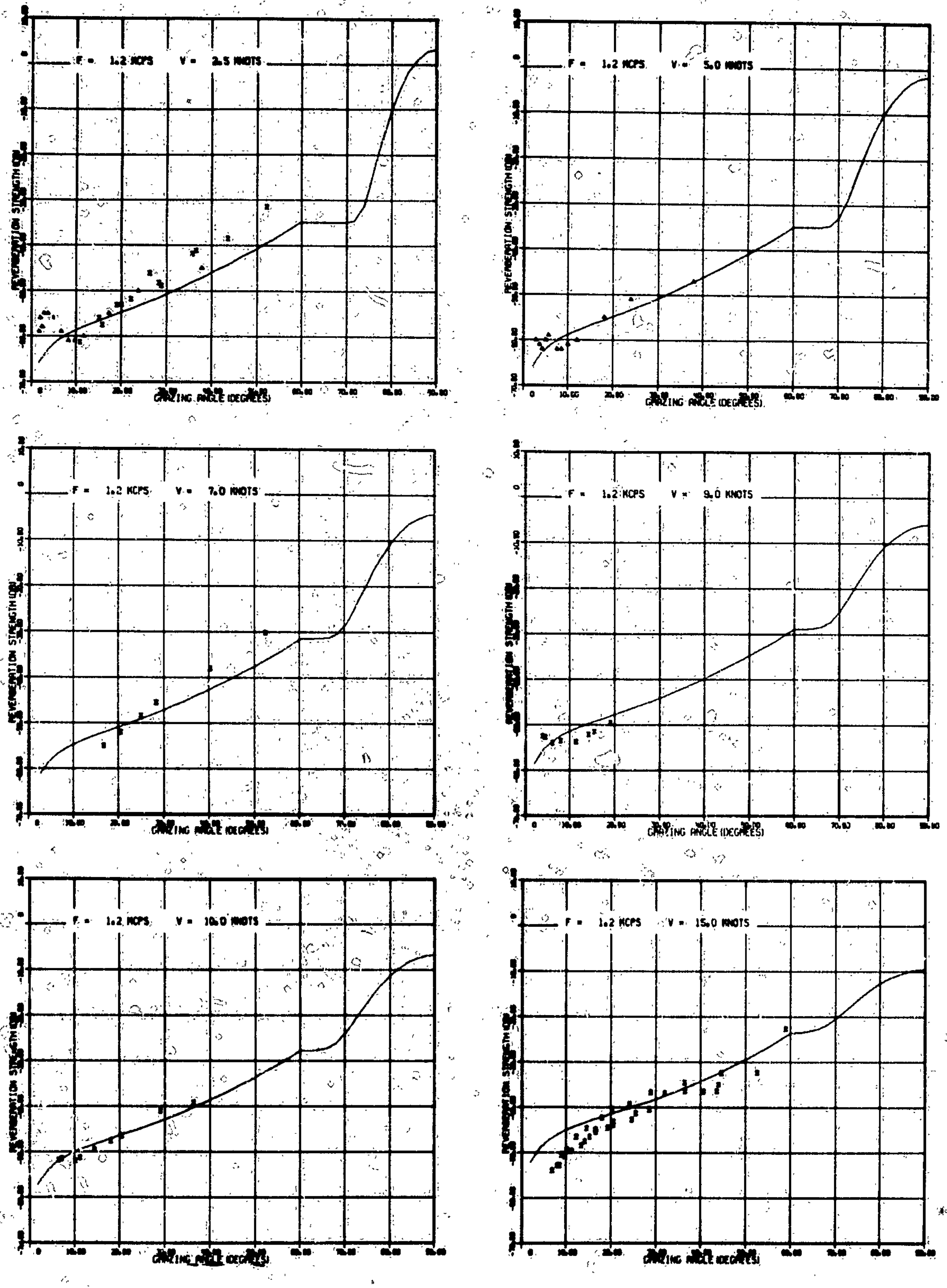

FIGURE B-3 Comparison of Experimental Acoustic Reverberation Data with Present Theory (1.2 kcps)

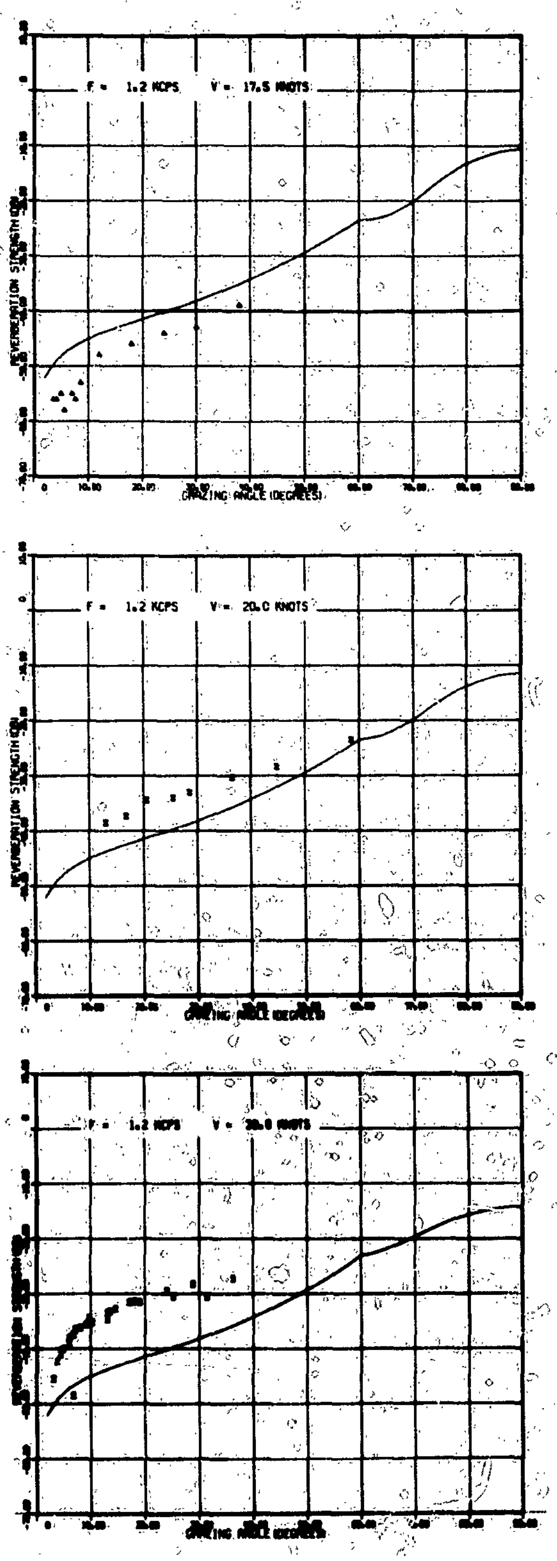

FIGURE B-3 (Cont'd) Comparison of Experimental Acoustic Reverberation Data with Present Theory (1.2 kcps)

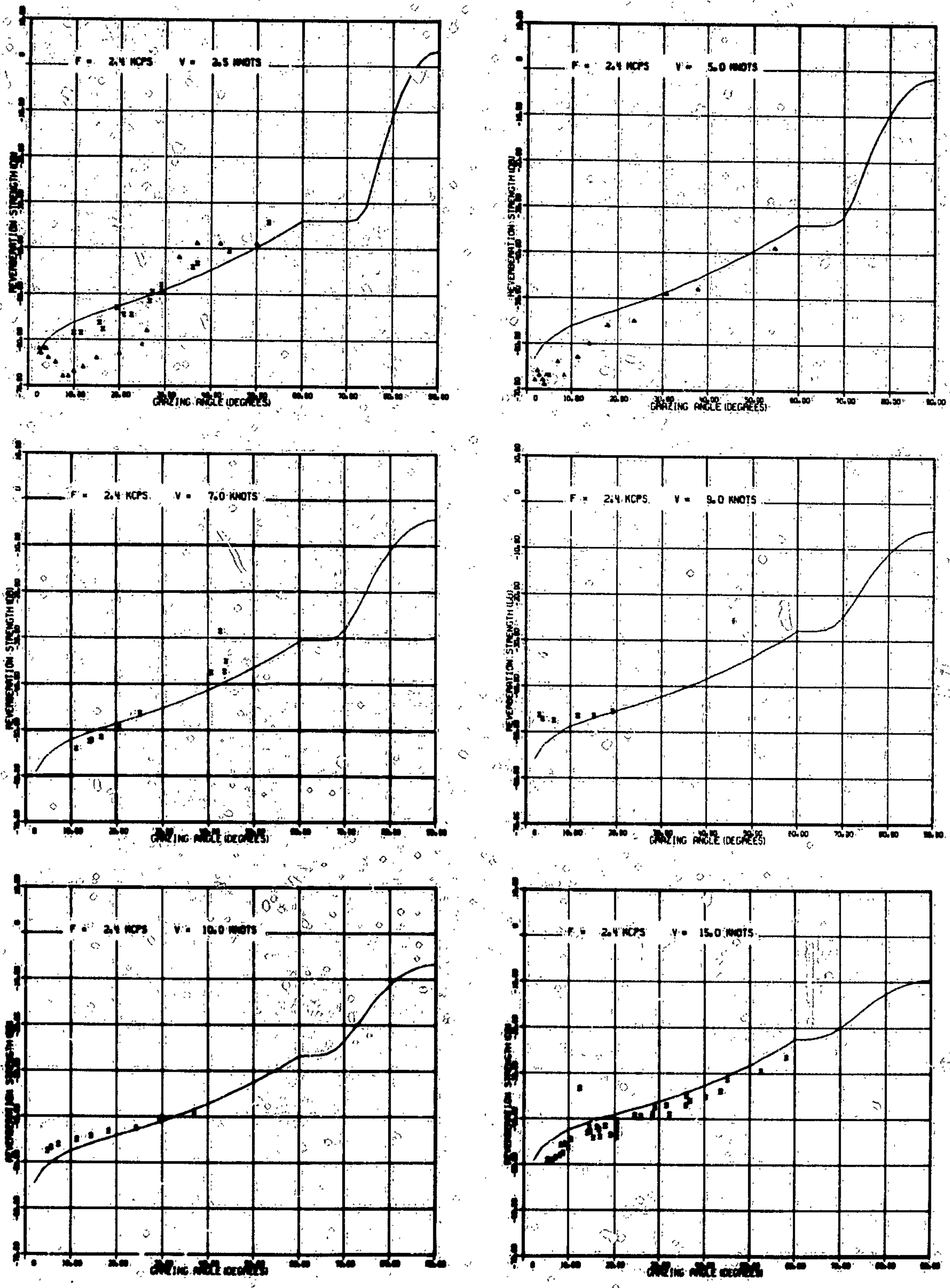

FIGURE B-4 Comparison of Experimental Acoustic Reverberation Data with Present Theory (2.4 kcps)

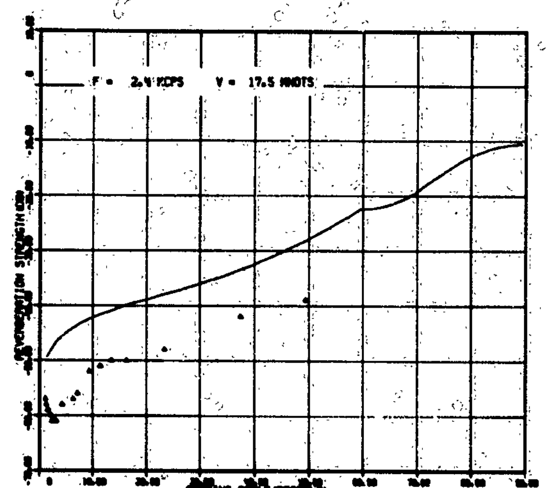

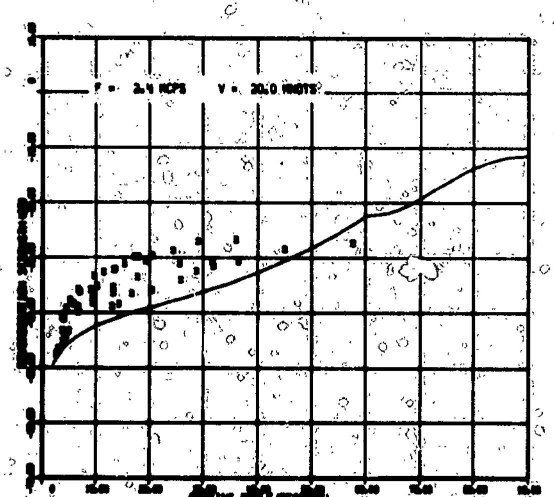

FIGURE B-4 (Cont'd) Comparison of Experimental Acoustic Reverberation Data with Present Theory (2.4 kcps)

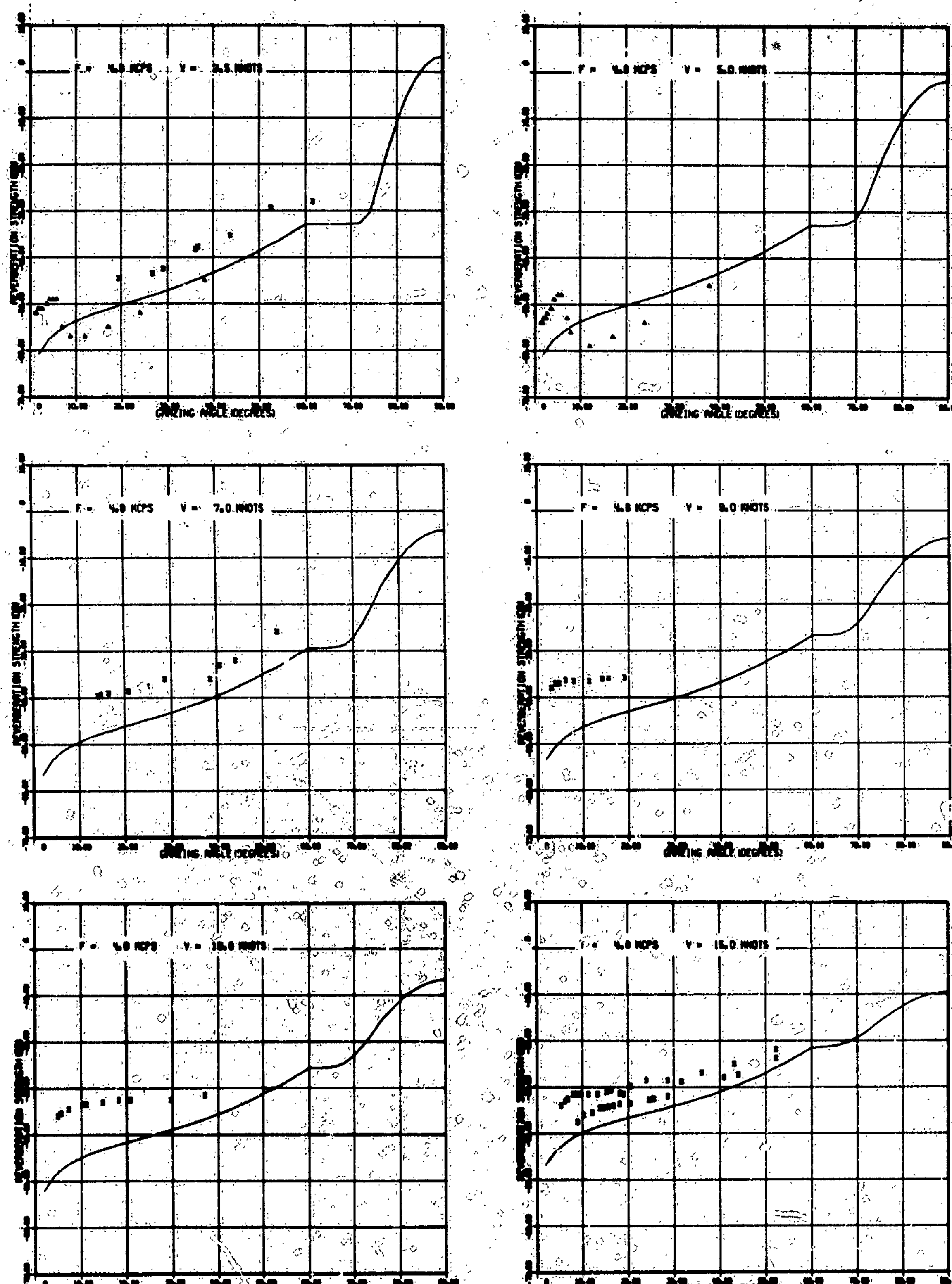

FIGURE B-5 Comparison of Experimental Acoustic Reverberation Data with Present Theory (4.8 kcps)

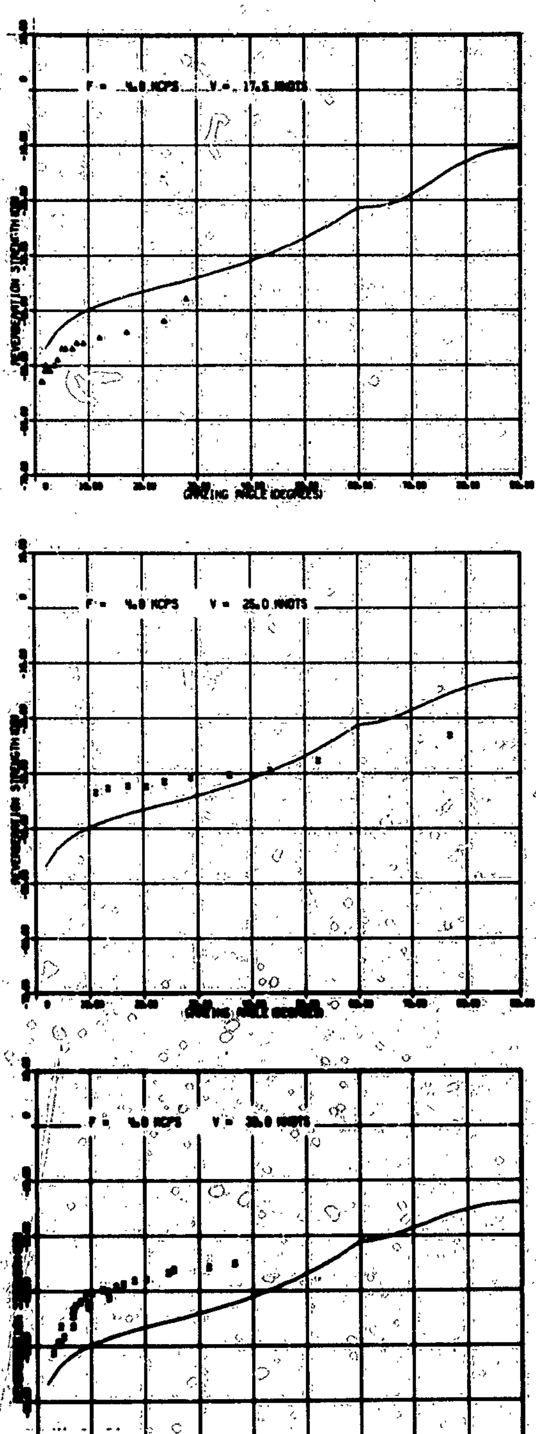

FIGURE B-5 (Cont'd) Comparison of Experimental Acoustic Reverberation Data with Present Theory (4.8 kcps)

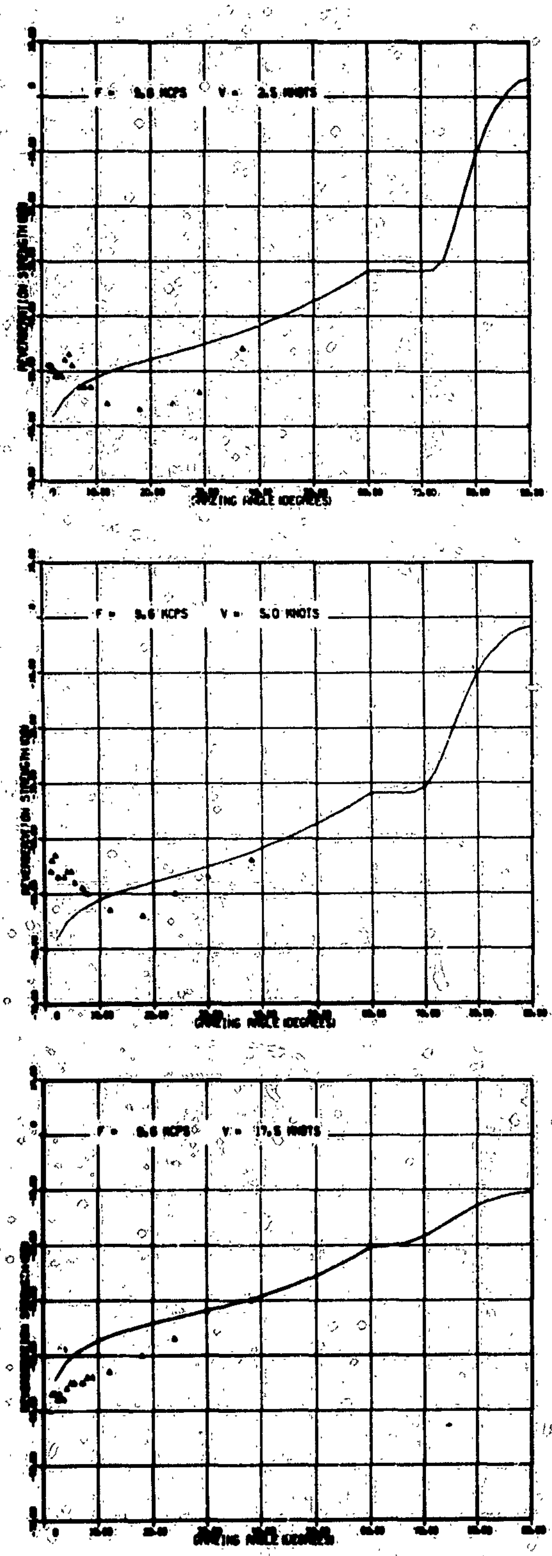

FIGURE B-6 Comparison of Experimental Acoustic Reverberation Data with Present Theory (9.6 kcps)

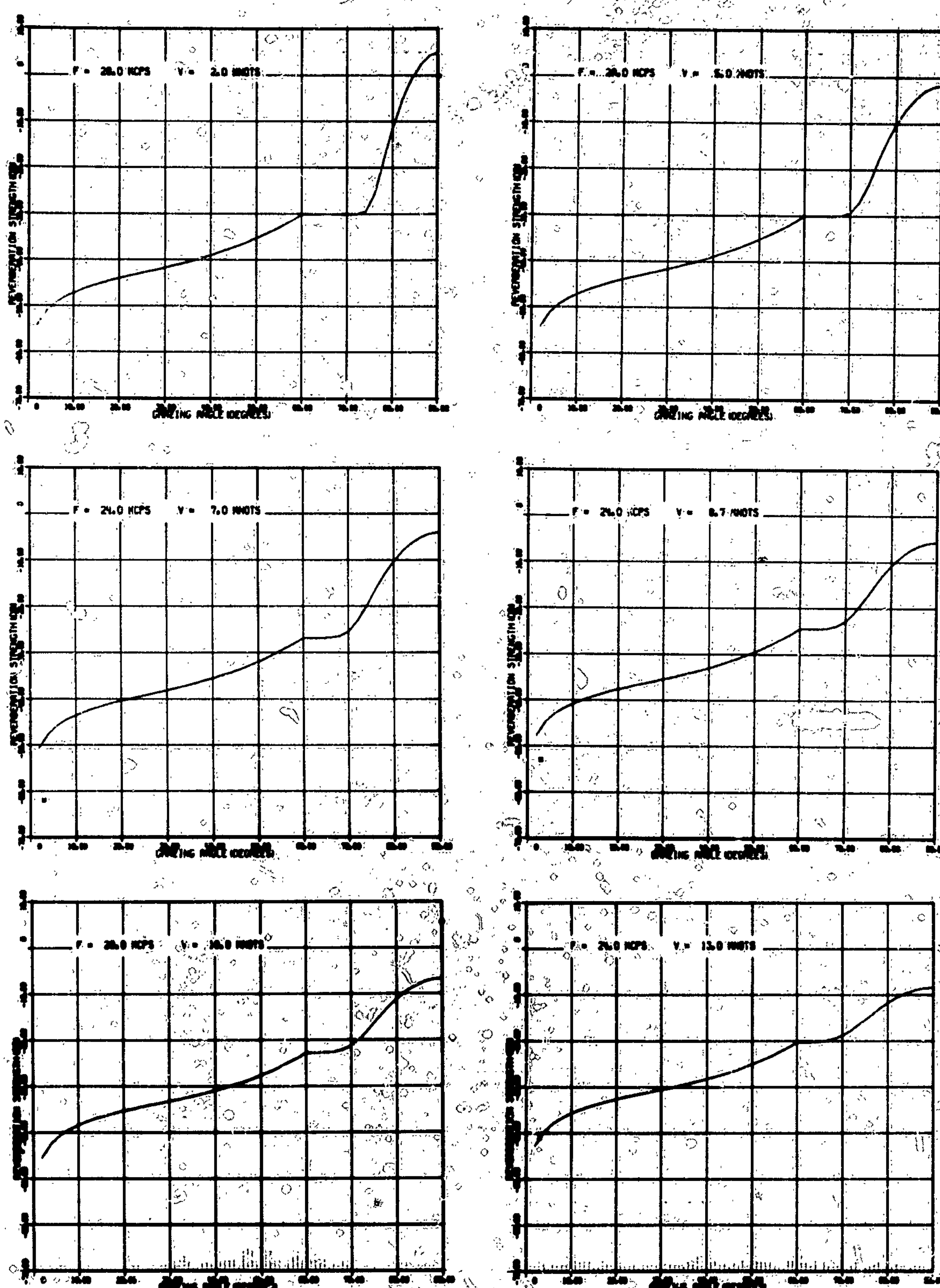

FIGURE B-7 Comparison of Experimental Acoustic Reverberation Data with Present Theory (24 to 28 kcps)

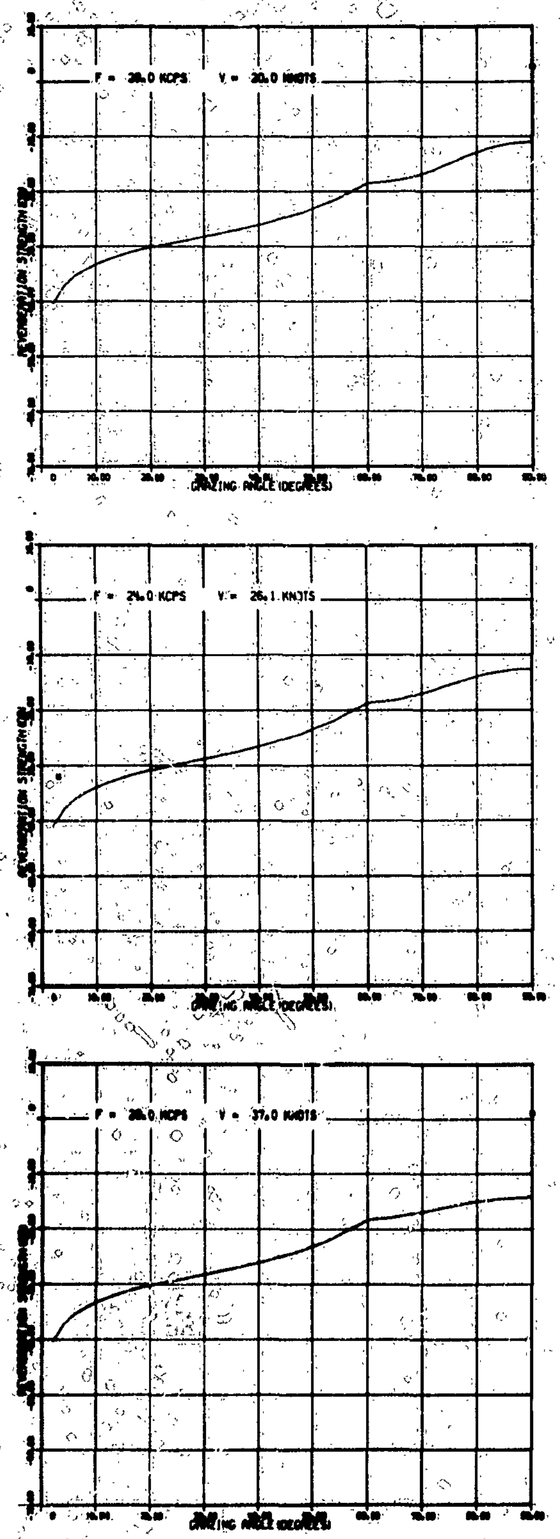

FIGURE B-7 (Cont'd) **Comparison of Experimental Acoustic Reverberation Data with Present Theory (24 to 28 kcps)**

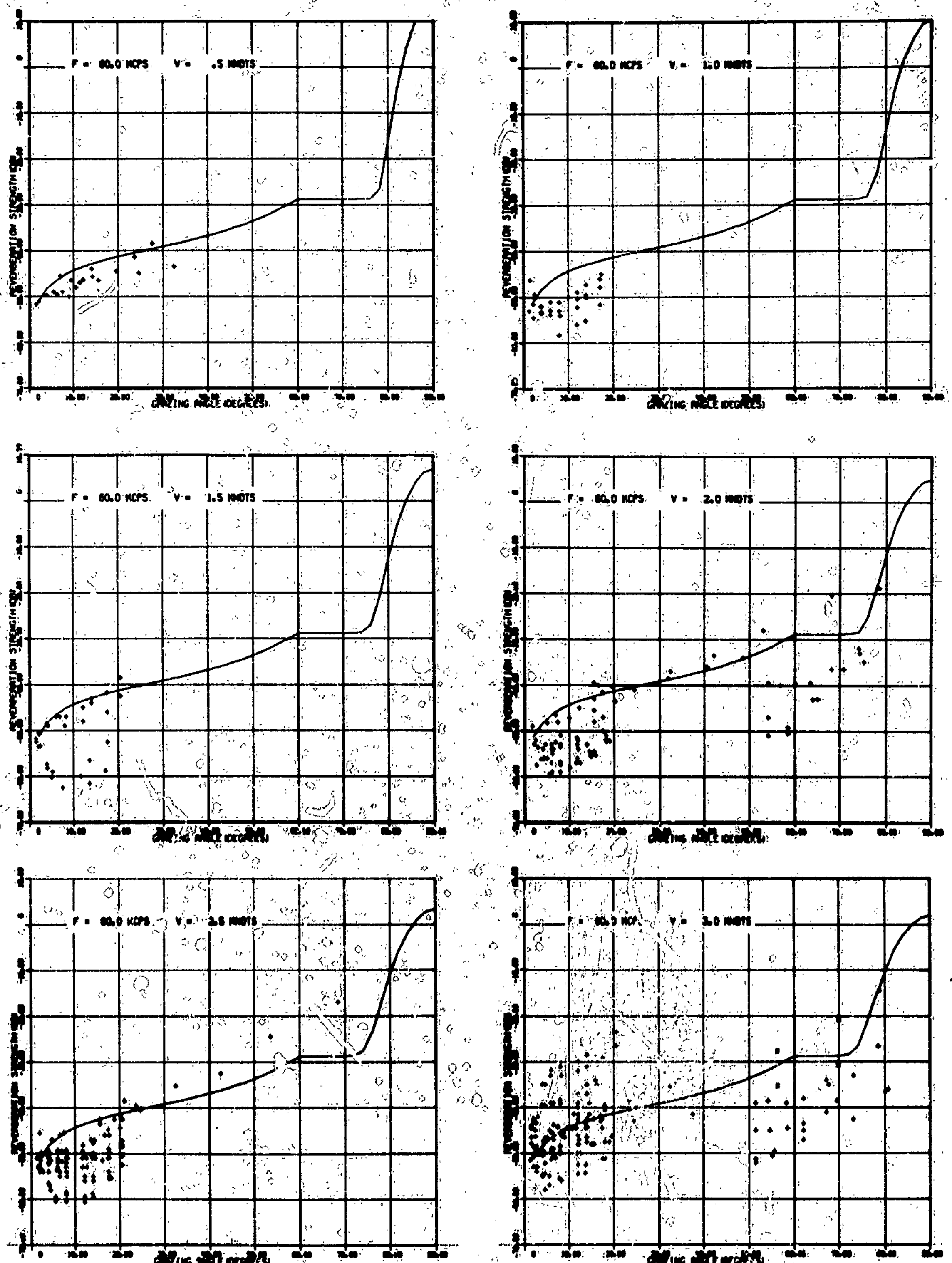

FIGURE B-8 Comparison of Experimental Acoustic Reverberation Data with Present Theory (60 kcps)

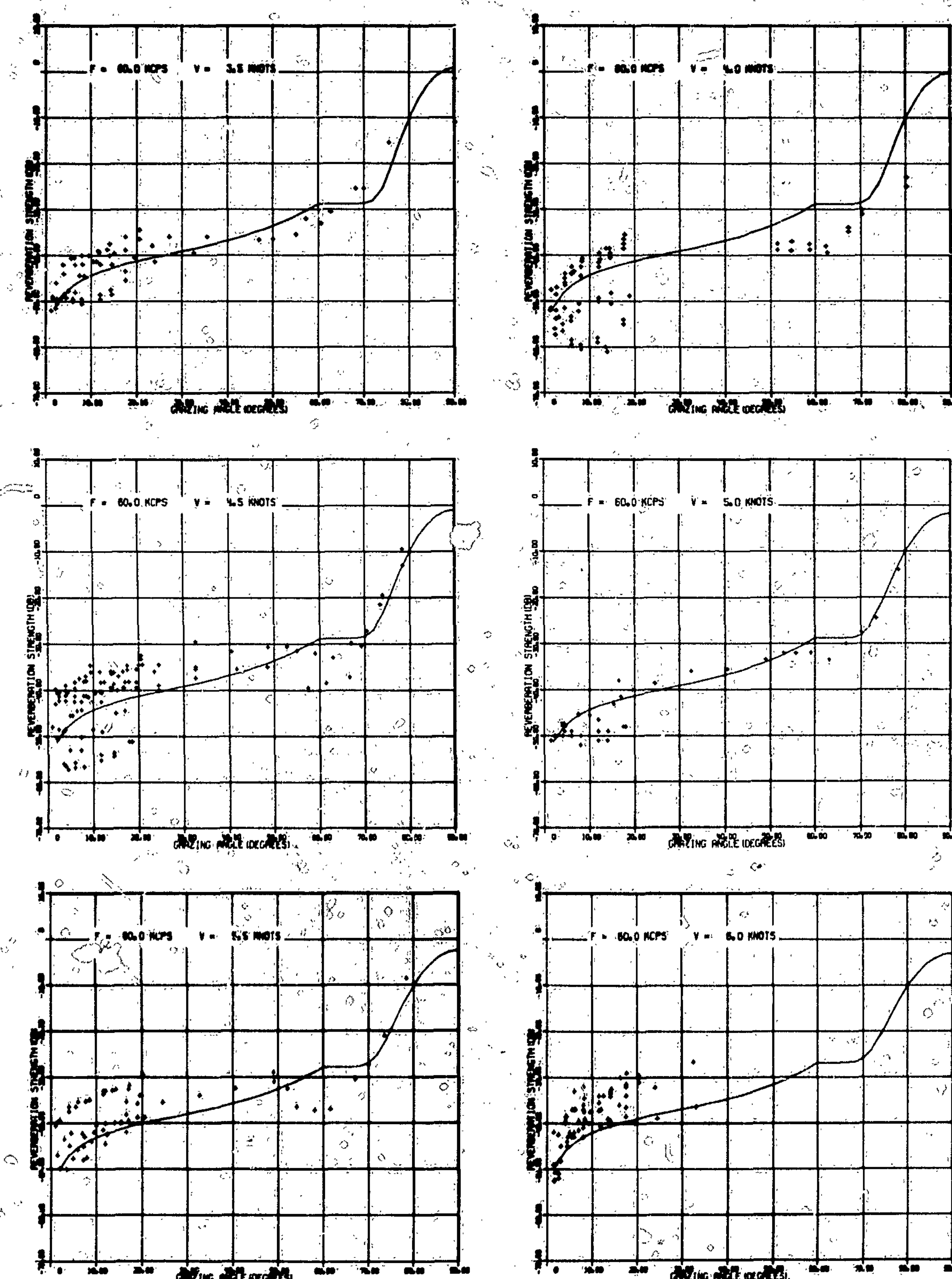

FIGURE B-8 (Cont'd) Comparison of Experimental Acoustic Reverberation Data with Present Theory (60 kcps)

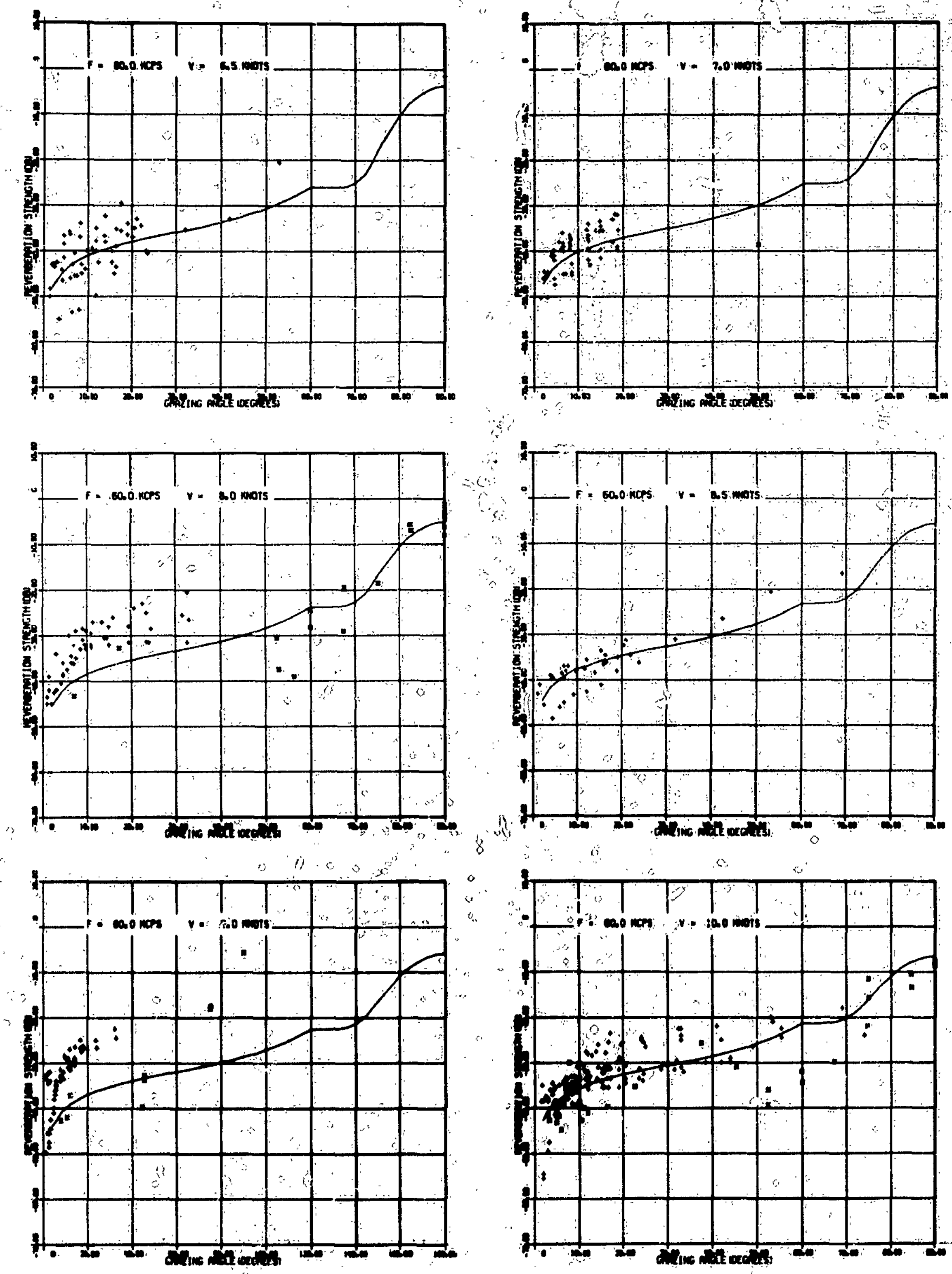

FIGURE B-8 (Cont'd) Comparison of Experimental Acoustic Reverberation Data with Present Theory (60 kcps)

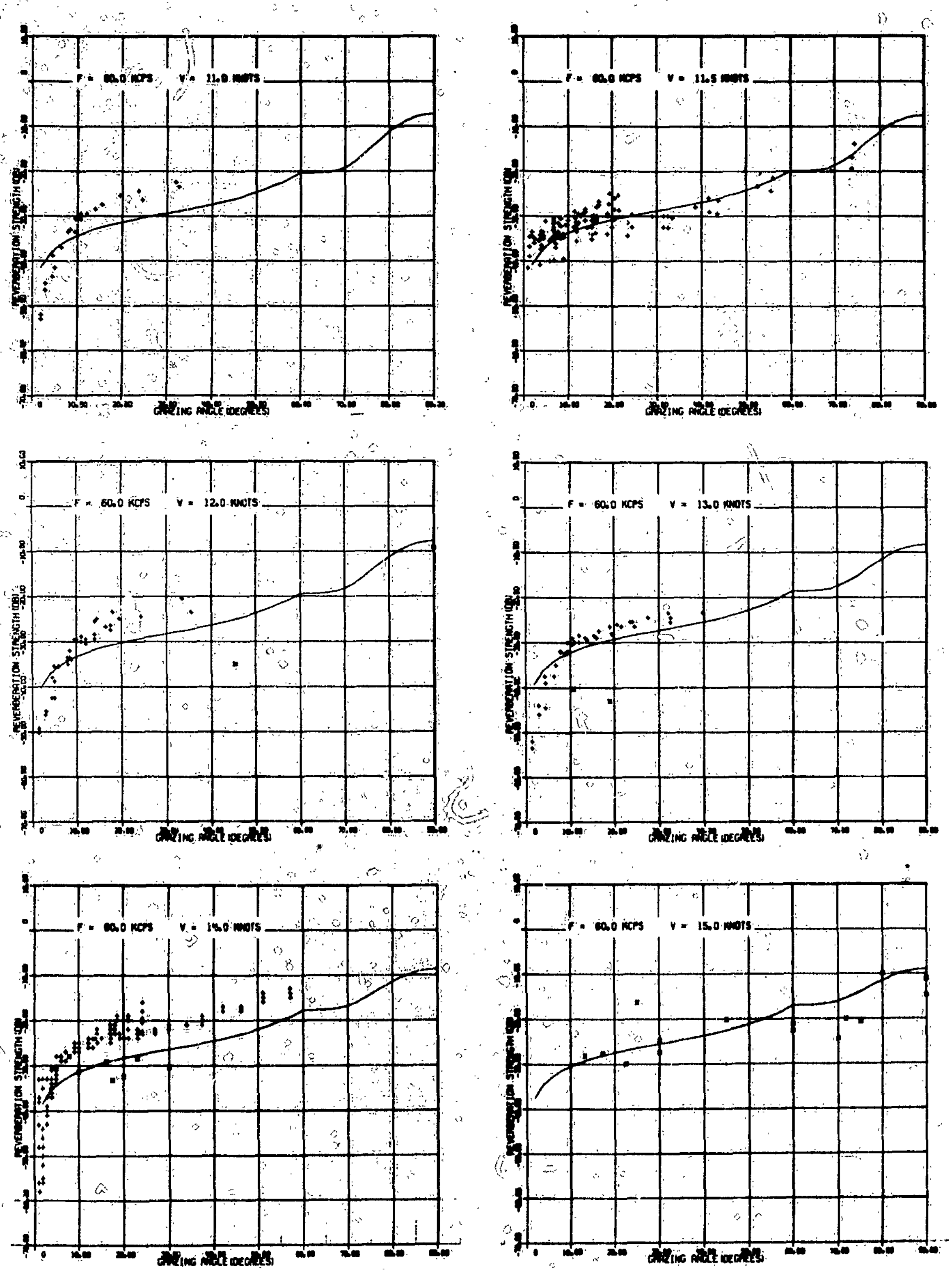

FIGURE B-8 (Cont'd) Comparison of Experimental Acoustic Reverberation Data with Present Theory (60 kcps)

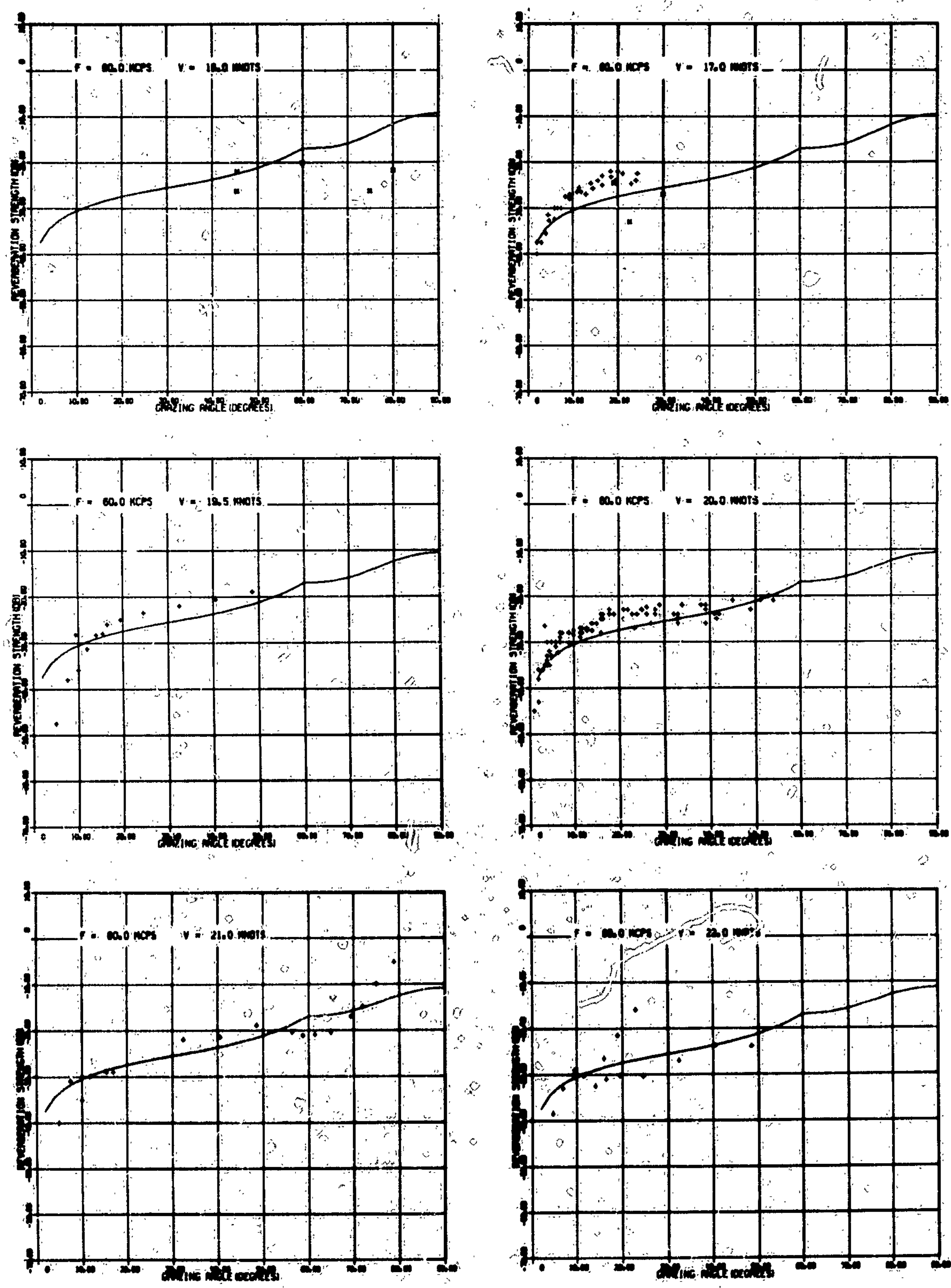

FIGURE B-8 (Cont'd) Comparison of Experimental Acoustic Reverberation Data with Present Theory (60 kcps)

APPENDIX C

OPTICALLY MEASURED AIR-DRIVEN WATER SURFACE SLOPE POWER SPECTRAL DENSITY DATA

The psd of water surface slopes as a function of air speed over water has been measured using the apparatus shown in Fig. C-1 (Fig. 1 of Ref. 19). The data obtained from this apparatus are shown in Fig. C-1 (Fig. 4 of Ref. 19) which shows fS(f) versus f where f is the slope frequency. In the nomenclature of this paper

$$fS(f) \equiv f \left[E_{z'}(f)\right]_l \tag{C1}$$

and the right-hand side of this identity will be employed. The data of Fig. C-1 are presented for air speeds at about 6 cm above the water surface of v_{lab} = 3.18, 6.08, 9.20, and 12.02 m/sec. The pertinence of these laboratory air speeds v_{lab} to wind speeds v_{sea} at sea will be discussed subsequently in this Appendix. The points of Fig. C-1 have been estimated and these readings are given in Tables C-1 and C-2 which contain the fundamental data upon which all optically measured slope psd are based; Table C-1 gives logarithmic values and Table C-2, absolute values.

At the foot of Table C-2, two summations are given: as $\sigma^2_{z'}$ is given by

$$\sigma^2_{z'} = \int_0^\infty \left[E_{z'}(f)\right]_l \, df \tag{C2}$$

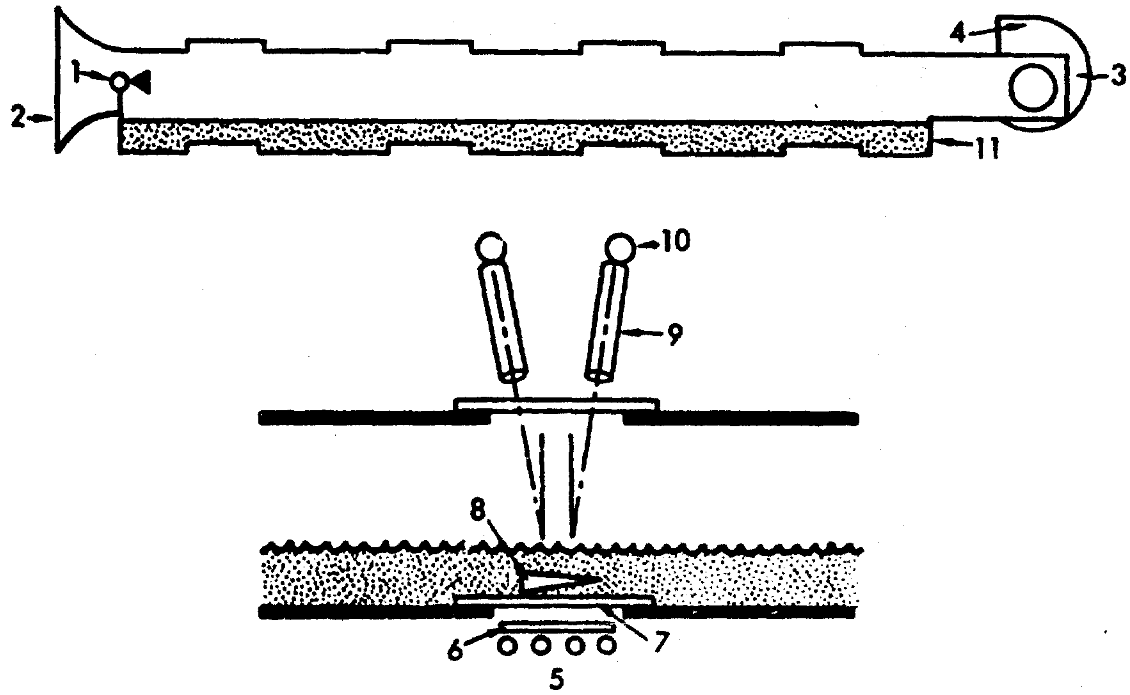

The stippled area in the lower third of the tank indicates water. The cross-sectional area of the air passage is 26.3 by 26.3 cm. The dimensions of the water channel are: 14 cm (depth), 26.3 cm (breadth), 6.1 m (length). Numerals refer to the following details: 1. cup anemometer; 2. entrance nozzle; 3. suction centrifugal fan; 4. damper for controlling wind speed; 11. gravel beach for absorbing waves. On an enlarged scale are shown: 5. light source composed of four cylindrical incandescent light bulbs operated on direct current; 6. diffusing glass; 7. plate glass windows (top and bottom of tank); 8. hollow wedge filled with inky water (placed directly upon or beneath lower plate glass window but here shown raised for clarity); 9. telescope tube which focusses an image of water surface on a pin-hole directly in front of photocell; 10. photocell.

FIGURE C-1 Wind and Water Tunnel for Measurements of Slopes of Waves Generated by Wind

R10-7-68-12

Table C-1 -- FREQUENCY-BIASED SLOPE SPECTRUM, LOGARITHMIC VALUES (After Ref. 19)

$$\log_{10}\left\{f\left[E_z,(f)\right]_1\right\}$$

Frequency, cps	v_{lab}, m/sec			
	3.15	6.08	9.20	12.02
0.857	-4.2	-3.9	-3.5	-2.7
1.07	-3.9	-3.6	-3.0	-2.3
1.35	-4.0	-3.5	-3.0	-2.4
1.71	-3.0	-2.7	-2.6	-2.0
2.15	-4.3	-3.3	-3.0	-1.7
2.71	-4.3	-3.5	-2.1	-0.8
3.41	-3.6	-3.1	-1.0	-0.6
4.29	-3.6	-1.8	-0.6	-0.9
5.40	-2.6	-1.0	-1.1	-1.0
6.80	-1.9	-1.0	-1.3	-1.0
8.57	-1.4	-1.4	-1.2	-0.9
10.7	-1.6	-1.6	-1.5	-0.8
13.5	-2.0	-1.5	-1.4	-0.8
17.1	-1.9	-1.6	-1.6	-0.9
21.5	-1.7	-1.5	-1.6	-1.0
27.1	-1.6	-1.3	-1.6	-1.0
34.1	-1.6	-1.3	-1.6	-1.0
42.9	-1.8	-1.1	-1.5	-1.1
54.0	-2.6	-0.9	-1.5	-1.0
68.0	-3.0	-1.2	-1.6	-1.4
85.7	-3.8	-1.4	-1.6	-1.4
107	-3.6	-1.7	-1.6	-1.5
135	-4.6	-2.2	-1.8	-1.6
171	--	-2.8	-2.0	-1.8
215	--	-3.5	-2.4	-2.1
271	--	-4.0	-2.9	-2.5
341	--	-4.5	-3.2	-2.7
429	--	-3.5	-3.6	-2.6
540	--	-2.6	-2.6	-2.0

Table C-2 -- FREQUENCY-BIASED SLOPE SPECTRUM,
ABSOLUTE VALUES
(After Ref. 19)

$$f\left[E_{l'}(f)\right]_1$$

Frequency, cps	v_{lab}, m/sec: 3.18	6.08	9.20	12.02
0.857	6.30 E-5	1.25 E-4	3.16 E-4	1.99 E-3
1.07	1.25 E-4	2.51 E-4	1.00 E-3	5.01 E-3
1.35	1.00 E-4	3.16 E-4	1.00 E-3	3.98 E-3
1.71	1.00 E-3	1.99 E-3	2.51 E-3	1.00 E-2
2.15	5.01 E-5	5.01 E-4	1.00 E-3	1.99 E-2
2.71	5.01 E-5	3.16 E-4	7.94 E-3	1.58 E-1
3.41	2.51 E-4	7.94 E-4	1.00 E-1	2.51 E-1
4.29	2.51 E-4	1.58 E-2	2.51 E-1	1.25 E-1
5.40	2.51 E-3	1.00 E-1	7.94 E-2	1.00 E-1
6.80	1.25 E-2	1.00 E-1	5.01 E-2	1.00 E-1
8.57	3.98 E-2	3.98 E-2	6.30 E-2	1.25 E-1
10.7	2.51 E-2	2.51 E-2	3.16 E-2	1.58 E-1
13.5	1.00 E-2	3.16 E-2	3.98 E-2	1.58 E-1
17.1	1.25 E-2	2.51 E-2	2.51 E-2	1.25 E-1
21.5	1.99 E-2	3.16 E-2	2.51 E-2	1.00 E-1
27.1	2.51 E-2	5.01 E-2	2.51 E-2	1.00 E-1
34.1	2.51 E-2	5.01 E-2	2.51 E-2	1.00 E-1
42.9	1.58 E-2	7.94 E-2	3.16 E-2	7.94 E-2
54.0	2.51 E-3	1.25 E-1	3.16 E-2	1.00 E-1
68.0	1.00 E-3	6.30 E-2	2.51 E-2	3.98 E-2
85.7	1.58 E-4	3.98 E-2	2.51 E-2	3.98 E-2
107.	2.51 E-4	1.99 E-2	2.51 E-2	3.16 E-2
135.	2.51 E-5	6.30 E-3	1.58 E-2	2.51 E-2
171.	-- --	1.58 E-3	1.00 E-2	1.58 E-2
215.	-- --	3.16 E-4	3.98 E-3	7.94 E-3
271.	-- --	1.00 E-4	1.25 E-3	3.16 E-3
341.	-- --	3.16 E-5	6.30 E-4	1.99 E-3
429.	-- --	3.16 E-4	2.51 E-4	2.51 E-3
540.	-- --	2.51 E-3	2.51 E-3	1.00 E-2
$(\Delta \ell n f)\Sigma f E_{l'}(f)$	6.78 E-2	1.87 E-1	2.07 E-1	4.61 E-2
$\sigma^2_{l'}$, (Eq. 35)	1.32 E-2	5.18 E-2	6.21 E-2	1.26 E-1

then

$$\sigma_{z'}^2 = \int_0^\infty f\left[E_{z'}(f)\right]_1 \, d(\ln f) \tag{C3a}$$

$$\cong \Delta(\ln f) \, \Sigma \, f_i \left[E_{z'}(f_i)\right]_1 \tag{C3b}$$

$$\cong 0.23 \, \Sigma \, f_i \left[E_{z'}(f_i)\right]_1 \tag{C3c}$$

where $\sigma_{z'}^2$ is the 1-D (along the length of the apparatus of Fig. C-1) variance of surface slopes. The value $\sigma_{z'}^2$ at the foot of Table C-2 is according to Eq. 35, and the summation given is that of the foregoing values in each column. The discrepancy between the values $\sigma_{z'}^2$ and the summation is, on the average, about four.

For the purposes of the theory of this paper, it is more convenient to use wave numbers k_s rather than frequency, so the data of Fig. C-2 and Table C-1 have to be transformed. Now the elevation psd of a surface is related to the slope psd as[3]

$$\left[E_z(k_s)\right]_1 = k_s^{-2} \left[E_{z'}(k_s)\right]_1 \quad , \tag{C4}$$

and the slope spectrum in wave number space is related to that in frequency space by

$$\left[E_{z'}(k_s)\right]_1 = \frac{1}{f}\left\{f\left[E_{z'}(f)\right]_1\right\} \frac{df}{dk_s} \quad , \tag{C5}$$

where

$$(2\pi f)^2 = gk_s + \gamma k_s^3/\rho_w \tag{C6}$$

relates f and k_s and determines df/dk_s. Thus, Eqs. C4, C5, and C6 transform $f[E_{z'}(f)]_1$ to $[E_z(k_s)]_1$. $[E_z(k_s)]_1$ is the form required in Appendix A for transformation to $[E_z(k_s)]_{s1}$ the 2-D representation of the psd of an homogeneous isotropically rough surface. In Eq. C6, g is acceleration due to gravity, γ is surface tension of water, and ρ_w,

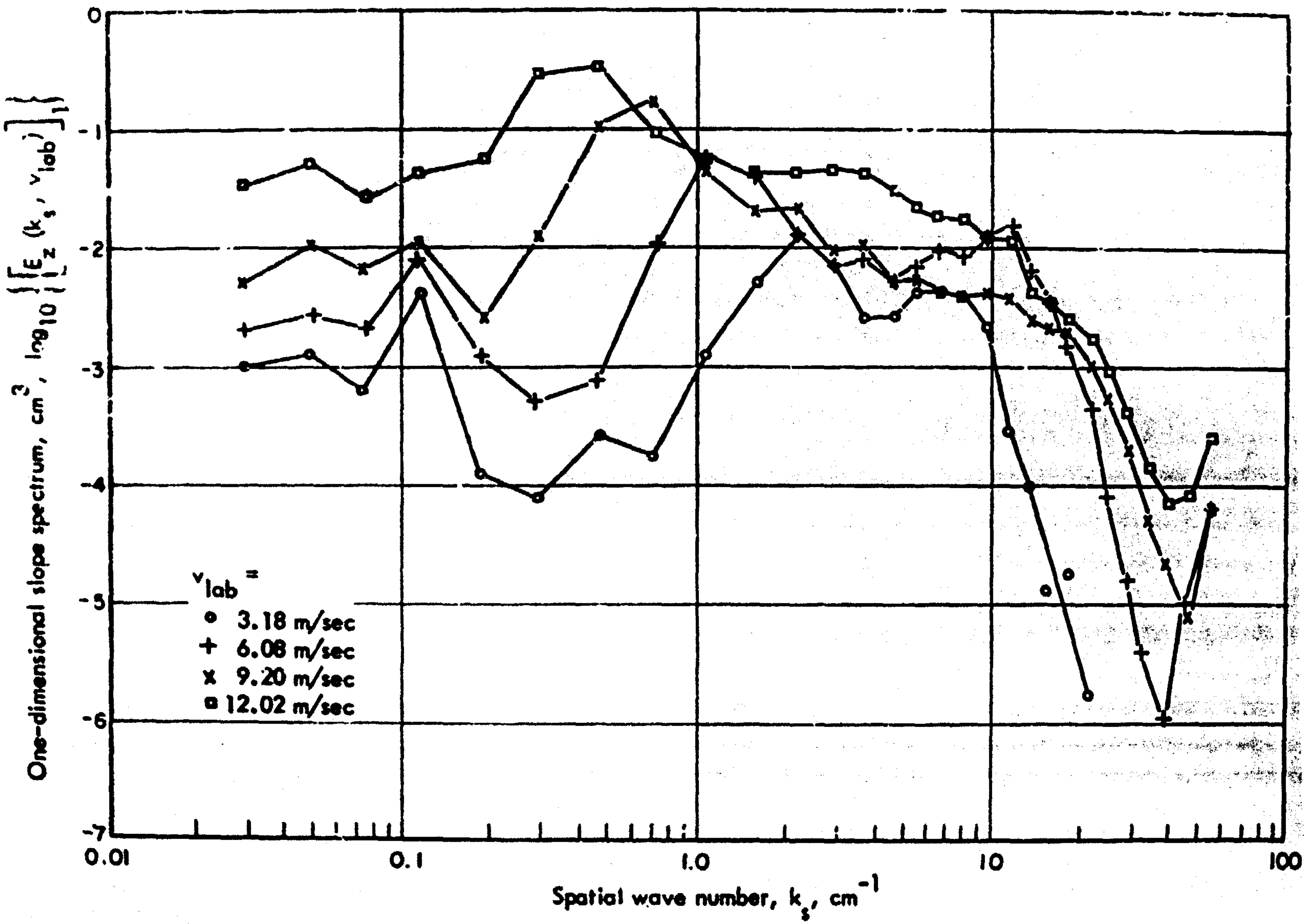

FIGURE C-2 One-Dimensional Water Surface Slope Power Spectral Density vs. Wave Number and Air Speed

density of water. As a convenience in relating wave number, frequency phase velocity, and length, Table C-3 presents these variables with parametric wave number, based on Eq. C6 and $k_s = 2\pi f_s / c_{ph}$.

Figure C-2 shows the variation of $[E_{z'}(k_s)]_1$ as from Eq. C5; one notes that for $0.6 < k_s < 20\ cm^{-1}$ it frequently occurs that $[E_{z'}(k_s, v_{lab})]_1$ is not a strictly monotonically increasing function of wind speed v_{lab} as one would expect, perhaps, on an intuitive basis. When $[E_{z'}(k_s, v_{lab})]_1$ is transformed to $[E_z(k_s, v_{lab})]_1$ by Eq. C5, this non-monotonic behavior persists as shown in Fig. C-3. As a result, smoothed values of $[E_z(k_s, v_{lab})]_1$ are employed as shown in Fig. C-4. This smoothing does not affect psd for $v_{lab} = 3.18$ and 12.02 m/sec, and modified psd values for $v_{lab} = 6.08$ and 9.20 m/sec by about a factor of two at most. Thus, $[E_z(k_s, v_{lab})]_1$ is in Fig. C-4 a monotonically increasing function of v_{lab} at fixed wave number. The corresponding tabular values of $[E_z(k_s, v)]_1$ are given in Table C-4. At the foot of Table C-3 is shown an approximation according to Eq. 2 of surface elevation variance σ_z^2 appropriate to the laboratory experiment. An analytical approximation to this which is useful below, is given by

$$\left(\sigma_z\right)_{lab} = 0.0435\ v_{lab}^{1.4} \tag{C7}$$

with v_{lab} in m/sec and σ_z in cm.

It is assumed in Ref. 19 that the boundary layer distribution of air (wind) speed above water (sea) surface is logarithmic in which case laboratory and at-sea measurements are related as

$$v_{sea} \ln(h/\sigma_z)_{sea} = v_{lab} \ln(h/\sigma_z)_{lab} \tag{C8}$$

where h is the height of measurement of v. Now $(\sigma_z)_{sea}$ is given (in cm and m/sec) as

$$\sigma_z = 0.41\ v^{5/2} \tag{C9}$$

Table C-3 -- WAVE FREQUENCY, PHASE VELOCITY, AND LENGTH VERSUS WAVE NUMBER

Wave Number, (cm^{-1})	Wave Frequency, cps	Phase Velocity, cm/sec	Wavelength, cm
0.001	0.158	990	6280
0.002	0.223	700	3140
0.003	0.273	572	2090
0.004	0.315	495	1570
0.005	0.352	443	1260
0.006	0.386	404	1050
0.007	0.417	374	898
0.008	0.446	350	785
0.009	0.473	330	698
0.01	0.498	313	628
0.02	0.705	221	314
0.03	0.863	181	209
0.04	0.997	157	157
0.05	1.11	140	126
0.06	1.22	128	105
0.07	1.32	118	89.8
0.08	1.41	111	78.5
0.09	1.50	104	69.8
0.1	1.58	99.0	62.8
0.2	2.23	70.1	31.4
0.3	2.74	57.3	20.9
0.4	3.17	49.8	15.7
0.5	3.56	44.7	12.6
0.6	3.91	41.0	10.5
0.7	4.24	38.1	8.98
0.8	4.56	35.8	7.85
0.9	4.87	34.0	6.98
1	5.16	32.4	6.28
2	8.03	25.2	3.14
3	11.1	23.4	2.09
4	14.7	23.2	1.57
5	18.8	23.7	1.26
6	23.4	24.5	1.05
7	28.4	25.5	0.898
8	33.8	26.6	0.785
9	39.6	27.7	0.698
10	45.8	28.7	0.628
20	124	38.8	0.314
30	225	47.1	0.209
40	345	54.2	0.157
50	482	60.5	0.126
60	633	66.2	0.105
70	797	71.5	0.0898
80	973	76.4	0.0785
90	1160	81.0	0.0698
100	1360	85.4	0.0628

NOTE: The minimum phase velocity is 23.12 cm/sec and this occurs at a wave number of 3.668 cm^{-1} for 35 parts/thousand (35 ‰) salt water at 20°C.

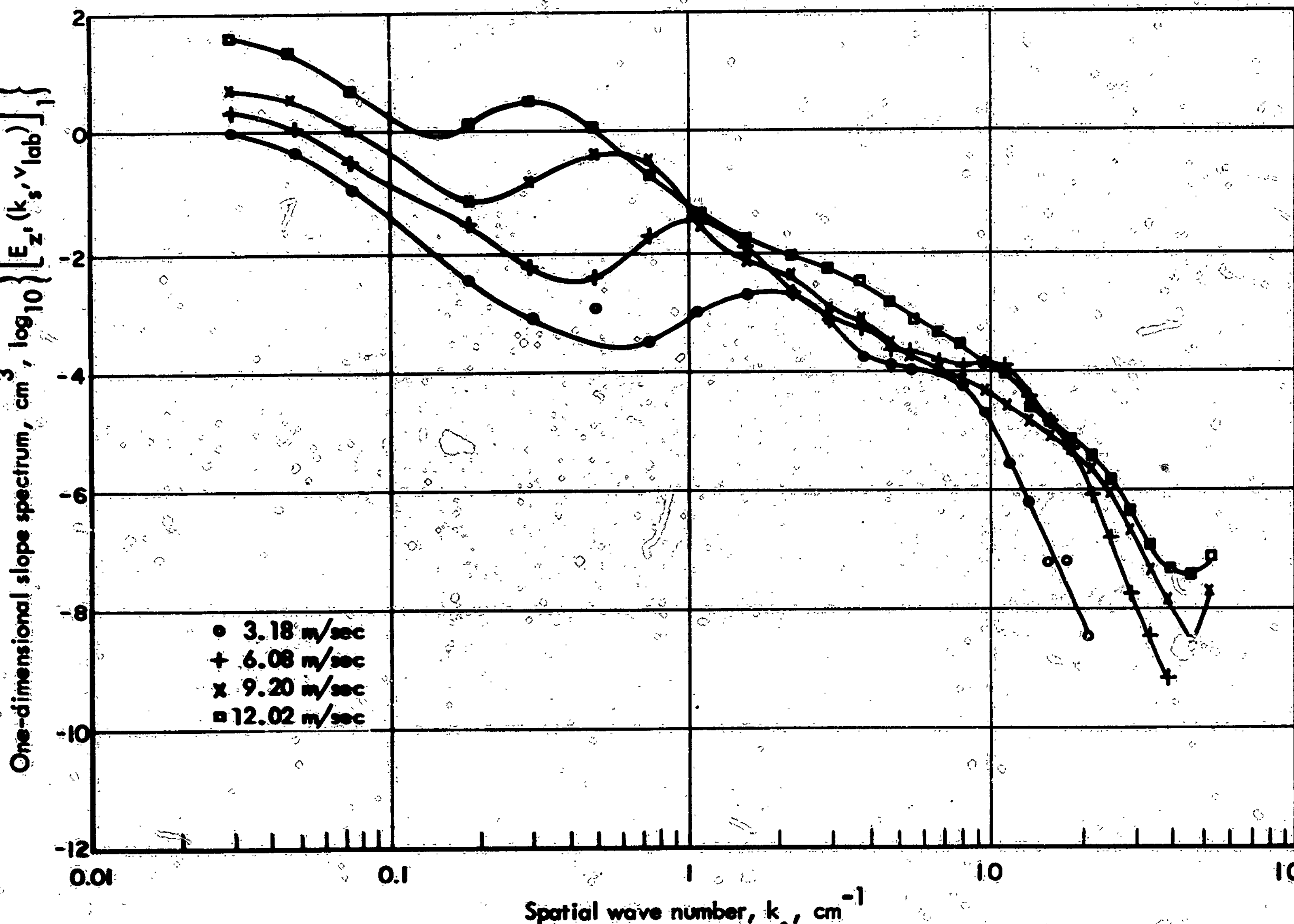

FIGURE C-3 One-Dimensional Water Surface Elevation Spectrum, Optically Based vs. Wave Number and Air Speed

RIO-7-66-14

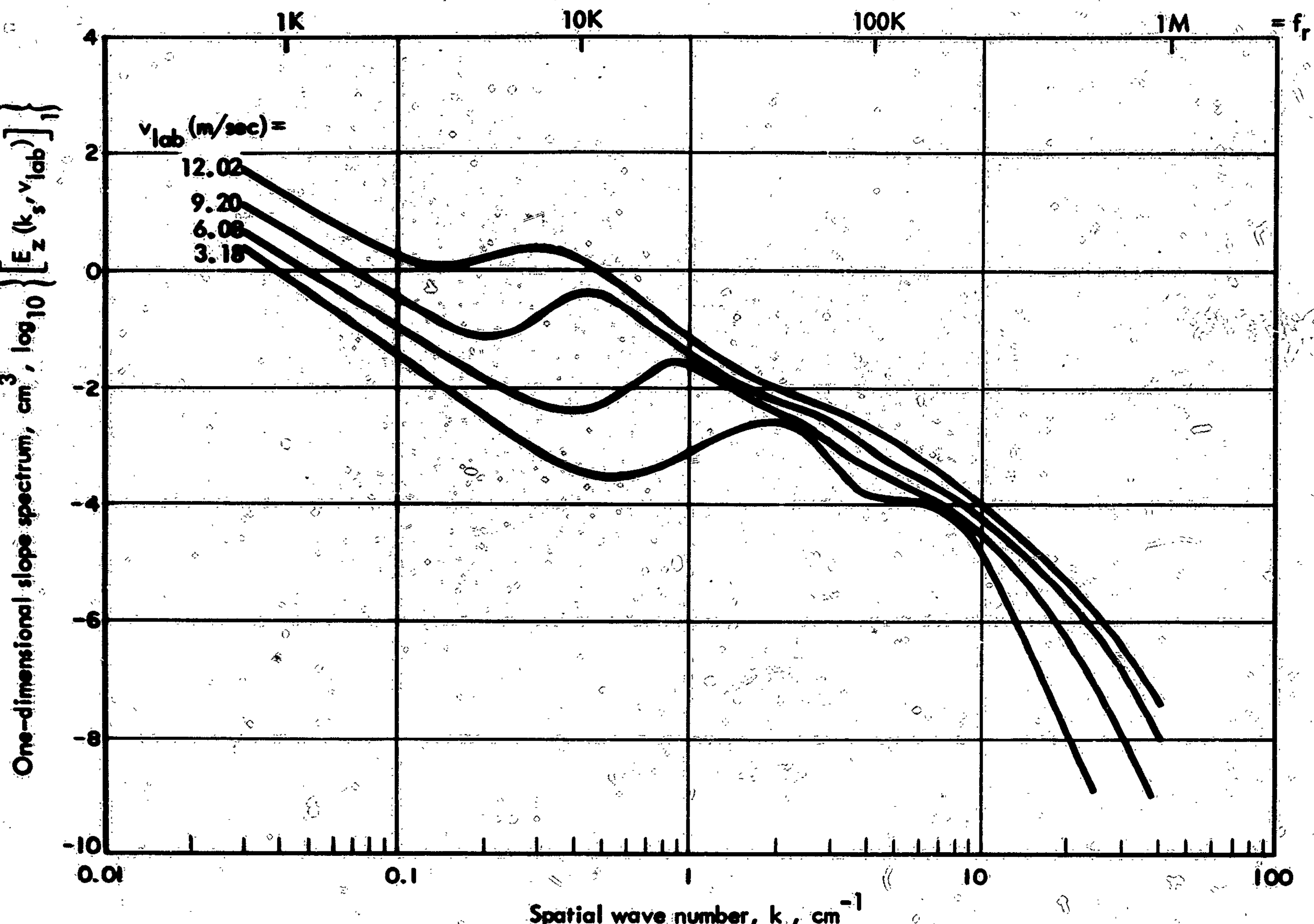

FIGURE C-4 One-Dimensional Water Surface Elevation Spectrum, Optically Based vs. Wave Number and Air Speed, Smoothed

R10-7-66-15

Table C-4 -- SMOOTHED ONE-DIMENSIONAL ELEVATION PSD

$\left[E_\zeta(k_s)\right]_1$ (cm^3)

Wave Number, k_s (cm^{-1})	v_{lab}, m/sec			
	3.18	6.08	9.20	12.02
0.0294	2.51	5.01	25.1	70.7
0.047	5.88 E-1	1.25	4.46	17.7
0.047	1.20 E-1	3.54 E-1	1.20	4.78
0.117	2.23 E-2	8.91 E-2	2.51 E-1	1.48
0.185	3.98 E-3	2.51 E-2	7.94 E-2	1.58
0.293	1.00 E-3	6.30 E-3	1.58 E-1	3.16
0.46	3.54 E-4	4.46 E-3	5.01 E-1	1.77
0.713	3.98 E-4	2.23 E-2	1.41 E-1	2.51 E-1
1.08	1.12 E-3	2.51 E-2	3.54 E-2	6.30 E-2
1.57	2.51 E-3	7.94 E-3	1.25 E-2	1.99 E-2
2.17	2.81 E-3	3.98 E-3	6.30 E-3	1.00 E-2
2.87	1.00 E-3	1.99 E-3	3.98 E-3	6.30 E-3
3.66	1.99 E-4	6.30 E-4	1.58 E-4	3.54 E-3
4.55	1.58 E-4	3.54 E-4	7.94 E-4	1.99 E-3
5.55	1.41 E-4	2.51 E-4	4.46 E-4	1.00 E-3
6.63	1.12 E-4	1.77 E-4	2.81 E-4	4.46 E-4
7.98	7.07 E-5	1.00 E-4	1.58 E-4	2.81 E-4
9.46	2.51 E-5	3.98 E-5	7.94 E-5	1.25 E-4
11.2	2.51 E-6	1.77 E-5	3.98 E-5	6.30 E-5
13.1	6.30 E-7	6.30 E-6	1.77 E-5	3.16 E-5
15.4	1.25 E-7	2.81 E-6	1.00 E-5	1.77 E-5
18.0	2.51 E-8	1.00 E-6	3.98 E-6	7.94 E-6
21.1	3.98 E-9	3.16 E-7	1.58 E-6	3.98 E-6
24.7	-- --	1.12 E-7	7.94 E-7	1.58 E-6
28.9	-- --	1.99 E-8	1.99 E-7	5.62 E-7
33.7	-- --	3.98 E-9	5.62 E-8	1.77 E-7
39.3	-- --	7.94 E-10	1.25 E-8	5.01 E-8
$\left(\sigma_\zeta^2\right)_{lab}$ (cm^2)	3.8 E-2	1.03 E-1	4.80 E-1	1.98

with the same units as Eq. C7. Thus, it is possible by numerical means to determine values of v_{sea} equivalent to v_{lab} if values of h are available. Reference 19 apparatus has h_{lab} = 6 cm and assumes a typical value of h_{sea} = 12.5 m (41 ft). Therefore, v_{lab} is transformable to v_{sea} by the foregoing and the results are given by Table 5 of the main text.

As the spectrum of elevation roughness plays a critical role in scattering and reflection of waves from a surface, one ought to consider the effect of the finite dimensions of the apparatus of Fig. C-1 upon the spectrum of roughness. Figure C-1 shows the water depth to be z_w = 14 cm, and the tank length to be ℓ_w = 6.1 m. Thus, one would expect no wavelengths $\lambda_s = \ell_w \geq 6.1$ m, corresponding to $k_s = 2\pi/610 \text{ cm} \cong 0.01 \text{ cm}^{-1}$. In fact, no data are reported for $k_s < 0.0294 \text{ cm}^{-1}$, i.e., about three times larger than the minimum expected and therefore presumably not greatly affected by tank length. In any case, finite length of the apparatus tends to diminish $[E_z(k_s, v_{lab})]$.

The other possibility of affecting the water surface condition is at small wave numbers by way of the finite depth of the tank. It is known that a particle near a wavy water surface undergoes more or less circular orbits and that if the water bottom is sufficiently near the surface, orbits are affected, thence wavelengths and heights. Now a wave in shallow water suffers its greatest dimunition[C1] of height near $z_w k_s = 1$ and if z_w = 14 cm, then $k_s \cong 0.07 \text{ cm}^{-1}$ corresponds to this minimum condition, at which point the wave height is about 91 percent of the deep water height. Corresponding to this condition, the change in wave phase velocity c_{ph} causes the wave number for shallow water to take on a value about 20 percent larger than would occur for deep water. As $z_w k_s \to 0$ from the vicinity of unity, wave height tends to increase (the surface takes on greater variance) and apparent wave number, as compared with deep water, increases. At $k_s = 0.0294 \text{ cm}^{-1}$, corresponding to the lower limit of Fig. C-2 and others, wave height is again at the deep water value and the corresponding wave number is about 65 percent greater than the deep water

value. Hence, in general, the finite dimensions of the tank tend to affect elevations of the water surface less than the reading accuracy of Fig. 1, and to shift wave numbers slightly at the lower limit of the optical data. The tendency of this is to increase $[E_z(k_s, v_{lab})]_1$. A typical correction is shown for v_{lab} = 12.02 m/sec in Fig. C-4; the effect of the correction therefore is to accentuate the postulated energetically isolated elevation spectral intervals and to cause a better match with mechanically taken elevation data in Fig. 3. Because finite depth and length of laboratory apparatus[C1] tend to compensate one another, no change in the data of Fig. C-4 was attempted.

UNCLASSIFIED
Security Classification

DOCUMENT CONTROL DATA - R & D

(Security classification of title, body of abstract and indexing annotation must be entered when the overall report is classified)

1. ORIGINATING ACTIVITY (Corporate author) Institute for Defense Analyses	2a. REPORT SECURITY CLASSIFICATION Unclassified
	2b. GROUP None

3. REPORT TITLE
Acoustic Reverberation At The Sea Surface: Surface And Sublayer Spectra Vis-A-Vis Scattering And Reflection

4. DESCRIPTIVE NOTES (Type of report and inclusive dates)
Research Paper P-284

5. AUTHOR(S) (First name, middle initial, last name)
John J. Martin

6. REPORT DATE December 1966	7a. TOTAL NO. OF PAGES 99	7b. NO. OF REFS 36
8a. CONTRACT OR GRANT NO. DAHC15 67 C 0011	9a. ORIGINATOR'S REPORT NUMBER(S) P-284	
b. PROJECT NO. T-37		
c.	9b. OTHER REPORT NO(S) (Any other numbers that may be assigned this report) N/A	
d.		

10. DISTRIBUTION STATEMENT
Distribution of this document is unlimited.

11. SUPPLEMENTARY NOTES N/A	12. SPONSORING MILITARY ACTIVITY N/A

13. ABSTRACT

On the basis of theoretical estimates of acoustic scattering an reflection strengths of rough surfaces and turbulent volumes, acou tic and optical data are interpreted so as to develop, on the one hand, spectra of sea surface roughness and of the turbulent sea su surface layer and, on the other, an acoustic reverberation strengt correlation formula. The range of application of both of these is for wind speeds up to about 20 knots (about 10 m/sec); the spectra range between 0.05 and 5 radians/cm, and the acoustic reverberatio strength correlation formula applies between acoustic frequencies of 0.6 kcps and 60 kcps.

DD FORM 1 NOV 65 1473

UNCLASSIFIED
Security Classification